UNIVERSITÁ DEGLI STUDI DI MILANO

Dipartimento di Scienze Farmacologiche e Biomolecolari

Corso di Dottorato in Scienze Farmacologiche

Sperimentali e Cliniche

Ciclo XXIX

“Pharmacological modulation of lactate levels affects the formation of long-term memory and the structure of excitatory synapses in mice hippocampus”

Settore scientifico disciplinare: BIO/14

Tesi di Dottorato di:

Elena VEZZOLI

Matricola n° R10407

TUTOR: Chiar.mo Prof. Alberto PANERAI

COTUTOR: Dott.sa Maura FRANCOLINI

COORDINATOR: Chiar.mo Prof. Alberto CORSINI

Anno Accademico 2015-2016

INDEX

LIST OF ABBREVIATIONS

Common abbreviations are not shown.
Of note, the International System of Units was applied throughout this study.

$[K^+]_i$	Intracellular potassium concentration
$[K^+]_o$	Extracellular potassium concentration
2D	Two dimensional
3D	Three dimensional
a.u.	Arbitrary units
Acetyl-CoA	Acetil-coenzyme A
ACSF	Artificial cerebrospinal fluid
ADP	Adenosine diphosphate
AGC	Aspartate/glutamate carrier
ANLS	Astrocyte-neuron lactate shuttle
ANLSH	Astrocyte-neuron lactate shuttle hypothesis
AP	Antero-posterior
ATP	Adenosine triphosphate
BBB	Blood brain barrier
BSA	Bovine serum albumin
CA1	Cornu Ammonis-1
CaMKIIa	Ca2+/calmodulin-dependent protein kinase II a
cAMP	Cyclic adenosine monophosphate
CBF	Cerebral blood flow
CNS	Central nervous system
CoA	Coenzyme A
CREB	cAMP response element-binding protein
CSF	Cerebrospinal fluid
Ctrl	Control
DAB	1,4-dideoxy-1,4-imino-D-arabinitol
EAAT1	Astrocytic excitatory amino acid transporter 1
EAAT2	Astrocytic excitatory amino acid transporter 2
ECS	Extracellular space
EM	Electron microscopy
ER	Endoplasmic reticulum
ERK	Extracellular signal-regulated kinases
F	Familiar object
FAD	Flavin adenine dinucleotide
FAD	Flavin-adenine dinucleotide
FADH	Flavin-adenine dinucleotide fully reduced form
$FADH_2$	Reduced flavin adenine dinucleotide
fMRI	Functional magnetic resonance imaging
GABA	Gamma-aminobutyric acid
GFAP	Glial fibrillary acidic protein
GLAST	Glutamate aspartate transporter
GLT-1	Glutamate transporter-1
GLUT1	Glucose transport-1
GP	Glycogen phosphorylase
i.e.	Id est

IC_{50}	Half maximal inhibitory concentration
IEG	Immediately Early Gene
K_M	Michaelis–Menten constant
L	Lateral
LDH	Lactate dehydrogenase
LTP	Long term potentiation
M	Mitochondrion
MAPK	Mitogen-activated protein kinase
MCT	Proton-coupled monocarboxylate transporter
MRS	Magnetic resonance spectroscopy
N	Novel object
NAD	Nicotinamide-adenine dinucleotide
NAD^+	Oxidized nicotinamide adenine dinucleotide
NAD^+	Nicotinamide-adenine dinucleotide oxidized form
NADH	Reduced nicotinamide adenine dinucleotide
NADPH	Nicotinamide-adenine dinucleotide phosphate reduced form
NMDA	N-methyl-D-aspartate
NMDAR	N-methyl-D-aspartate receptor
NOR	Novel object recognition
PA	Passive avoidance
PBS	Phosphate buffer saline
pCREB	Phospho- cAMP response element-binding protein
PDK	Pyruvate dehydrogenase kinase
PET	Positron emission tomography
PFK	Phosphofructokinase
Pfkfb3	6-phosphofructose-2-kinase/fructose-2,6-bisphosphatase-3
PKA	Protein kinase A
PKC	Protein kinase C
PMT	Photomultiplier
PNS	Peripheral nervous system
PSD	Post-synaptic density
ROS	Reactive oxygen species
RT	Room temperature
SBF-SEM	Serial block face scanning electron microscopy
SLC	Solute carrier
SMCTs	Sodium-coupled monocarboxylate transporters
SV	Synaptic vesicle
T1	Test time 1
T2	Test time 2
TCA	Tricarboxylic acid
TEM	Transmission electron microscope
TJs	Tight junctions
V	Ventral
Zif268	Zinc finger family 268

ABSTRACT

The block of glycogenolysis in the rat hippocampus impairs memory while L-lactate (but not equicaloric concentrations of glucose) rescues amnesia, suggesting that the metabolic coupling between astrocytes and neurons via lactate is required for long-term memory formation. The inactivation of glycogen metabolism and the consequent decrease of lactate production in hippocampal astrocytes leads to an impairment of long-term memory and defects in long-term potentiation (LTP). Since it has been demonstrated that LTP defects are associated with alterations in dendritic spines morphology and density, we studied whether anatomical differences in hippocampal excitatory synapses were related to defects in long-term memory in mice treated with the inhibitor of glycogen phosphorylase, 1,4-dideoxy-1,4-imino-D-arabinitol (DAB), and if these defects were rescued by L-lactate administration.

We first tested the effects associated to DAB administration on long-term memory using the passive avoidance (PA) task, a fear-aggravated test used to evaluate learning and memory in rodents. DAB was injected 15 minutes before training and long-term memory was tested 24 hours after the administration of the drug. The analysis of the PA test shows that DAB did not affect long-term memory. We then performed the novel object recognition (NOR) test to study intermediate- and long-term episodic memory after DAB injection into the hippocampus and here we showed that this treatment affected both intermediate- and long-term episodic memory, in a dose dependent manner. We performed low resolution analyses of spine density in apical dendrites from CA1 pyramidal neurons by means of the Golgi-Cox staining technique, 24 hours after training of mice treated with DAB and challenged with both PA and NOR tasks, to determine whether behavioural impairments are paralleled by defects on dendritic spine density. Our data demonstrated that 24 hours after treatment with DAB and following memory training, hippocampal neurons showed a marked reduction in dendritic spine density if compared to that of mice injected with vehicle, regardless of the memory paradigm used. To evaluate if this defect in spine density was associated to ultrastructural defects in hippocampal excitatory synapses, we performed a morphometric analysis on 2D transmission electron microscopy projections. These analyses highlighted a significant reduction of vesicle density in synapses of mice treated with DAB and an unvaried pre-synaptic surface. Interestingly, despite the effect of DAB on spine density, the post-synaptic density (PSD) architecture is unaffected as length and thickness were the same in animals treated with vehicle or DAB.

We then analysed the astrocyte-neuron lactate shuttle's role on the 3D architecture of excitatory synapses and mitochondria as a consequence of DAB administration. These data confirmed the observations obtained with the Golgi and the 2D analyses: the density of the dendritic spines was reduced and the PSD volume remained unvaried in mice treated with DAB. Altered brain metabolism is associated with changes in mitochondria dynamic cycles of fission and fusion. The remodelling of mitochondrial cristae and mitochondrial morphology are sensitive to the energetic demand of the cell, and they directly affects the development and maintenance of synapses. We analysed the mitochondrial structure in order to see whether the block of glycogen metabolism in astrocytes could affect the architecture of these organelles in neurons. We observed a significant change in dendritic mitochondria number, shape, and volume in DAB treated mice. Compared to uniformly compact and well-separated mitochondria in the hippocampi of mice treated with vehicle, DAB-treated neurons exhibited elongated mitochondria, in which two or more units were interconnected by tubular membrane extensions. Dendritic mitochondria in DAB treated mice were longer, reduced in number and bigger compared to dendritic mitochondria of mice treated with vehicle, suggesting that the alteration of glycogen metabolism induced by DAB could be the basis of mitochondria dynamics changes.

L-lactate, was administered to investigate its ability to revert the DAB-induced memory impairment. Co-injection of DAB and L-lactate was able to revert the memory impairment induced by DAB, 24 hours after NOR training. Besides behavioural rescue, the Golgi-Cox staining showed that in mice treated with DAB and L-lactate there was a rescue of spine density in apical dendrites of CA1 pyramidal neurons, bringing back its value to that of mice treated with vehicle. Focusing our attention on the ultrastructure of excitatory synapses, we measured the pre-synaptic surface and vesicle density of these samples and we showed that the vesicle density was comparable to that found in the synapses of mice treated only with DAB.

Our results suggest that, bilateral hippocampal injection of DAB caused an impairment of long-term memory formation 24 hours after NOR test. This behavioural alteration was accompanied by a strong morphological alteration of excitatory hippocampal synapses and dendritic mitochondria. L-lactate is able to rescue the behavioural phenotype, the reduction in spine density and the morphological alterations of dendritic mitochondria induced by this drug, but not the pre-synaptic effect induced by DAB on excitatory hippocampal synapses.

RIASSUNTO

Un crescente numero di evidenze sperimentali dimostra che gli astrociti hanno un ruolo attivo nello svolgimento delle funzioni cerebrali, comprese quelle cognitive. Il metabolismo del glicogeno, selettivamente localizzato negli astrociti, porta alla produzione di lattato che viene trasportato nei neuroni e usato come fonte di energia. Il blocco della glicogenolisi nell'ippocampo dei ratti provoca fenomeni di amnesia che è possibile revertire dopo la somministrazione di L-lattato ma non con concentrazioni equi-caloriche di glucosio. Questo indica che è necessaria un'azione coordinata tra astrociti e neuroni per la formazione della memoria a lungo termine. Il mancato consolidamento della memoria a lungo termine causato dall'inattivazione del metabolismo del glicogeno e dalla conseguente diminuzione dei livelli di lattato negli astrociti ippocampali, è accompagnato inoltre da difetti nei meccanismi di plasticità sinaptica.

Partendo da questi presupposti abbiamo studiato la morfologia delle sinapsi eccitatorie ippocampali in topi trattati con un inibitore della glicogeno fosforilasi, l'1,4-dideoxy-1,4-imino-D-arabinitol (DAB), per verificare se i difetti nella formazione della memoria a lungo termine fossero accompagnati anche da difetti nell'anatomia delle sinapsi e se questi effetti fossero revertiti dalla somministrazione di L-lattato.

Abbiamo verificato l'effetto del DAB sulla formazione della memoria a lungo termine attraverso due test comportamentali, la *passive avoidance* (PA) e il *novel object recognition* (NOR). Abbiamo dimostrato che DAB, iniettato bilateralmente nell'ippocampo dei topi 15 minuti prima del PA *training*, non ha effetti sulla memoria a lungo termine testata 24 ore dopo il *training*; al contrario, se iniettato 15 minuti prima del NOR *training* causa difetti sia alla memoria intermedia (testata 120 minuti dopo il *training*) che a lungo termine (24 ore dopo il *training*).

Abbiamo dimostrato, attraverso Golgi-Cox *staining,* che nei topi trattati con DAB e testati per la memoria a lungo termine con entrambi i test, i dendriti apicali dei neuroni piramidali presenti nella regione CA1 dell'ippocampo, hanno un ridotto numero di spine dendritiche rispetto ai topi trattati con il solo veicolo. Al fine di investigare se la ridotta densità delle spine dendritiche fosse associata a difetti nella loro struttura, abbiamo condotto un'analisi morfometica sui terminali sinaptici eccitatori utilizzando la microscopia elettronica a trasmissione. I risultati di quest'analisi ci mostrano che nonostante il DAB riduca la densità delle spine dendritiche, l'ultrastruttura della loro densità post-sinaptica (PSD) rimane inalterata, mentre si riduce significativamente la densità delle vescicole sinaptiche nei

terminali eccitatori ippocampali. Per completare l'analisi dell'architettura delle sinapsi, abbiamo condotto un'analisi 3D su un'ampia porzione di tessuto, che ci ha permesso di confermare la ridotta densità delle spine dendritiche, già dimostrata con l'analisi del Golgi in 2D e ci ha permesso di studiare la morfologia dei mitocondri presenti sia nei dendriti che nei terminali sinaptici.

Recenti studi hanno dimostrato che un'alterazione del metabolismo del cervello è associata a cambiamenti nei cicli di fusione e fissione dei mitocondri che portano a modificazioni della loro morfologia e funzione. La sensibilità di questi organelli al consumo energetico delle cellule provoca alterazioni nello sviluppo e nel mantenimento delle sinapsi.

Abbiamo studiato la morfologia dei mitocondri per valutare se il blocco del metabolismo del glicogeno negli astrociti avesse degli effetti sull'architettura di questi organelli nei neuroni. Abbiamo dimostrato che i mitocondri presenti nei dendriti degli animali trattati con DAB sono più allungati e sono formati da diverse unità interconnesse tra di loro, oltre ad essere presenti in numero ridotto e avere un volume maggiore rispetto ai mitocondri presenti negli animali trattati con il solo veicolo. Questi dati dimostrano che l'alterazione del metabolismo del glicogeno negli astrociti causa un drammatico cambiamento nell'architettura dei questi organelli.

Per verificare se L-lattato fosse in grado di revertire gli effetti di DAB sia sulla memoria degli animali che sulla morfologia delle spine, abbiamo co-iniettato L-lattato con il DAB nell'ippocampo dei topi. La somministrazione di L-lattato con DAB non causa alcun difetto nella memoria a lungo termine (24 ore dopo NOR *training*) e, sia la densità delle spine dendritiche che la morfologia dei mitocondri, non presenta alcuna alterazione rispetto ai topi trattati con il solo veicolo. Rimane però, negli animali trattati con L-lattato e DAB una ridotta densità delle vescicole sinaptiche nei terminali eccitatori ippocampali.

In conclusione, i nostri risultati dimostrano come il blocco del metabolismo del glicogeno negli astrociti causa un difetto nella formazione della memoria a lungo termine accompagnato da evidenti alterazioni della densità delle spine dendritiche, della morfologia delle sinapsi eccitatorie e nell'architettura dei mitocondri. La co-iniezione di L-lattato con DAB ripristina il difetto della memoria, l'alterazione della densità delle spine dendritiche e della morfologia dei mitocondri ma non la ridotta densità delle vescicole sinaptiche nei bottoni pre-sinaptici eccitatori.

INTRODUCTION

1. ENERGY METABOLISM IN THE NERVOUS SYSTEM

The energy requirements of the central nervous system (CNS) in mammals are very high, as the brain performs many different functions that are fundamental for survival. While in humans the brain represents only 2% of the body mass, it consumes about 20% of the oxygen and 25% of the glucose to accomplish all the cerebral functions. Glucose is the main energy source of the brain, and neurons are the cells that have the highest energy demand, neurons use this energy for information and signalling processing. The focus of this first part of introduction is to give a general overview of brain energy metabolism in order to understand how glucose metabolism sustains basal brain physiology.

2. GLUCOSE METABOLISM

Glucose plays a pivotal role in the energy metabolism of all cell types; it represents the starting molecule of this process and can be used by all the cells in the body. Glucose is a carbohydrate ($C_6H_{12}O_6$), in particular, a simple monosaccharide that is transported into cells and through a cascade of reactions (glycolysis and oxidative metabolism) that take place both in the cytosol and mitochondria, it is transformed in energy. The mammalian brain consumes about 5.6 mg of glucose per 100 g of brain tissue per minute with glucose being continuously taken-up from the blood. In neurons, glucose metabolism, through the production of ATP, represent the main energy source to sustain all physiological brain functions, to maintain neuronal and non-neuronal cellular viability, and to synthetize neurotransmitters starting from their precursors. To accomplish all these different functions, glucose localization and transport in the CNS, are tightly regulated and closely related to local regulation of the blood flow, under the control of glucose-sensing neurons. Besides its roles in the physiological functions of neurons, glucose metabolism is also intimately connected to cell death pathways by glucose-metabolizing enzymes. Thus, interference with glucose delivery and metabolism can cause a number of pathological brain conditions (Mergenthaler et al., 2013).

In the following paragraphs, the glycolysis and oxidative metabolism that are the major carbohydrate energy producing reactions are described.

2.1 Glycolytic pathway

The glycolytic pathway represents the first step of intracellular glucose metabolism and, in all eukaryotic cells, it takes place in the cytoplasm. Glycolysis can be described as the series of biochemical reactions that transforms glucose into pyruvate with the release of ATP, the energy source that can be used by cells.

Glycolysis can be divided into three main steps. In the first step glucose is converted into fructose-1,6-bisphosphate upon phosphorylation, isomerization, and a second phosphorylation reaction. This step requires two molecule of ATP per glucose molecule. In the second step, the six-carbon molecule (fructose-1,6-bisphosphate) is cleaved into two three-carbon fragments. In the third step, ATP is produced when the three-carbon fragments are oxidized to pyruvate, a reaction that produces one molecule of NADH and two of ATP (Figure 1) (Berg et al., 2002). Under aerobic conditions, the pyruvate molecule produced at the end of the glycolytic pathway can either enter the mitochondria and be transformed through the tricarboxylic acid cycle (TCA) where it is oxidatively metabolised to form Acetyl CoA and to produce ATP or remain in the cytoplasm to be further processed by the lactic fermentation pathway.

Figure 1

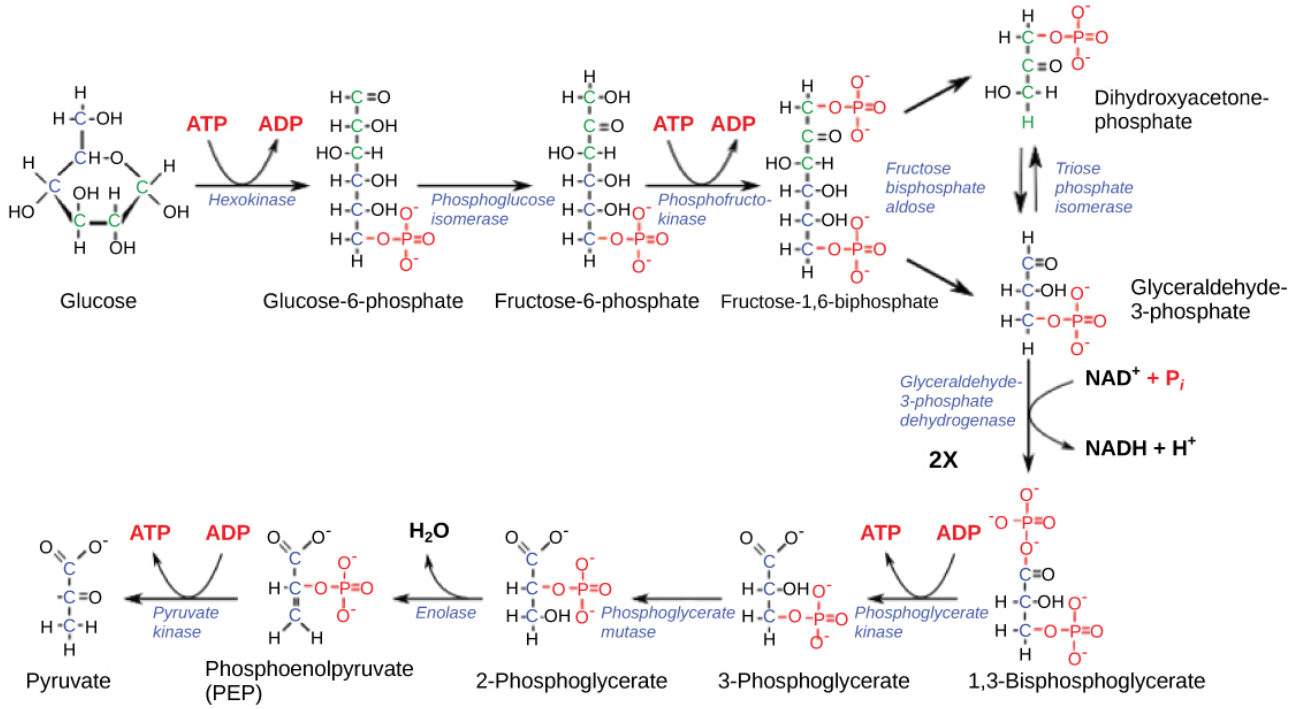

Figure 1. *Schematic representation of the three steps of the glycolytic pathway and the enzymes that are involved in all chemical reactions. During the first step glucose is converted into fructose-1,6-bisphosphate that, in the second step, is divided into two three-carbon moieties. In the third and last step, ATP is generated (modified from Berg et al., 2002).*

2.2 Oxidative metabolism: tricarboxylic acid cycle and electron-transport chain

The oxidative metabolism produces the majority of the ATP in the body; all chemical reactions involved take place in the mitochondria and the overall cycle needs oxygen (Fernie et al., 2004). Oxidative metabolism is achieved by the reactions of the tricarboxylic acid cycle (also known as Krebs cycle or citric acid cycle), which encompasses the final oxidation reactions, and the electron transport chain. The starting point of the oxidative metabolism is the pyruvate that is produced from the glycolysis. Under aerobic conditions, pyruvate is oxidatively decarboxylated to generate Acetyl CoA that enters in the TCA cycle.

As shown in figure 2, initially the two-carbon acetyl unit, the Acetyl CoA, is linked to a four-carbon compound, the oxaloacetate, to generate a six-carbon tricarboxylic acid, the citrate. The isocitrate, an isomer of citrate, is oxidatively decarboxylated to generate a five-carbon compound, the α-ketoglutarate. The following step is the formation of a four-carbon compound, the succinate, that leads to the de-novo formation of oxaloacetate. As result of this series of reactions, three hydride ions are transferred to three molecules of nicotinamide adenine dinucleotide (NAD^+), whereas one pair of hydrogen atoms (two electrons) is transferred to one molecule of flavin-adenine-dinucleotide (FAD). The main function of the TCA cycle is to synthetize the electron donor molecules (NADH and FADH) necessary during the next step of the oxidative metabolism: the electron transport chain. During the oxidative phosphorylation, the re-oxidation of NADH and $FADH_2$ causes a release of electrons that are then transferred to a series of enzymatic complexes, located in the mitochondrial inner membrane, to generate a proton gradient across the membrane. These protons flow through ATP synthase to generate ATP from ADP and inorganic phosphate. Oxygen is required for the TCA cycle indirectly as it represents the electron acceptor at the end of the electron-transport chain, necessary to regenerate NAD^+ and FAD (Berg et al., 2002). Besides energy production, during the TCA cycle, non-essential amino acids are synthetized. The TCA, together with oxidative phosphorylation, provides the vast majority of the energy used by aerobic metabolism in human beings, more than 95%. It is a highly

efficient chain of reactions as a limited number of molecules can generate large amounts of NADH and $FADH_2$. In the brain, as in almost all tissues, oxidative metabolism is the largest contributor to ATP synthesis. However, not all the glucose up-taken and used by the brain is totally oxidized. The brain consums 31 mmol of glucose per 100 gr of tissue per minute, more than the oxidized 26.6 mmol/100gr/min that were calculated based on the brain's oxygen consumption, thus, 4.4 mmol/100gr/min of glucose are free to enter other metabolic pathways (Magistretti, 2000).

Figure 2

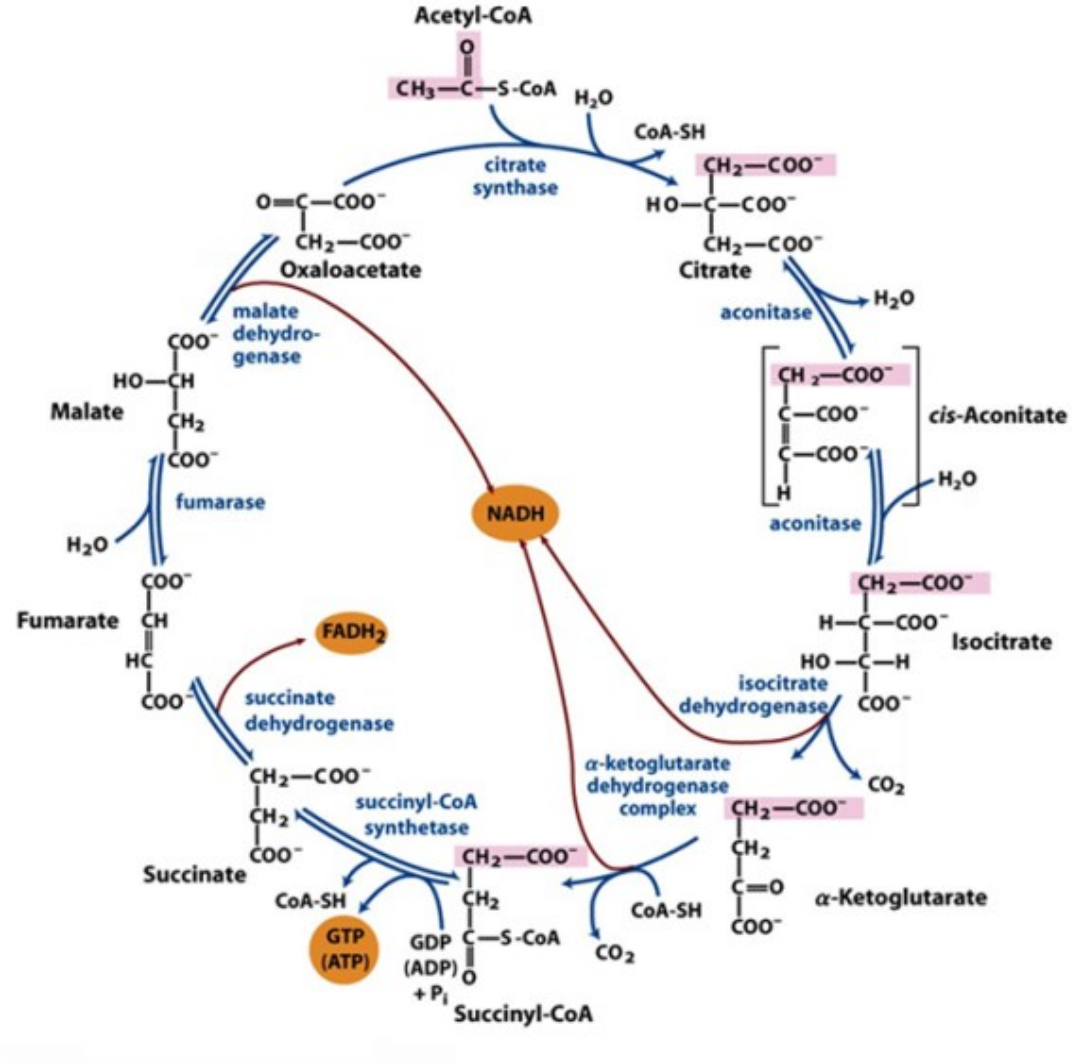

Figure 2. *Schematic representation of the tricarboxylic acid cycle (TCA) and the enzymes that are involved in its reactions. At the end of this series of reactions, that oxidizes two-carbon units, two molecules of CO_2, one molecule of GTP, and high-energy electrons in the form of NADH and $FADH_2$ are generated (modified from Nelson et al., 2008).*

2.3 Lactate

Lactate is a hydroxycarboxylic acid that may exist in the human body as two stereoisomers, L-lactate and D-lactate; L-lactate enantiomer is the most abundant in physiological condition (Adeva-Andany et al., 2014). Lactate is produced under anaerobic condition in the cell cytoplasm by the reactions of the fermentation pathway, starting from the reduction of the pyruvate with the parallel oxidation of NADH to NAD. This reaction is catalysed by lactate dehydrogenase (LDH). This enzyme is able to catalyse the reverse reaction thus producing pyruvate from lactate. The direction of the reaction depends both on the lactate and pyruvate concentration and on the LDH isoenzyme. This enzyme is a tetramer composed of an union of two different subunits: the H (heart) and the M (muscle) subunit, which respectively have a predominant expression in the heart or muscles. It is known that there are five different isoenzyme: LDH-1 (H_4), LDH-2 (H_3M_1), LDH-3 (H_2M_2), LDH-4 (H_1M_3), and LDH-5 (M_4) that are characterized by differential reactivity toward substrates, sensitivity to inhibitors, heat and cold lability (Sola-Penna, 2008). The oxidation of lactate into pyruvate is catalysed by the LDH1 isoform, whereas LDH-5 is responsible for the conversion of pyruvate to lactate and is mostly expressed in those tissues that produce lactate (i.e. muscle) (Cahn et al., 1962).

Lactate has long be considered a mere by-product of anaerobic metabolism, generated in conditions of oxygen shortage. During the last thirty years, however, this view has changed, as it was shown by many independent researchers that lactate can be used as an alternative energy source by several different cell types. First, it was demonstrated that lactate can be transported among different cells and within the cell itself. It is now well known that glycolytic muscle fibers can produce and release lactate that can be taken-up by surrounding oxidative fibers where it can be converted into pyruvate for aerobic oxidation (Brooks, 1986). More recently a novel example of intercellular lactate shuttle among astrocytes and neurons was described and indeed lactate is now considered as the second energy source of the brain (Barros, 2013). This phenomenon can be considered as one of the many aspects of the glial-neuronal metabolic coupling (Pellerin and Magistretti, 1994).

Lactate is transported across the cell membrane by the monocarboxylate transporters (MCTs). The MCTs are symporters that are able to move equimolar amounts of monocarboxylates, such as lactate, pyruvate and butyrate and H^+. The most important members of this family, with regards to lactate transport, are MCT1-MCT4 as these have been shown to transport lactate and other monocarboxylates such as pyruvate and ketone

bodies (Halestrap and Meredith, 2004). Generally, MCT1 and 2 are associated with lactate uptake in the liver, heart, kidney and red skeletal muscle. MCT4 is expressed by cells that exhibit a high rate of glycolysis and is associated with lactate efflux (Juel and Halestrap, 1999). MCT1, 2 and 4 are extensively expressed in the brain, with MCT3 is present in the choroidal plexus and retinal pigmented cells (Simpson et al., 2007). Because of its limited expression in the brain, MCT3 is not considered strictly a neuronal isoform and most studies on brain MCTs are centred on MCT1, 2 and 4. The relation of MCT subtypes with lactate up-take or release is crucial to understand the role of lactate in the brain, and it will be introduced in the paragraph 3.6 of the introduction.

2.4 Carbohydrate storage

Glycogen is the most important carbohydrate storage form in mammalian cells; actually, it is defined as the readily mobilized storage form of glucose. Glycogen is the very large, branched polymer of glucose, which can be broken down to provide glucose molecules when cells need energy (Berg et al., 2002*)*.

Glycogen is the fuel reserve of the body for several reasons: i) the controlled breakdown of glycogen and release of glucose increase the amount of glucose that is available between meals; ii) glycogen serves as a buffer to maintain blood-glucose levels. Glycogen's role in maintaining blood-glucose levels is especially important because glucose is virtually the only fuel used by the brain, except during prolonged starvation. iii) The glucose from glycogen is readily mobilized and is therefore a good source of energy for sudden, strenuous activity. Unlike fatty acids, the released glucose can provide energy in the absence of oxygen and can thus supply energy for anaerobic activity.

The two major sites for glycogen storage are the liver and the skeletal muscle. The volume of glycogen represents the 9-10% of the total tissue mass in the liver and 1-2% in the skeletal muscle. However, given the larger mass of skeletal muscles compared to liver, in absolute terms more glycogen is stored in skeletal muscle.

The functions of the glycogen are different in the different storage sites. In the liver, glycogen synthesis and degradation are regulated to maintain glucose levels in the blood high (or low) enough to meet the needs of the organism as a whole. By contrast, in the skeletal muscle, these processes are regulated to meet the energy needs of the muscle itself.

Glycogen metabolism involves a series of reactions that are shown in figure 3. The key enzyme for glycogenolysis is glycogen phosphorylase (GP). GP only acts on the linear chains of glucose residues contained within the glycogen molecule, thus a de-branching enzyme is required to completely digest glycogen.

Figure 3

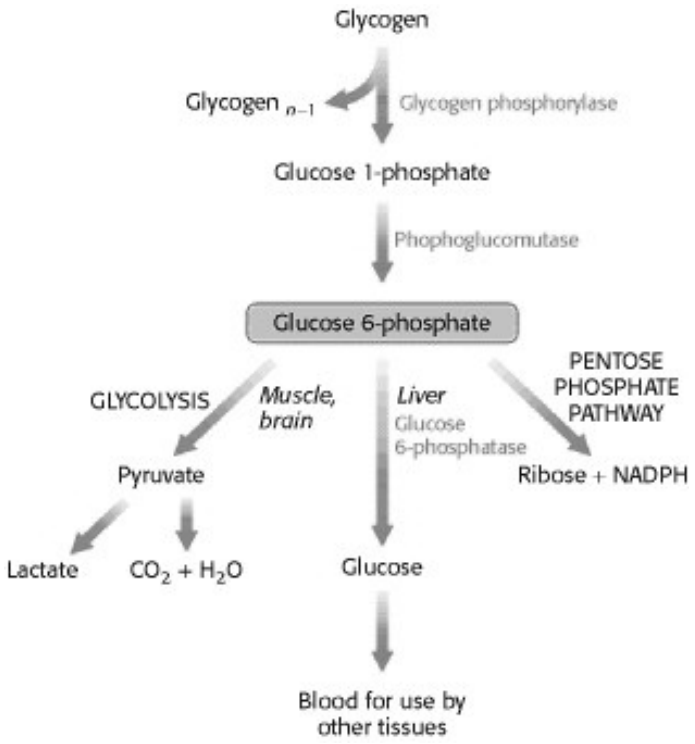

Figure 3. *Upon glycogen degradation, glucose 1-phosphate is released and converted into glucose 6-phosphate. Free glucose 6-phosphate can then be used as a fuel for anaerobic or aerobic metabolism in muscle and brain; or be converted into free glucose in the liver and subsequently released into the blood; finally it can be processed through the pentose phosphate pathway to generate NADPH or ribose in a variety of tissues* (modified from Berg et al., 2002).

As reported in figure 3 the pathway of glycogen degradation consists of three main steps: i) a molecule of glucose 1-phosphate is release from glycogen, ii) the glycogen that remain is remodeled to allow further degradation, and iii) the molecule of glucose 1-phosphate is converted into glucose 6-phosphate for further metabolism. The molecule of glucose 6-phosphate derived from the breakdown of glycogen can be further processed following three different fates: i) it can be used as the first substrate for the glycolytic pathway, ii) it can be processed along the pentose phosphate pathway to yield NADPH and ribose derivatives; and iii) it can be converted into free glucose to be released into the

bloodstream. This last conversion takes place mainly in the liver and to a lesser extent in the intestines and kidneys (Berg et al., 2002).

The limiting step in glycogenolysis is represented by the activation/inactivation of GP; GP is active in its phosphorylated form. The phosphorylation of GP is performed by phosphorylase kinase (Brown, 2004). The switch of GP from its inactive to active state is very rapid, and this allows glycogen to be quickly mobilized when needed (Shulman and Rothman, 2001). Glycogenolysis and therefore access to the stored glucose can be inhibited by compounds that bind to GP in its inactive state, an example of an inhibitor of GP is the compound DAB (1,4-dideoxy-1,4-imino-D-arabinitol) (Walls et al., 2008).

3. BRAIN ENERGY METABOLISM

3.1 Energy requirements of the brain

The Central Nervous System (CNS) has a very high-energy demand in terms of its requirements of both glucose and oxygen supply. As mentioned above, the brain represents only 2% of the body mass, but it consumes about 20% of the oxygen and 25% of total plasma glucose (Raichle and Gusnard, 2002). As demonstrated by many evolutionary studies, higher cognitive functions in humans are associated with an increased glucose consumption and an increased expression of genes related to energy metabolism. Indeed, with the two principal functional brain imaging techniques, positron emission tomography (PET) and functional magnetic resonance imaging (fMRI) -which are widely used in human neuroscience studies- it has been possible to monitor energy delivery to the brain and to parallel energy consumption with neuronal activity. Furthermore, through the use of high-field magnetic resonance spectroscopy (MRS), it is now possible to study metabolic fluxes *in vivo* in laboratory animals and humans under physiological and pathological conditions (Shulman and Rothman, 2001; Duarte et al., 2012).

The first pioneering studies conducted by Sokoloff and colleagues (Sokoloff et al., 1955) in awake human beings, demonstrated that glucose was almost fully oxidized in the brain where it represented the obligatory energy substrate. However, more recently, other studies at the whole organ level on awake patients, demonstrated that, under particular conditions (i.e. fasting, uncontrolled diabetes, and maternal milk diet in new-born), the

energetic requirements of the brain can be sustained not only by glucose but also by ketone bodies (Magistretti et al., 1999, reviewed in Magistretti and Allaman, 2015).

It has to be noted, however, that other methodological approaches, besides studies on entire organs in awake patients or animal models, can be used to investigate neuroenergetics in search for specific metabolites, and/or to assess the relative contributions of each cell type to the overall metabolic processes of the brain. These last aspects represent indeed one of the major challenge in modern neuroscience and the answers to these questions might derive from the integrated use of methodological approaches (both in vitro and ex-vivo) whose results can be gathered to provide a comprehensive view of brain energy metabolism.

3.2 The Blood-Brain Barrier

The blood brain barrier (BBB) is a diffusion barrier essential for the normal function of the central nervous system. BBB isolates the brain from circulating blood, in this way it blocks influx of most compounds from blood to brain thus creating a protected environment for neurons and glial cells. The BBB is composed by three different cells types and cellular structures: i) brain capillary endothelial cells, ii) astrocyte end-feet, and iii) pericytes. The endothelial cells are closely held together by tight junctions (TJs), that forms a diffusion barrier, which is able to block para-cellular fluxes of molecules flowing in the blood from entering into the brain. Astrocytic end-feet strengthen this barrier, surrounding the outside of the endothelial wall, their presence is crucial for the maintenance of the TJs complexes. The last type of cell that are represented in the BBB is the pericyte that plays a key role in the structural stability of the vessel wall.

Thanks to the presence of the BBB, in order to enter the brain parenchyma, molecules have to be either lipophilic, thus be transported through cells by diffusing through the plasma-membrane, or to be recognized by specific molecules, called transporters, that are able to mediate trans-cellular crossing of the endothelial cell layer (Proia et al., 2016). The brain energy metabolism is strictly dependent on the selective permeability of the energy substrates with respect to the BBB. In fact, the primary energy substrate of the brain, glucose, enters in the brain thanks to a glucose transporter (GLUT1), which is abundantly expressed in brain capillary endothelial cells (Barros et al., 2007). The relevance of the selectivity of the BBB toward energy substrates like glucose, is demonstrated by the observation that in humans, patients bearing mutations in the gene coding for GLUT1 that

result in a reduced surface expression of this protein, are characterized by low glucose concentrations in the cerebrospinal fluid (CSF), seizures and impaired development (De Vivo et al., 1991).

Similarly, the second brain energy source, lactate, enters into the brain by specific transporters that are located in the BBB, the monocarboxylate transporters (MCT), that, as mentioned above, are also are able to transport pyruvate and ketone bodies.

3.3 Neuroglial Cells and the Astrocytes

Glial cells are the most abundant cells in the brain, the group is represented by highly heterogeneous cellular populations of neural origin, the macroglia (astrocytes, oligodendrocytes, and Neuro-Glial antigen 2 glial cells) and non-neural origin, the microglia. All macroglial cell types are essential for maintaining and modulating efficient neurotransmission, homeostatic cascades, supply of energy metabolites, turnover of neurotransmitters, and establishment of the blood-brain barrier (Wang et al., 2016).

Microglial cells represent the immune competent cells of the central nervous system, being in fact a specialized sub-population of macrophages. Microglia is responsible for CNS health and protection against many types of pathogenic factors as well as for removal of damaged neuronal debris (Buttgereit et al., 2016).

Macroglia in the CNS is represented by astrocytes, oligodendrocytes, and Neuro-Glial antigen 2 glial cells. In the peripheral nervous system (PNS) macroglia also comprises Schwann cells, satellite cells and enteric glial cells. Many are the roles of the neuroglial cells in the CNS, in this thesis I will discuss about the role of the astrocytes in the brain.

3.4 Astrocytes

One of the neuroglial cell types that populates the brain is astrocytes that occupy 25-50% of the brain volume. This type of cell has a stellate morphology with many fine processes but, differently from excitable cells, they lack of axons, action and synaptic potentials. In the last 25 years, however, numerous investigations focused on astrocytic functions have highlighted the fundamental nature of the interactions between neurons and astrocytes for normal brain function.

The astrocytes present in the white matter are called fibrous astrocytes and are characterized by a complex cellular architecture with 50 to 60 long branching processes that can be extended from the cell body to the pial surface, around the blood vessels, or among neurites. In the gray matter a different type of astrocytes is found, the protoplasmic astrocytes that are characterized by short stubby processes that surround the capillaries, pial surfaces and neurons. The astrocytic processes that surround the blood vessels are called end-feet and they are involved in glucose uptake, for this reason they express on their surface many glucose transporters, in particular the GLUT1 type. Every synapse, in the gray matter is virtually enclosed by astrocytic lamellar process that play very precise and specific roles (Magistretti and Ransom, 2002).

Astrocytes are the cells that contain glycogen, which is the brain energy storage. The relevance of this specific property of astrocytes will be discussed below. Cytoplasm of astrocytes also contain a peculiar intermediate filament protein, the Glial Fibrillar Acidic Protein (GFAP) that is organized in filaments (9 nm). Fibrous astrocytes contain more of these intermediate filaments than protoplasmic astrocytes.

Astrocytes do not have functional chemical or electrical junctions with neurons; however, these two cells types communicate in many diverse ways through the extracellular space (ECS) separating them. ESC is an active compartment both for its contents and for its extension. It is represented by a very thin space (0.02 μm) between adjacent cell membranes. In ECS, all the molecules released by one cell diffuse instantly to adjacent cells and this diffusion is crucial for most correct brain functions. Within ECS in fact neurons can find and uptake ions (Na^+, K^+, Ca^{2+} and Cl^-) that are necessary to maintain neuronal electrical activity. Through the ECS movements of the energetic metabolites and the neurotransmitters are granted, thus allowing them to diffuse and permeate into the brain parenchyma. The homeostatic control of ECS potassium concentration $[K^+]_o$ is crucial as it can influence a number of physiological functions like neuronal activity (Baylor and Nicholls, 1969) and neurotransmitter release (Balestrino et al., 1986), cerebral blood flow (Kontos, 1981), ECS volume (Ransom et al, 1985), and glucose metabolism (Salem et al., 1975). The uncontrolled increase of $[K^+]_o$ leads to an unstable positive feedback loop increasing excitability; in fact higher $[K^+]_o$ is measured during intense neuronal activity as epileptic discharge (Ransom et al., 2000). Astrocytes maintain the extracellular potassium concentration at the physiological level and they limit its accumulation to a maximum level of 10 to 12 mM (Figure 4),

Figure 4

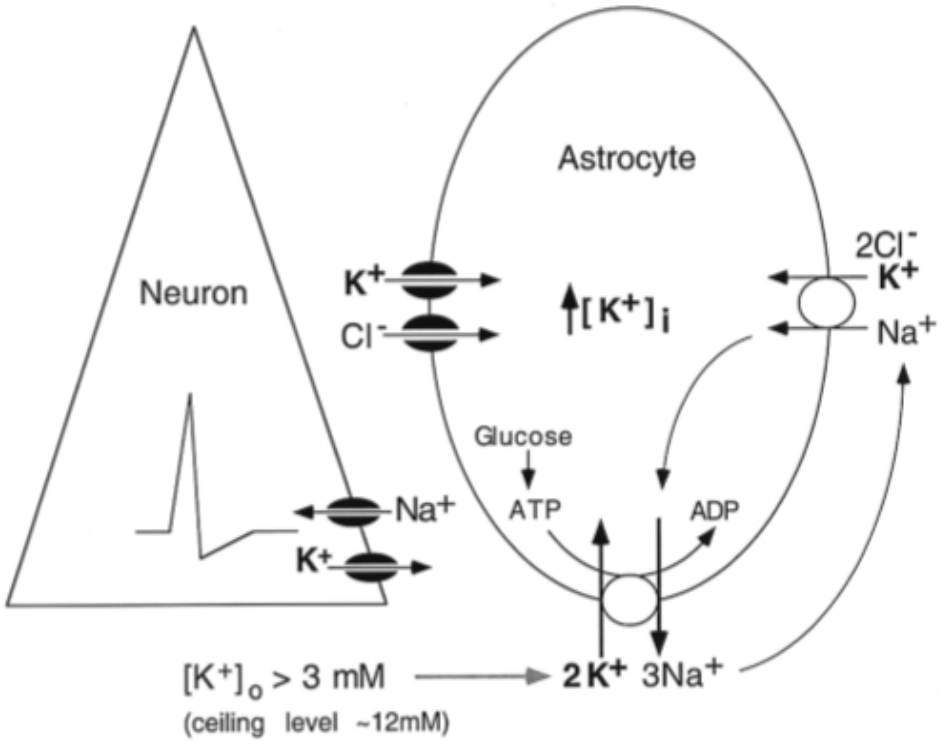

Figure 4. *Astrocytes control the increase of K^+ in the extracellular space caused by firing neurons thank to three molecules expressed at their surface. 1) The ATP sodium-potassium pump; 2) the anion transporter and 3) the Cl^- and K^+ channels, with these three strategies astrocytes limit the $[K^+]_o$ under 12 mM. (Modified from Magistretti and Ransom, 2002).*

The second important function astrocytes in the brain is the synthesis and the removal of neurotransmitters, in particular glutamate, the most diffuse excitatory neurotransmitter in the brain. Glutamate is originated from i) neuronal glucose metabolism and ii) from astrocyte-derived glutamine, the main precursor of synaptically released glutamate (Fonnum, 1984). Astrocytes synthesized and released glutamine by the "glutamate-glutamine cycle" (Figure 5). This chain of reactions represents a biochemical shuttle where glutamate, after being released from the pre-synaptic terminal, is taken-up by astrocytes (Anderson and Swanson, 2000) and it is converted into glutamine by glutamine-synthetase, an ATP dependent enzyme (Norenberg and Martinez-Hernandez, 1979). This enzyme is present in the astrocytic lamellae that surround the glutamatergic synapses. Glial cells released glutamine that then enters in the neurons through specific carriers. When glutamine reaches the pre-synaptic terminal, it is converted into glutamate by glutaminase, a phosphate-dependent

enzyme, localized in synaptic mitochondrial matrix (Westergaard et al., 1995); before being transported into synaptic vesicles and ready for the release. The glutamate-glutamine cycle is an example of the active interplay between astrocytes and neurons. On one hand astrocytes mediate the removal of the potentially toxic excess of glutamate from the ECS while on the other they provide neurons with a precursor for its re-synthesis.

Figure 5

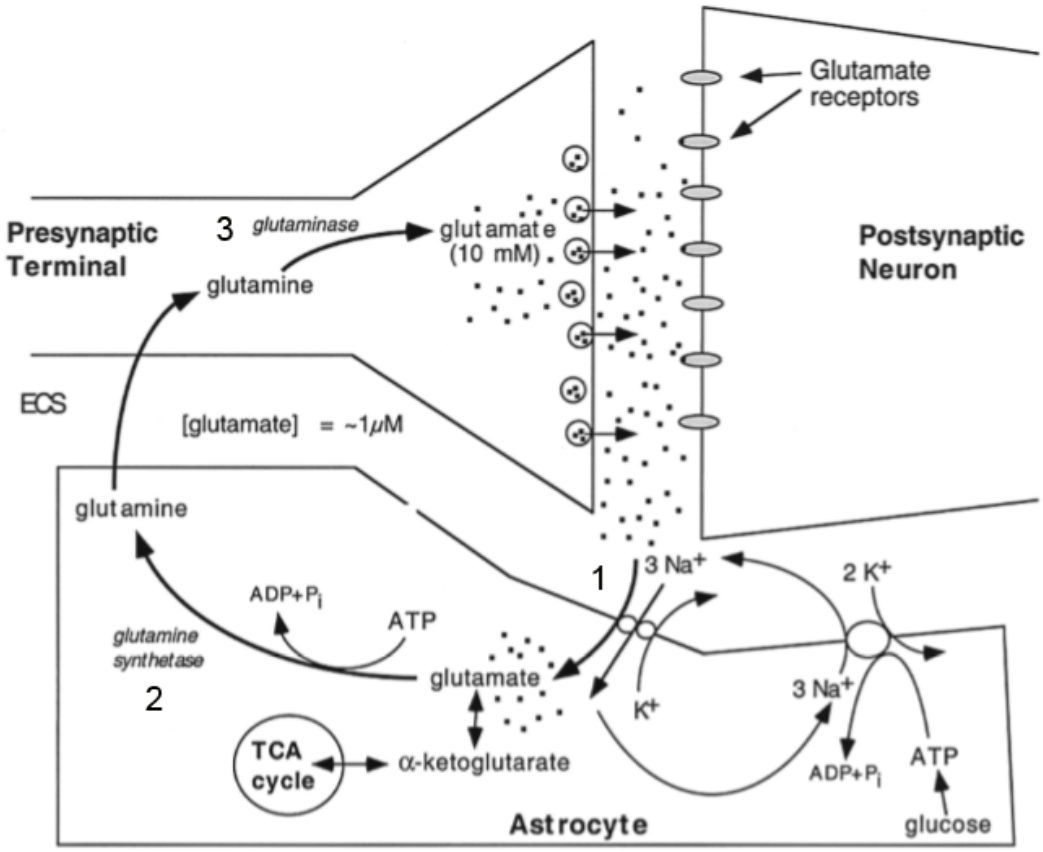

Figure 5. *Scheme of glutamate-glutamine cycle. The glutamate release from the pre-synaptic terminal is taken-up by the high affinity glutamate uptake system of the astrocytes that contains the glutamine synthetase, which converts glutamate to glutamine in an ATP-dependent mechanism. The following step is the release of the glutamine that enters into neurons where it is converted into glutamate for synaptic release. (Modified from Magistretti and Ransom, 2002).*

The extracellular physiological concentration of glutamate is about 2 μM (Benveniste et al., 1984), it is important that this value remains stable without increase as, besides being the most important neurotransmitter in the CNS, this amino-acid is also a potent neurotoxin

and glutamate excito-toxicity been implicated in a number of pathological CNS conditions as stroke, amyotrophic lateral sclerosis, and epilepsy.

Both neurons and glial cells express glutamate transporters on their surface, however the amount of glutamate transported by astrocytes is quantitatively the most important in the fine tuning of glutamate levels at synapses and in the extracellular space. Glutamate uptake by astrocytes is primarily achieved 1) by the astrocyte-specific sodium-dependent high-affinity glutamate transporters (GLT-1 in rodents, EAAT2 in humans) and it is driven by the electrochemical gradients of Na^+ and K^+ (3 Na^+ and 1 H^+ in and 1 K^+ out with the uptake of each glutamate anion (Anderson and Swanson, 2000) and 2) by the glutamate aspartate transporter (GLAST in rodents, EAAT1 in humans) (Bak et al., 2006). Indeed, astrocytic membranes facing a glutamatergic synapse express higher levels of GLAST than membranes facing other structures such as *pia mater* or capillaries (Chaudhry et al., 1995). In fact, most of the glutamate released by synaptic vesicle exocytosis is taken up by adjacent astrocytes (Bergles and Jahr, 1998).

3.5 Metabolic profiles of neurons and astrocytes

The mammalian brain is a high-energy consuming organ, its proper function depends upon the energy substances that reach the organ from the blood flow, however it is able to store only little energy reserves. Glucose, lactate, pyruvate, glutamate and glutamine can all be used as energy source by cells in the brain (Zielke et al., 2009). Among these substances, lactate has raised the higher interest in recent years. The lactate extracellular concentration in the brain is similar to that of glucose, between 0.5 and 1.5 mM, and many studies indicate that it represents an important energy source for the brain instead of being only a metabolic dead-end (Schurr et al., 1999; Smith et al., 2003; Gallagher et al., 2009; Boumezbeur et al., 2010).

Both astrocytes and neurons are able to fully oxidize glucose and lactate (Zielke et al., 2009), however, as they are characterized by different expression patterns of genes involved in energy metabolism, under physiological condition they used different metabolic pathways, (Lovatt et al., 2007; Vilchez et al., 2007; Herrero-Mendez et al., 2009). Oxidative pathways are predominant in neurons, whereas glycolysis is mostly used in astrocytes. Neurons and astrocytes are thus characterized by complementary metabolic profiles, which indeed reflect their extensive metabolic cooperativity.

Metabolic profile of neurons

In the brain, neurons are the cells that require more energy and they sustain a high rate of oxidative metabolism compared to glial cells. It was shown that, not only neurons can use lactate as an energy substrate, but also that, when both substrates are present, neurons tend to use preferentially lactate over glucose (Magistretti and Allaman, 2015 and references therein).

These neuronal metabolic characteristics can be explained by different neuronal features:

1) neurons virtually lack the enzyme 6-phosphofructose-2-kinase/fructose-2,6-bisphosphatase-3 (Pfkfb3) that is constantly degraded by the proteasome, by contrast this enzyme is highly express and active in the astrocytes (Almeida et al., 2004; Herrero-Mendez et al., 2009), where it produces the fructose-2,6-bisphosphate (fructose-2,6-P2), a potent activator of the glycolytic enzyme phosphofructokinase-1 (PFK). Low level of fructose-2,6-P2 leads to a reduction in the rate of the glycolytic pathway in neurons as compared with the astrocytes.

2) In neurons, glucose is almost entirely processed by the oxidative way of the pentose phosphate that is responsible for the production of the neuronal NADPH, which is used to regenerate reduced glutathione, the principal molecular effector for scavenging reactive oxygen species (ROS) produced by the marked oxidative activity of neurons. Accordingly, the overexpression of Pfkfb3 in neurons causes oxidative stress and apoptosis (Herrero-Mendez et al., 2009), this suggest that neuronal cells cannot maintain a high glycolytic rate.

3) Neurons and astrocytes are characterized by cell-specific differential splicing of the enzyme pyruvate kinase (PK): the isoform PKM1 is exclusively expressed in neuronal cells, while the PKM2 isoform is present in astrocytes. PK is the key regulator of the glycolysis, it promotes the conversion of phosphoenolpyruvate to pyruvate. The PKM2 isoform is present in cells that sustain high rate of aerobic glycolysis (i.e. cancer cells) (Ward and Thompson, 2012), and it can increase the glycolytic flux in response to higher energy demands, whereas PKM1, the neuronal isoform, cannot.

Figure 6

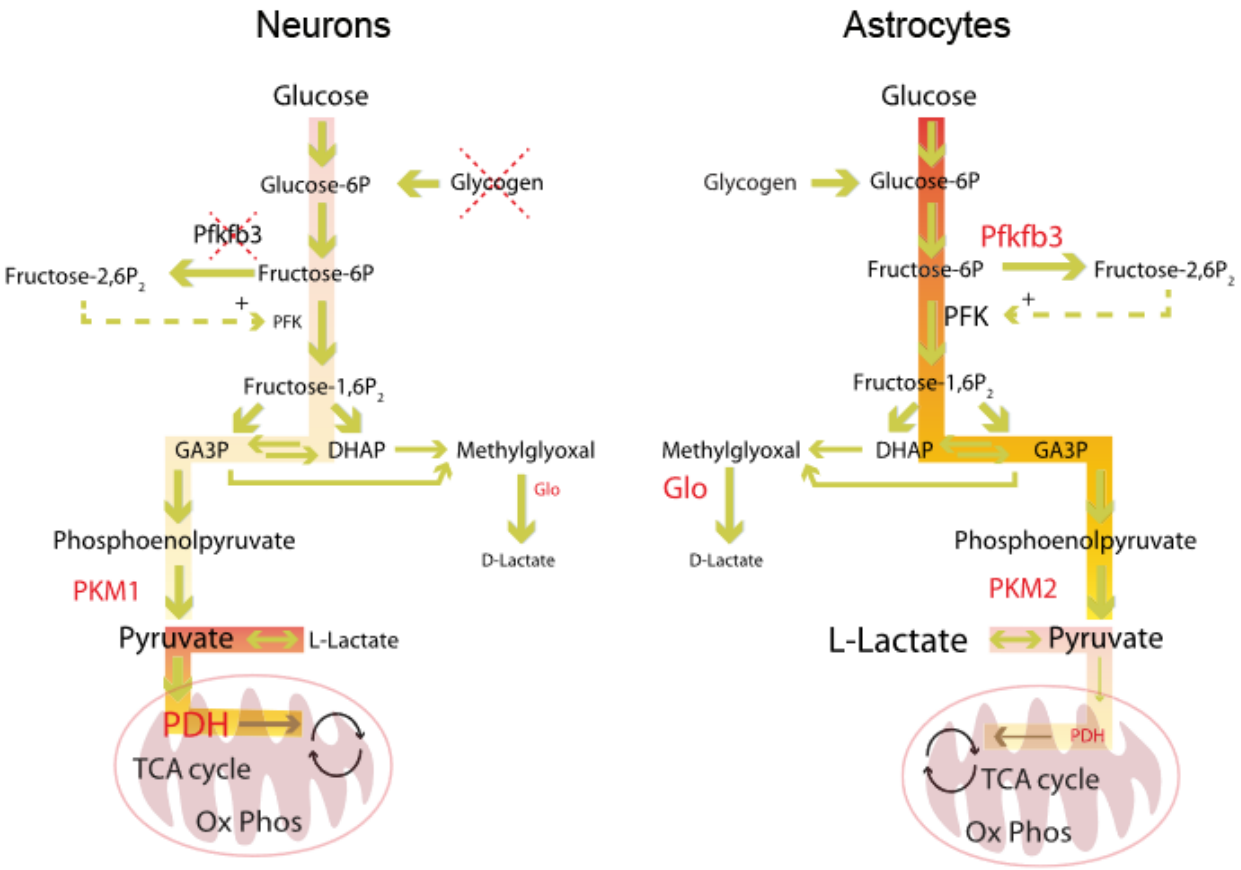

Figure 6. *Metabolic profiles of neurons and astrocytes (see text for the description of the respective metabolic pathways) (Modified from Magistretti and Allaman 2015).*

Metabolic profile of astrocytes

The metabolic profile of astrocytes is almost completely glycolytic is characterized by a low level of oxidative metabolism if compared with neurons (Itoh et al., 2003; Herrero-Mendez et al., 2009; Bittner et al., 2010). A number of different studies have shown that the glucose that enters into astrocytes is then released as lactate in the extracellular space (Pellerin and Magistretti, 1994; Itoh et al., 2003; Bouzier-Sore et al., 2006; Lovatt et al., 2007). This particular glycolytic metabolic nature of the astrocyte is again the product of the profile of gene expression involving different enzymes and transporters that act in a coordinate manner to generate the astrocytic phenotype.

1) The first aspect that characterizes the metabolic profile of the astrocytes is the high expression of Pfkfb3, which is able to activate PFK by fructose-2,6-P2 and in this way to assure a high glycolytic rate.

2) The second specific aspect is the low levels of expression of the aspartate/glutamate carrier (AGC) that is part of the malate aspartate shuttle that determines the relocation of reducing equivalents (i.e., NADH) from the cytosol to the mitochondria (Ramos et al., 2003; Berkich et al., 2007). Conversion of pyruvate (derived from glycolysis) to lactate in the cytosol ensures the maintenance of a high NAD+/NADH ratio, which, in turn is needed to maintain a high glycolytic rate.

3) The third aspect is that, pyruvate dehydrogenase, the key enzyme that regulates the entry of pyruvate in the TCA cycle is either expressed at very low level (Laughton et al., 2007), or efficiently inactivated through phosphorylation (Itoh et al., 2003; Halim et al., 2010).

4) PDK4 is the enzyme that phosphorylates pyruvate dehydrogenase and reduces its activity. PDK4 is highly expressed in astrocytes (its level of expression is more than 30-fold higher with respect to neurons). The functional consequence of this increased expression is that increases in the glycolytic flux in astrocytes will result in lactate production, as the entry of pyruvate into the TCA cycle cannot be upregulated.
All these circumstances may favor the conversion of pyruvate to lactate in astrocytes.
Finally, a strong indication that astrocytes are possibly the source of lactate for neurons comes from the observation that hippocampal and cortical astrocytes express the type 5 isoform of lactate dehydrogenase (LDH-5), which catalyzes the conversion of pyruvate into L-lactate. Although both neurons and astrocytes express LDH-1, which catalyzes the formation of pyruvate from L-lactate, neurons do not express LDH-5 (Cahn et al.,1962; Bittar et al., 1996). Thus, the differential expression of these enzymes strongly supports the idea that lactate is produced by astrocytes and shuttled to neurons, where it is then metabolized.

3.6 Astrocyte-Neuron Lactate Shuttle Hypothesis (ANLSH)

The interaction between neurons and glial cells is fundamental for the correct functioning of the brain and it is important for its energy metabolism. It is known that neurons are the most energy-demanding cells in the brain in terms of consumption while astrocytes consumes only 5% to 15% of the brain energy (Attwell and Laughlin, 2001; Magistretti, 2008). However, it was demonstrated that astrocytes internalization of energy substrates is very high when compared with their actual needs (Chuquet et al., 2010; Jakoby, et al., 2012). One explanation for this apparent paradox is given when considering the Astrocyte-Neuron Lactate Shuttle (ANLS) hypothesis that was originally proposed over two decades ago (Fig. 7) (Pellerin and Magistretti, 1994).

Figure 7

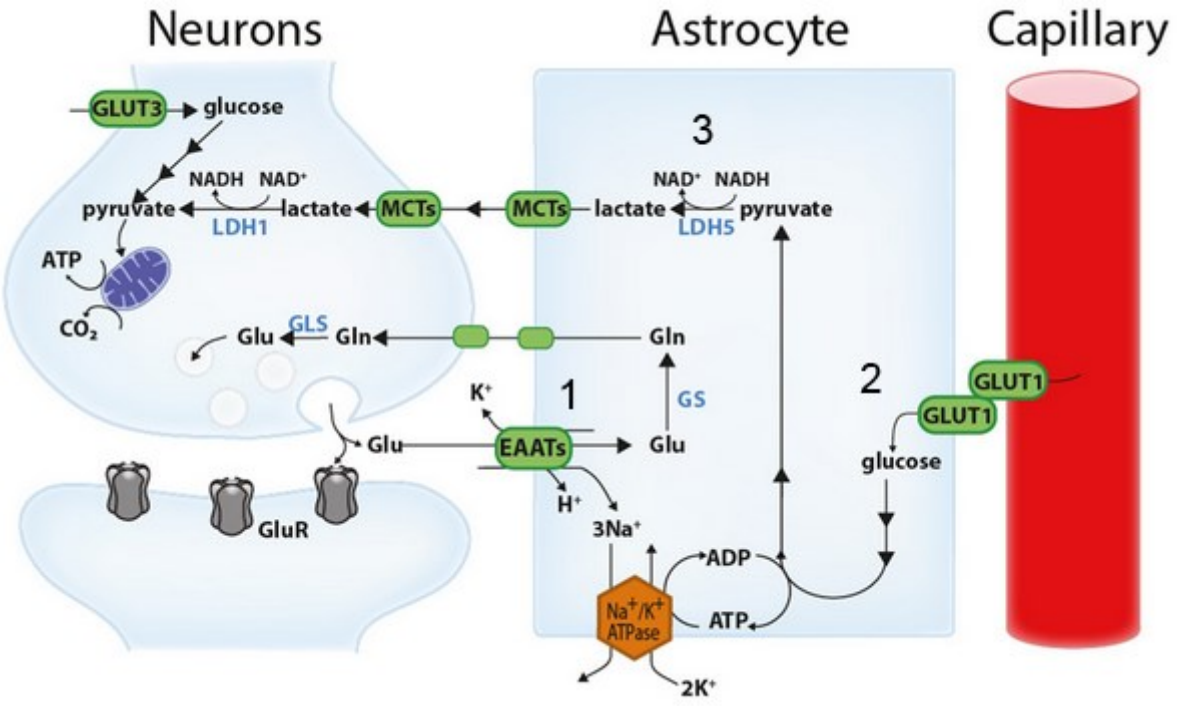

Figure 7. *Schematic representation of the astrocyte-neuron lactate shuttle (ANLS) (for a detailed description see text.)(Modified from Allaman et al., 2015).*

According to this hypothesis, i) neuronal activity leads to an increase of glutamate in the extracellular space that is rapidly taken-up by EAATs (or GLT-1) by a Na^+ dependent mechanism; ii) the consequent increase of intracellular Na^+ concentration in astrocytes

activates the Na^+/K^+ ATPase, ATP consumption (Magistretti and Chatton, 2005), glucose uptake, and astrocytic glycolytic pathway activation; iii) the result of this activation is the production of high level of lactate that is released in the extracellular space where; iv) lactate is taken-up by the neurons and it is used as energy source for oxidative ATP production (Pellerin et al., 2007; Magistretti, 2009).

While it is now established that lactate can be used as fuel to support neuronal activity, the relative contribution of this pathway in the support of this activity is still debated and this issue in central in all discussions about the ANLS hypothesis.

However, the validity of the model is supported by a number of evidences that complemented the initial discovery of astrocytic lactate release. Firstly, neurons express the LDH-1 subunit which is involved in the conversion of lactate to pyruvate suggesting that neurons are able to oxidize lactate. The LDH-1 subunit is also present in astrocytes where the LDH-5 subunit is expressed as well, favoring the formation of lactate from pyruvate (Bittar et al., 1996). Indeed, LDH-5 subunit expression is a characteristic of glycolytic, lactate-producing cells; a role that in the ANLSH model is attributed to astrocytes. Finally, the particular membrane expression of MCTs has also been considered as a further demonstration that astrocytes predominantly release lactate into the extracellular space while neurons are responsible for its uptake (Pellerin and Magistretti, 2003). Neurons express high levels of MCT2, that has the higher affinity for lactate (Debernardi et al., 2003), indicating that they are less prone to release lactate and more prone to retain oxidized lactate, whereas, astrocytes express MCT1 and MCT4. Astrocytes expressing MCT4 are, on the contrary, able to rapidly release lactate when the intracellular concentration rises (Broer et al., 1997).

However, it has to be noted that not all experimental evidences collected so far confirm the validity of the ANLSH model, thus the hypothesis of a lactate flow from astrocytes to neurons is not universally accepted (Hertz and Dienel, 2005). Evidences that do not support the ANLSH come from experiments in which MCT inhibitors were used to block lactate transport. Experiments in rodent optic nerve and hippocampal slices, have shown that lactate shuttling is important for neuronal survival only when the supply of energy substrate is restricted (Cater et al., 2001; Tekkok et al., 2005). On the other hand, it was shown that downregulation of MCTs with antisense nucleotides disrupts long-term memory formation in rats, indicating that lactate transport has a role in this physiological function (Suzuki et al., 2011).

Overall, a considerable body of evidence supports the notion of a net transfer of energy from astrocytes to neurons in the form of lactate as a result of glutamatergic transmission.

3.7 Mono-Carboxylate Transporters – localization and function

The entrance of lactate into the brain is mediated by specific carriers that are present in the membranes of the cellular components of the BBB and that belong to the family of the monocarboxylate transporters (MCTs). MCTs are able to transport not only lactate but also other monocarboxylic acids, such as pyruvate and ketone bodies. The family of the MCTs is formed by 14 transmembrane proteins, and altogether, they belong to the solute carrier family (SLC16). Lactate can cross the cell plasma membranes both with sodium-coupled transporters (SMCTs) or proton-coupled monocarboxylate transporters (MCTs). In the brain lactate transport is achieved through MCTs. Specifically, in the brain four carriers are expressed, that are able to catalyse bidirectional and electroneutral co-transport of protons and monocarboxylic acid. All the MCTs, from MCT1 to MCT4, are able to transport lactate, but with different affinities.

In rodent and human brain, MCT1 is the transporter isoform that is responsible for the transport of lactate across the BBB.

As briefly mentioned before, MCT2 is the transporter with the highest affinity for lactate (K_M: 0.7 mM), it is expressed in neurons, and more precisely it is inserted in the plasma membrane of the postsynaptic compartments of glutamatergic synapses, where its level of expression has been suggested to be regulated to provide increased supply of lactate as energy fuel during increased neuronal activity.

MCT3 has been detected at the basolateral membrane of the retinal pigment epithelium, where it regulates the pH and the lactate concentration.

The last carrier is MCT4 that is present in the plasma membrane of the astrocytes both in the lamellae that surround the synapses and in the end-feet (reviewed in Proia et al., 2016).

As mentioned before, the specific and different localization of the MCTs in neurons and astrocytes is suggestive of different aspects of lactate metabolism, possibly involving differences in the preferential direction of inter-cellular lactate transport. It has to be stressed, however, that the levels of expression of these transporters might change upon environmental stimuli. It has been shown, in fact, that oxygen- and glucose-deprivation induces an up-regulation of MCT4 expression in astrocytes.

3.8 Pharmacological control of glycogen biosynthesis and degradation

The most modern views of the synapse in the CNS, tend to consider this structure as a tripartite complex, with the pre- and post-synaptic neuron and the astrocytic processes. Neuronal activity induces energy-fluctuations in this microenvironment and in several circumstances, glycogen may represent a readily accessible energy source. The role of astrocytic glycogen as an energy supply for neurons can be studied and dissected by using pharmacological tools that enable to block glycogenolysis in astrocytes thus finally interfering with lactate supply to neurons. As shown before, the key enzyme for glycogenolysis is glycogen phosphorylase (GP), thus inhibitors of this enzyme will block glycogen degradation.

DAB,1,4-dideoxy-1,4-imino-D-arabinitol, was shown to be a useful inhibitor of GP in vitro on liver homogenates, thus potently inhibiting glycogen degradation with an IC50-value of 740 ± 9 nM (Andersen et al., 1999; Fosgerau et al., 2000; Latsis et al., 2002). A similar inhibitory effect was also observed in homogenates from brain and cultured astrocytes with an IC50-value of 400 nM. The concentration of the drug necessary for complete inhibition of glycogen breakdown in intact cells and tissues however was much higher (about 300 μM and up to 3 mM) (Suh et al., 2007) and before being effective, the drug needed a pre-incubation period to allow the molecule to cross cell membranes and to reach its intracellular targets.

DAB was also shown to have a secondary function in blocking on glycogen synthesis. In fact the inhibition of GP by DAB was accompanied by a decreased glycogen synthase activity in hepatocytes. However, the concentration of DAB required for half-maximal inhibition of glycogen synthesis was an order of magnitude higher than the IC_{50}-value for inhibition of GP (Latsis et al., 2002). Importantly, DAB does not interfere with glucose uptake nor with the activity of the enzymes involved in the glucose-6-phosphate pathway, i.e. hexokinase, phosphoglucoisomerase and glucose-6-phosphate dehydrogenase. Based on all these characteristics it was demonstrated that DAB could be safely used as a pharmacological tool to investigate the functional roles of glycogen degradation.

4. WHAT IS LEARNING AND WHAT IS MEMORY?

Experimentally in mice, short-, intermediate- and long-term memory are characterized by different training-testing intervals and it was shown that these types of memory are limited to temporal constraints that are specified by unique molecular profiles. Short-term memory occurs on a time-scale of minutes and is independent of new protein synthesis and gene transcription, relying only on post-translational modifications of pre-existing molecules. Intermediate-term memory occurs in a time span of several hours, its occurrence is dependent on new protein synthesis but not on new gene transcription while long-term memory relies on both new protein synthesis and transcription of genes, and is characterized by memory retention intervals longer than 24 hours (Taglialatela et al., 2009 and references therein).

In the last decades, numerous scientists have investigated to dissect the molecular and cellular mechanisms underlying memory formation and processing. In the last 30 years, investigations were mostly focused on the exclusive role of neuronal mechanism, even if, as we have seen before, the brain is composed not only by neurons but also by other, different cell types that, together with neurons and in tight association with them, cooperate to mediate all brain functions.

Recent studies however, took into account the role of these different cell types and in particular the role of astrocytes with their glycogen and glucose metabolisms. Their chemical and functional coupling to neuronal functions via lactate release in the ECS was specially investigated. Interestingly these studies demonstrated that this last aspect of neuron-astrocyte coupling is an essential mechanism for long-term memory formation.

4.1 Structural synaptic modifications occur during long–term potentiation and behavioural learning in the hippocampus

During the consolidation process, a memory that is initially temporary and labile, can become long-lasting. Memory consolidation is a pivotal event that depend on a number of molecular and cellular events that, when interrupted, might result in amnesia. From a molecular point of view, both long-term memory and long-term potentiation (LTP, the electrophysiological correlate of long-term memory), require de-novo gene expression and imply the activation of shared molecular pathways which include MAPK, CaMKIIα, PKA and PKC signalling cascades (Martin et al.,1997). Memory consolidation involves the activation

of different signalling cascades including the one involving the transcription factor CREB (cAMP response element binding protein) which has an evolutionary conserved role in memory formation (Alberini, 2009); the induction of the immediate early gene activity-regulated cytoskeletal protein (Arc/Arg3.1) and the activation of the pathway leading to actin filament severing mediated by the protein p21-activated kinase-cofilin, all functions are necessary for the regulation of anatomical changes at the synapse (Fischer et al., 2004; Chen et al., 2007; Bramham, 2008; Mantzur et al., 2009).

From the cellular point of view, upon learning, these molecular changes are accompanied by synapse structural modifications that can be transient or stable (Toni et al., 1999) and that can include new synapse formation, and/or synapse remodelling but also activation or potentiation of existing synapses (Bailey et al., 2015 and references therein).

Modifications/potentiation of pre-existing synapses is emerging as a relevant mechanism to support structural plasticity in both LTP and behavioural learning. Ultrastructural studies demonstrated that synaptic plasticity was accompanied by structural changes in both size and shape of dendritic spines, while functional investigations showed that increases in synaptic strength correlated with enlargements of the spine head (Caroni et al., 2012 and references therein). All these mechanisms could be linked to increased surface expression of receptors, and mobilization of intracellular resources as PSD proteins and other cytoskeletal elements. Among synaptic structural changes, activation of existing silent synapses (through the insertion or the migration of active AMPA receptors to the PSD) is of relevance (Kerchner and Nicoll, 2008 and references therein). This event takes place, on a large scale, in the hippocampus during postnatal development and it was suggested that several neurodevelopmental disabilities might originate from the inability to transform inactive synapses into active ones during brain development (Durand et al., 1996; Liao et al., 1999; Petralia et al., 1999). Conversion of silent synapses into functional ones may then be crucial for synaptic plasticity associated with LTP (Isaac et al., 1995; Liao et al., 1995) but also, importantly, for synaptic plasticity associated with behavioural learning (Geinisman, 2000). Taking into account all the evidences indicating that memory formation induced by behavioural learning and memory formation upon LTP share common molecular pathways, it is reasonable to suppose that the cellular mechanisms of memory formation following behavioural learning include the establishment of new synaptic connections and the remodelling of existing synapses. It is important to remember however that, as in LTP only those newly emerging spines that are contacted by axon terminals activated by the stimulation are subjected to potentiation (Toni et al., 1999), similarly the effects of

behavioural learning in promoting synaptogenesis and spinogenesis may be restricted to a subset of neurons and terminals, that are activated upon training, in pertinent brain areas. When looking at dendrites and spines, this may have a confounding effect as only a subset of neurons/dendrites would be potentiated and a population based analysis may fail to reveal this effect (Geinisman, 2000 and references therein).

4.2 Glycogen, lactate and astrocytic-neuronal interplay in plasticity and memory

Astrocytes actively participate in many complex brain functions, including cognitive ones (Haydon and Nedergaard, 2015). Non-neuronal contributions to learning and memory and synaptic plasticity have been increasingly investigated in the past 10 years and it was shown that long-term memory formation and neuronal plasticity need tight interaction between neuron and glia in terms of both signalling and transmission (Stehberg et al., 2012; Moraga Amaro et al., 2014). It was also suggested that astrocyte contribution to all architectural remodelling occurring upon synaptic plasticity is crucial in the spatial and temporal integration of neural activity and plasticity (Bourne and Harris, 2008; DePittà et al., 2016). Synaptic plasticity and memory formation are energetically demanding function, thus they are dependent on nutrient availability that is under the control of astrocytes. In this context, not only glucose entry into the brain and its subsequent metabolism are well studied aspects (Nedergaard et al., 2003; Halassa and Haydon, 2010), but also glycogen metabolism and the subsequent release of lactate and how these events are linked in long-term memory formation and plasticity are considered.

Indeed when neurons are engaged in high energy demanding tasks, such as during intense stimulation and frequent generation of excitatory postsynaptic potentials (i.e. during learning and memory tasks or LTP induction) but also when de novo transcription, translation and structural modification of synapses are needed to consolidate memories, the oxidation of the sole glucose present in the neuron itself may not be sufficient, thus additional sources of energy are required. Astrocytes, and the glycogen in their cytoplasm that, as we mentioned before, represents the main energy reserve for the brain, supply neurons with the energy needed.

A growing numbers of studies now indicate that when activity-dependent changes occur, thus requiring an elevated energy consumption and energy inputs from astrocytes, (i.e during long-term memory formation and consolidation in different brain areas),

glycogenolysis and glycolysis followed by lactate production by astrocytes and its release into the ECS are necessary for all the molecular and cellular modifications involved in memory consolidation, to occur.

The first evidence about the relevance of neuron-astrocyte cross-talk mediated by lactate in the formation of learning memory formation come from experiments in young chicks (Gibbs et al., 2006); and was then confirmed by further experiments in rats, where, besides pharmacological interference with glycogenolisis and lactate release during memory tasks, the effects of neuronal and astroglial lactate transporters downregulation were also examined. In this work, it was shown that synaptic plasticity and long-term memory formation were dependent on the presence of lactate, but that these events were also critically dependent on the capability of the astrocytes to transfer lactate into the extracellular space and of the neurons to internalize it from this same compartment, through the expression of the specific lactate transporters. Interestingly, in trained rats, inhibition of lactate release from astrocytes completely blocked the activation of CREB and cofilin pathways as well as the induction of Arc (Suzuki et al., 2011). That lactate controls the molecular events that are required for memory consolidation in neurons is further demonstrated by the administration of L-lactate to primary neuronal cortical cultures, or lactate injection into the mouse sensory-motor cortex. In both experimental configurations lactate induces the expression of Arc, c-Fos and Zif268. The authors of this work demonstrated also that these changes were mediated by the activation of the N-methyl-D-aspartate (NMDA) glutamate receptor, and the involvement of the extracellular-signal-regulated kinase 1/2 (ERK1/2) pathway, indicating that the de-novo expression of these immediate early genes is activity-dependent (Yang et al., 2014).

Different memory circuits are affected by breaking the the astrocyte–neuron lactate transfer system, as it was recently demonstrated that its integrity is also crucial in the retrieval of addictive drug memories; DAB injection into basolateral amigdala in rat brains was able to persistently reduce conditioned responses to cocaine (Boury-Jamot et al., 2016).

Altogether these data indicate that the metabolic coupling of neurons with astrocytes mediated by lactate is needed to supply the energy that is necessary to all neuronal functions that are related to training, learning and memory consolidation, differently all survival or homeostatic neuronal process seem to be independent from this supplemental energy supply, thus lactate may actually play a specific and distinct role in neuronal functions.

4.3 Lactate as a signaling molecule in brain plasticity

A number of data derived from cell culture experiments, where application of lactate was associated with increased intracellular levels of NADH, that alone induces similar effects as lactate on NMDAR signalling, suggested additional regulatory mechanisms for lactate (Yang et al., 2014). In the mitochondria, lactate is oxidized to pyruvate while regenerating NADH, this conversion affects the redox state of mitochondria and ultimately of cells. Changes in the redox balance have been proposed to represent a signalling mechanism by themselves (Brooks, 2009). According to this view, lactate transport may serve as a signalling mechanism in itself or again it may trigger a further signalling pathway that involves the production of reactive oxygen species (ROS). In fact, even if excess of ROS production is toxic for all cell types, physiological levels of these molecular species are needed for promoting synaptic plasticity (Massaad and Klann, 2011). Thus, coordinated action of all these lactate-mediated events may be necessary for the multiple molecular and cellular effects that result learning and in the formation of long-term memory.

AIMS OF THE WORK

In the last thirty years, several studies have demonstrated that the astrocytes play an active role in the control of several brain functions, including the cognitive ones: learning and memory. Recent studies have shown that blocking glycogenolysis or the transport of lactate between astrocytes and neurons, in different animal models and brain areas impairs long-term memory formation. Lactate administration rescues amnesia suggesting that metabolic coupling between astrocytes and neurons via lactate is required for long-term memory formation. This project aims to investigate the effects of the pharmacological inhibition of glycogen degradation and lactate production (thus impairing the astrocyte-neuron metabolic coupling) on the anatomy of mice hippocampal excitatory synapses that are involved in learning and memory-related process.

The first task of this project was to characterize the behavioural phenotype of C57Bl/6N adult mice bilaterally intra-hippocampal injected with 1,4-dideoxy-1,4-imino-D-arabinitol (DAB), an inhibitor of glycogen phosphorylase, in order to pinpoint behavioural memory defects (as already observed in chicks and rats). We studied intermediate- and long-term memory formation using two different behavioural memory tests: the passive avoidance (PA) and the novel object recognition (NOR). We evaluated the memory impairment associated with DAB treatment and if and how the effect of the drug was persistent in time.

Following behavioural phenotyping, the same animals were used to achieve the second task, namely to carefully characterize the architecture of neuronal connectivity in the hippocampal CA1 region, more precisely in the apical dendrites layer of this area.

We first verified that our pharmacological treatment was not toxic for astrocytes, as inflammation and astrogliosis might have had undesired and confounding effects on the parameters that we wanted to evaluate. Then, with the Golgi-Cox staining, we evaluated whether DAB administration had any effects on dendritic spine density and with serial-block face scanning electron microscopy analyses, we focused our attention on the 3D architecture of dendritic spine and synaptic and dendritic mitochondria. In particular, we measured the spine head and the PSD volume as well as the mitochondria volume, number and shape. Furthermore, we performed ultrastructural analysis on 2D TEM images to characterize the hippocampal excitatory synapses features, measuring the surface of the pre-synaptic terminal, the synaptic vesicle density and the PSD length and thickness. We

also performed a detailed analysis of mitochondrial ultrastructure, by the investigation of the number of the cristae and the dendritic or synaptic area occupied by these organelles.

Finally, as a third objective, we performed a series of experiments to evaluate the effect of L-lactate hippocampal injection in the rescue of both anatomical and behavioural phenotypes in mice treated with DAB. In this case we decided to use as behavioural test the NOR, to see whether the co-injection of DAB and L-lactate was able to rescue the phenotype.

From all our data we can conclude that the block of the glycogenolysis in mice hippocampus leads to an impairment of memory formation accompanied by dramatic effects on dendritic spine density, dendritic mitochondria morphology and synaptic vesicle density. Through the simultaneous administration of DAB and L-lactate, we were able to rescue the behavioural and the post-synaptic effects on spines and dendrites phenotype, but not the pre-synaptic ones.

MATERIALS AND METHODS

1. ANIMALS

Male C57Bl/6N mice (3 month old) were housed individually in polycarbonate cages with food and water freely available through wire lids. Cob-bedding were changed weekly, and the vivarium was 21°C with a 12 hours light cycle (lights on at 08:00). All the experimental procedures followed the guidelines established by the Italian Council on Animal Care and will be approved by the Italian Government decree. All efforts were made to minimize the number of subjects used and their suffering.

2. INTRAHIPPOCAMPAL INJECTION PROCEDURE

2.1 Surgeries

Mice were anesthetized with intraperitoneal injection of chloral hydrate (450 mg/kg in a volume of 0.1 ml/10 g) and placed in a stereotaxic apparatus. The skin was incised and the skull was cleaned. One 22-gauge guide cannula (2biological instruments S.N.C., Besozzo, VA, Italy) was placed 1 mm above the intended site of injection according to the atlas of Paxinos and Franklin (2001). Stereotaxic coordinates for the CA1 region of the dorsal hippocampus were anteroposterior: −2 mm from bregma, medio-lateral: −1.9 from the sagittal suture and dorso-ventral: −1.9 mm from the skull surface. The cannula was secured to anchor jewellers' screws with dental acrylic. A stainless steel stylet was inserted into the guide cannula to keep it free of debris. All animals were allowed 1 week to recover from surgery and to clear anaesthetic.

2.2 Drug injection

For drug injection, the animals were gently restrained by hand; the stylet was removed from the guide cannula and replaced by injection needle (0.5 mm below the tip of the guide cannula). The injection solutions were administered in a total volume of 0.5 µl/mouse/side over a 60 seconds period through an infusion pump (KDS Model 100 KD Scientific Inc., Hill Road Holliston, MA, USA). The injection needle was left in place for an additional 60 seconds to facilitate the diffusion of the drugs. To verify the appropriateness of the coordinates of stereotactic injection site and procedure, 4 animals were injected with

0.5 µl of 0.4% Evans blue solution (E2129 Sigma-Aldrich®, St. Louis, MO, USA). One hour after injection, the animals were sacrificed and the brain dissected, sectioned at the level of the dorsal hippocampus and directly imaged under a stereomicroscope (M205 FA Stereo Microscope Leica Microsystem, Wetzlar, Germany).

2.3 Treatments

Mice were treated with the inhibitor of glycogen phosphorylase, 1,4-dideoxy-1,4-imino-D-arabinitol (DAB, D1542 Sigma-Aldrich® St. Louis, MO, USA), L-Lactate (L7022 Sigma-Aldrich® St. Louis, MO, USA) or vehicle (artificial cerebrospinal fluid). Injections into the hippocampus were made 15 minutes before the beginning of the tasks. When DAB was given in combination with L-Lactate, one solution was prepared. The volume was 0.5 µl/mouse/side. All the drugs were dissolved in artificial cerebrospinal fluid prepared fresh (124 mM NaCl, 2.5 mM KCl, 2.0 mM $MgSO_4$, 1.25 mM KH_2PO_4, 26 mM $NaHCO_3$, 10 mM glucose, 4 mM sucrose, 2.5 mM $CaCl_2$).

We injected bilaterally 0.5 µl/side of DAB (1000, 2000, 4000 and 8000 µM; 500, 1000, 2000 and 4000 pmol respectively), 0.5 µl/side of vehicle (artificial cerebrospinal fluid) or 0.5 µl/side of L-lactate 100 nmol.

3. BEHAVIORAL TESTS ON C57Bl/6N ADULT MICE

3.1 Spontaneous motor activity

Spontaneous motor activity was evaluated using an automated activity cage (Ugo Basile, Varese, Italy) placed in a sound-attenuating room as described in Ferri et al. (2004). Each system consists of an animal cage (43×43×32 cm) containing 16 photocells 3 cm above the floor under transparent cover, an electronic unit incorporating a counter and a printer. The rectangular animal cage has transparent sides and lid to allow for observations. The cage floor has horizontal and vertical infrared sensors. The counter sums up the photocell disruptions, and a printer displays the results at pre-set intervals. On the day of the test, each mouse was habituated to the room for 60 minutes in the home cage and then in the activity cage for 30 minutes. Cumulative horizontal and vertical beam breaks, every 5 minutes interval period, during 30 minutes observation period were counted. Results were

statistically analyzed with the software GraphPad Prism® 6.0c version, with One-way Analysis of Variance (ANOVA) corrected with Tuckey multiple comparison procedure. Means were considered statistically different when $P < 0.05$.

3.2 Visual cliff

Visual acuity was tested in the visual cliff paradigm according to Van't Veer et al. (2013). The apparatus consisted of a platform with a checkered pattern positioned 1 m above the ground. A clear piece of Plexiglas was placed on the platform and extended 0.5 m beyond the platform edge. A checkered pattern was also placed on the floor below the extending Plexiglas, creating the illusion of a sudden drop-off. At the interface between the shallow side and the deep side, there was a ridge of aluminium (1 cm). Each mouse was placed on the aluminium ridge and was allowed to step off to either side. Choices were manually recorded as safe if the mouse stepped towards the platform side (good visual acuity) and as unsafe if the mouse chose the overhang side (poor visual acuity). Each mouse was tested in 10 consecutive trials.

3.3 Passive Avoidance training

Passive (or inhibitory) avoidance test was carried out as previously described (Braida et al., 2004). The test chamber consists of a rectangular-shaped Perspex box, divided into a safe compartment and a shock compartment. The safe compartment is white and illuminated by a light on the cage lid. The shock compartment is dark and blackened. Foot shocks are delivered through the grid floor of the dark chamber via a constant current scrambler circuit. The two compartments are separated by an automatically operated sliding door. During the training session, each mouse is placed in the safe compartment with its head facing away from the door. After 1 second, the door automatically opens, allowing the mouse to move into the preferred, dark chamber. The door is closed 1 second after the mouse enters the shock chamber, and a brief foot shock (1 mA for 1 second) is administered to the animal. Latency to enter the shock compartment was taken as a measure of acquisition (Acq). The mouse is then returned to its home cage and tested for retention 24 hours later. Retention test is performed by placing the mouse back into the safe compartment and measuring its latency to enter the shock compartment. The latency to re-

enter the black compartment is recorded (Test). An increased retention latency indicates that the animal has learned the association between the shock and the dark compartment. A cut-off of 300 seconds is employed. Training and testing procedures are performed blind to treatments. Results were statistically analyzed with the software GraphPad Prism® 6.0c version, with One-way Analysis of Variance (ANOVA) corrected with Tuckey multiple comparison procedure. Means were considered statistically different when $P < 0.05$.

3.4 Novel Object Recognition Test

Object recognition was conducted in an open plastic arena (38 cm × 30 cm × 18 cm). The apparatus is illuminated by a fluorescent lamp placed centrally above it (75 W). The animals were first habituated to the test apparatus for 10 min on Day 1 and then subjected to the familiarization trial (T1) and to a novel object recognition trial (T2). In order to study the DAB effect on short and long-term memory the time course of the DAB starting from 120 minutes of delay until 72 hours of delay was investigated. A further experiment was done consisting of delivering a retraining 5 days after the last delay (72 hours) and testing 24 hours after animals differently pre-treated.

The total time spent exploring the two objects during T1 and T2 trial was taken as a measure of object exploration. To avoid the interference of olfactory cues, the sawdust was stirred and the objects were cleaned with 70% ethanol after each tested animal (Braida et al., 2013). The performance was evaluated by calculating a discrimination index (N−F/N+F), where N=time spent exploring the new object (T2novel) during T2, F=time spent exploring the familiar object (T2familiar) during T2. Results were statistically analyzed with the software GraphPad Prism® 6.0c version, with One-way Analysis of Variance (ANOVA) corrected with Tuckey multiple comparison procedure. Means were considered statistically different when $P < 0.05$.

4. HISTOLOGICAL ANALYSES

4.1 Adult mouse brain fixation, paraffin embedding and sectioning

Cannula placements were examined after behavioural testing to ensure correct placement. Mice were anaesthetized by intraperitoneal injection of chloral hydrate (450 mg/kg in a volume of 0.1 ml/10 g) and transcardially perfused with 2% paraformaldehyde (19200, Electron Microscopy Sciences Hatfield, PA, USA) in PBS 1x (137 mM NaCl, 2.7 mM KCl, 10 mM Na_2HPO_4, 2 mM KH_2PO_4) pH 7.4. Dissected brains were further fixed in Bouin's fixative (Sigma-Aldrich®, St. Louis, MO, USA) for 18-30 hours and then cleared and conserved in 70% (vol/vol) ethanol. Four transverse sections of each brain were obtained with an adult mouse brain matrix and processed together. Samples were processed using an automated tissue processor (ASP300, Leica Microsystem, Wetzlar, Germany) and paraffin embedded. Briefly, samples were rinsed in bi-distilled water for 30 minutes, then were gradually dehydrated through an ethanol (02860, Sigma-Aldrich®, St. Louis, MO, USA) series (50%, 70%, 90%, 100%) and xylene (95672, Sigma-Aldrich®, St. Louis, MO, USA) at room temperature (RT) and finally embedded in paraffin (327212 Sigma-Aldrich®, St. Louis, MO, USA) at 62°C. Blocks were cut in 8-15 μm sections with a microtome (RM 2255 Leica Biosystems, Nussloch GmbH, Germany).

4.2 Haematoxylin and eosin staining

Sections were stained with haematoxylin and eosin (Diapath S.p.A., Martinengo, BG, Italy) and studied under a light microscope (Leica DM750, Leica Microsystem, Wetzlar, Germany). The sections were deparaffinised in xylene and rehydrated, at room temperature, through a decreasing ethanol series (100%, 95%, and 70%) and rinsed in bi-distilled water. The staining consisted in the incubation of sections in haematoxylin for 3 minutes, in the rinsing in running water for 5 minutes and then in the counter-staining with eosin for 3 minutes. Sections were subsequently dehydrated with an increasing ethanol series (95% and 100%) and xylene and mounted with Micromount mounting medium (060200, Diapath S.p.A, Martinengo (BG), Italy).

Histological sections were visualized with an optical microscope (DM 2500, Leica Microsystem, Wetzlar, Germany) and acquired with a digital camera (DFC310FX, Leica Microsystem, Wetzlar, Germany) associated with the Leica Image Manager Software.

5. GOLGI-COX STAINING

After the behavioural tests, mice (at least 3 for each group) were anesthetized by intraperitoneal injection of chloral hydrate (450 mg/kg in a volume of 0.1 ml/10 g) and transcardially perfused with 15 ml of saline solution (0.9% NaCl). After perfusion, dissected brains were quickly immersed in Golgi-Cox solution (potassium dichromate 1%, mercuric chloride 1%, and potassium chromate 0.8%) (AnalaR B.D.H. Milan, Italy) and stored at room temperature for at least 6 days in the dark. After this period of impregnation, brains were washed in water several times to remove the excess Golgi-Cox solution and incubated in a 30% sucrose (Sigma-Aldrich®, St. Louis, MO, USA) solution for at least 2 days in the dark at 4°C. 100 μm coronal sections were obtained with a vibratome (Leica VT1000S) and were mounted on gelatin coated glass slides (2% gelatine, 1% $KCr(SO_4)_2$ 12 H_2O). After 24 hours, brain slices were treated in the dark as follows: slices were washed twice with water and incubated for 30 minutes in ammonium hydroxide (05002 Sigma-Aldrich®, St. Louis, MO, USA) at RT. Rinsed slides were fixed for 30 minutes in Kodak fix solution (P8307 Sigma-Aldrich®, St. Louis, MO, USA). Subsequently slices were dehydrated with an ethanol series (50%, 70%, 95% and 100%) for 5 minutes each, then a solution composed by 1/3 chloroform, 1/3 xylene and 1/3 ethanol for 15 minutes, and xylene (185566 Sigma-Aldrich®, St. Louis, MO, USA) for 15 minutes. Sections were subsequently mounted with a coverslip using Micromount mounting medium.

5.1 Images acquisition and quantitative analysis

Stained neurons from the CA1 region of hippocampus were acquired using an Axiovert 200M (Carl Zeiss, Oberkochen, Germany) spinning-disc confocal system (PerkinElmer Life Sciences Waltham, Massachusetts, USA). Stacks were collected every 0.5 μm with a 20x, 40x (oil) and 63x (oil) objective. Ten pyramidal neurons from the dorso-ventral hippocampal CA1 (*stratum radiatum*) were studied from 3 animals for each group (20 dendritic shafts and at least 1300 μm of dendrites per group were analysed). Pyramidal

neurons from the *stratum radiatum* of hippocampal CA1 were studied because in this region, the CA3-proceeding Schaffer collaterals synapse with dendritic spines from the dendritic arbor of pyramidal cells, mostly in the *stratum radiatum*. The spine density of the proximal apical dendrite area was analysed (minimum 100 μm from soma), the second- or third order of dendrite (protruding from its parent apical dendrite) was chosen for spine density quantification. Z-stacks were made from each dendrite in the whole of the analysed segment. To determine the spine density, ImageJ1.47v software (National Institute of Health, Bethesda, USA) was used. Results were statistically analyzed with the software GraphPad Prism® 5 version, with One-way Analysis of Variance (ANOVA) corrected with Tuckey multiple comparison procedure. Means were considered statistically different when $P < 0.05$.

6. GFAP IMMUNOFLUORESCENCE STAINING OF CORONAL BRAIN CRYOSTAT SECTIONS

24 hours after intra-hippocampal injection of vehicle and 1000 pmol DAB, mice were anesthetized by intraperitoneal injection of chloral hydrate (450 mg/kg in a volume of 0.1 ml/10 g) and transcardially perfused with 5% sucrose in PBS 1x followed by 4% paraformaldehyde in PBS 1x . After perfusion, dissected brains were quickly immersed in 4% paraformaldehyde, 4% sucrose in PBS 1x and stored at 4°C for 1 hour. After this period, brains were washed in PBS 1x and incubated in a 30% sucrose solution for 12 hours at 4°C. 24 hours later, brains were embedded in Optimal Cutting Temperature (OCT, Tissue-tek®, Sakura Finetek Europe B.V. KvK, Leiden, The Netherlands) and snap-frozen in liquid nitrogen. The frozen samples were cut with a cryostat (Reichert-Jung 2700-frigocut, Buffalo, NY, USA) in coronal sections with a thickness of 20 μm, collected on a glass slide and covered with PBS 1x. Sections were washed with PBS 1x for 15 minutes at RT and incubated at RT for 30 minutes in blocking solution: 3% Bovine Serum Albumin (BSA, A7906 Sigma-Aldrich®, St. Louis, MO, USA), 10% normal goat serum (Diapath S.p.A, Martinengo (BG), Italy) to reduce non-specific background staining, and 0.4% Triton™ X-100 (T8787, Sigma-Aldrich®, St. Louis, MO, USA)) in PBS 1x for 30 minutes. Sections were incubated at 4°C for 12 hours with the primary antibody: rabbit polyclonal anti-GFAP (glial fibrillary acidic protein, an astrocytes marker) 1:500 (Z0334, Dako, Glostrup, Denmark) in blocking solution. After rinsing with PBS 1x, sections were incubated at RT for 1 hour

with the secondary antibody: AlexaFluor® 488 F(ab')2 Fragment of Goat Anti-Rabbit IgG (H+L) 1:200 (A11070, Molecular Probes®, Life Technologies Europe BV, Monza (MB), Italy) in blocking solution. After rinsing with PBS 1x, stained sections were mounted in 9:1 glycerol and PBS 1x and stored at 4°C in the dark. Negative control was prepared by replacing the primary antibody solution with blocking solution.

6.1 Images acquisition

The immunofluorescence stained sections were acquired at the confocal microscope LSM 510 Meta confocal microscope (Carl Zeiss) with a 20x objective, 8-bit gray-scale, opened pinhole: 1 airy units, 4 lines averaging, scan speed 600 Hz, format: 1632 x 1632). We acquired 2 fields of apical dendrites of the CA1 region of the hippocampus (pixel size: 280 nm). To excite AlexaFluor® 488 we used the laser line with a wavelength of 488 nm and we collected the light emitted setting the photomultiplier (PMT) bandpass between 505 and 570 nm.

High magnification of astrocytes were acquired with the confocal microscope LSM 510 Meta confocal microscope (Carl Zeiss) with 63x oil-immersion objective. We used the laser line at 488 nm to excite AlexaFluor® 488 and we detected the wavelengths emitted between 505 nm and 570 nm. For each sample we acquired z-stacks containing the entire depth of the astrocytic cell with z-step size of 0.3 µm. For each animal, we collected 5-10 fields of 142.8 µm x 142.8 µm (pixel size: 90 nm, format 1632 x 1632).

6.2 Evaluation of reactive astrogliosis in the hippocampal CA1 region in mice treated with vehicle and 1000 pmol DAB

The fluorescence images collected were analyzed with the software ImageJ64. In each sample, we measured the ratio between the mean fluorescence intensity signal (in arbitrary units a.u.) in the CA1 region and the area of the same field (μm^2) for GFAP staining. To quantitatively evaluate the inflammatory infiltrate in the CA1 hippocampal region we measured the ratio between the surface occupied by the fluorescence signal and the total area under investigation and the percentage of the total fluorescent signal in the same area. The identification of GFAP positive cells was obtained first, through the generation of a binary mask for each fluorescence image using the Image > Adjust > Threshold function of

ImageJ in order to specifically isolate the signal associated to the inflammatory cells from the background and then using the function Process > Binary > Make Binary to produce a binary mask where fluorescent cells result black in a white background. With the function Analyze > Measure function we obtained the measure of the area occupied by the inflammatory cells and the mean fluorescence intensity associated.
Results were statistically analyzed with the software GraphPad Prism® 5 version, with unpaired Student t-test. Means were considered statistically different when $P < 0.05$.

7. TRANSMISSION ELECTRON MICROSCOPY

After the behavioural tests, mice (at least 3 for each group) were anaesthetized by intraperitoneal injection of chloral hydrate (450 mg/kg in a volume of 0.1 ml/10 g) and transcardially perfused with 2.5% glutaraldehyde (16220, Electron Microscopy Sciences Hatfield, PA, USA), 2% paraformaldehyde in 0.15 M sodium cacodylate buffer (12300, Electron Microscopy Sciences Hatfield, PA, USA). Coronal sections (100 µm thickness) where obtained with a vibratome (Leica VT1000S) and further fixed in the same fixative solution for 48 hours at 4°C. Subsequently, under a stereomicroscope, the CA1 region of hippocampus was manually dissected in small pieces of 1 mm x 1 mm and samples were rinsed 3 times for 10 minutes with sodium cacodylate buffer 0.1 M, post-fixed in 2% osmium tetroxide (19150, Electron Microscopy Sciences Hatfield, PA, USA) in 0.1 M cacodylate buffer for 1 hour. After multiple rinses with 0.1 M cacodylate buffer and bi-distilled water, samples were counter-stained with a saturated solution of uranyl acetate (73943, Sigma-Aldrich®, St. Louis, MO, USA) in 20% ethanol for 45 minutes in the dark. After rinsing with 20% ethanol, samples were gradually dehydrated with an ethanol series (70%, 80%, 90%, 100%) and propylene-oxide (110205, Sigma-Aldrich®, St. Louis, MO, USA). Meanwhile, Epon-Spurr resin was prepared mixing Epon and Spurr resins 1:1. Epon (18010, Eponate 12 kit (DMP30 catalyst), TED PELLA Inc., Redding, CA, USA) was prepared mixing properly dodecenylsuccinic anhydride (DDSA), methyl nadic anhydride (MNA), Epon 812 and Epon Accelerator DMP30, while Spurr (18300-4221, Low Viscosity "Spurr" Kit, TED PELLA Inc., Redding, CA, USA) component was prepared mixing vinylcyclohexene dioxide (VCD), diglycidyl ether of polypropylene glycol (DER), nonenyl succinic anhydride (NSA) and dimethylaminoethanol (DMAE) according to manufacturer specifications. Samples were gradually infiltrated first with a mixture of Epon-Spurr and propylene-oxide 1:3 for 12 hours,

then with Epon-Spurr and propylene-oxide 1:1 for 3 hours, 3 hours Epon-Spurr and propylene-oxide 3:1 and put in pure resin before polymerization at 60°C for 48 hours.

7.1 Ultra-thin sections preparation and samples observation at the transmission electron microscope

Resin embedded samples were cut with the ultramicrotome (Leica EM UC6, Leica Microsystem, Wetzlar, Germany) in semi-thin sections of 0.5 µm thickness with a glass knife, stained with 0.1% toluidine blue (22050, Electron Microscopy Sciences Hatfield, PA, USA) and 0.1% methylene blue (18600, Electron Microscopy Sciences Hatfield, PA, USA) in 0.1 M sodium phosphate buffer and observed at the optical microscope (Leica DM2500, Leica Microsystem, Wetzlar, Germany) to identify the region of the sample to investigate at the ultrastructural level. In particular, we studied the apical dendrites of the CA1 pyramidal hippocampal neurons. Ultra-thin sections of 70 nm were cut with a diamond knife (Ultra 45°, DiATOME, 2501 Biel, Switzerland) and collected on copper grids (G300-Cu, Electron Microscopy Sciences Hatfield, PA, USA) and counter-stained with uranyl acetate solution for 20 minutes and 1% lead citrate (17800, Electron Microscopy Sciences Hatfield, PA, USA) for 7 minutes. Samples were observed at the transmission electron microscope (TEM) (Philips CM10, 5656 AE, Eindhoven, The Netherlands) at 80 kV and images were acquired with a digital camera (Morada, Olympus, Münster, Germany).

7.2 Ultrastructural analyses of excitatory hippocampal synapses and dendrites

We performed qualitative ultrastructural analyses of pre and post-synaptic excitatory terminal, dendritic, and synaptic mitochondria in search of ultrastructural alterations in mice treated with DAB respect to vehicle. We performed the quantitative ultrastructural analyses of excitatory synapses and dendrites in the CA1 region of the hippocampus. We measured, on electron micrographs acquired at 25000x and 34000x (format 3708 x 2627 pixels, pixel size: 1.45 nm and 1.03 nm, respectively), synaptic boutons surface, synaptic vesicle density (Cappello et al., 2012), PSD length and thickness (Folci et al., 2016) of about 80 synapses and PSD in each animal group. The analyses of dendritic and synaptic mitochondria were

performed on TEM images at 10500x and 13500x (images format 3708 x 2627 pixels, pixel size: 3.5 nm and 2.9 nm, respectively). We measured the surface of the mitochondria and the number of the mitochondrial cristae in order to calculate the density of the cristae as the ratio between the number of the cristae and the mitochondria surface, in about 100 synaptic and dendritic mitochondria. Quantitative measurements were performed with ImageJ 1.47v, and results were statistically analysed with the software GraphPad Prism® 5 version, with One-way Analysis of Variance (ANOVA), corrected with Tuckey post-test or by Kruskal-Wallis test and corrected with Dunn's multiple comparison procedure. Mean were considered statistically different when $P < 0.05$.

8. SERIAL BLOCK FACE SCANNING ELECTRON MICROSCOPY (SBFSEM)

Coronal sections (100 µm thickness) were obtained with a vibratome (Leica VT1000S) and hippocampi were manually dissected from these sections. After washing with cold cacodylate buffer 0.1 M, samples were fixed in a reduced osmium solution containing 3% potassium ferrocyanide (P3289 Sigma-Aldrich®, St. Louis, MO, USA) in 0.3 M cacodylate buffer combined with an equal volume of 4% aqueous osmium tetroxide, for 1 hour, on ice. At the end of the first heavy metal incubation, the tissues were washed with bi-distilled water at RT and then were placed in the 0.22 µm-Millipore-filtered 1% thiocarbohydrazide (88535 Sigma-Aldrich®, St. Louis, MO, USA) in bi-distilled water solution for 20 minutes, at RT. Tissues were then rinsed again in bi-distilled water and incubated in 2% osmium tetroxide in bi-distilled water for 30 minutes, at RT. After several washed at RT in bi-distilled water they are then placed in 1% uranyl acetate (aqueous), and left overnight at 4°C. Samples were washed, and were than immersed *en- bloc* in Walton's lead aspartate solution (0.066 g lead nitrate dissolved in 10 ml of 0.003 M aspartic acid solution, pH 5.5) (228621 and A9256 Sigma-Aldrich®, St. Louis, MO, USA) at 60°C for 30 minutes. The tissues were washed, and dehydrated using ice-cold solutions of freshly prepared ethanol series, then placed in anhydrous ice-cold acetone (650501 Sigma-Aldrich®, St. Louis, MO, USA) for 10 minutes and embedded in Durcupan resin (44610-1EA Sigma-Aldrich®, St. Louis, MO, USA) cured at 60°C for 48 hours. Resin blocs were mounted on aluminium specimen pins (10-006002-10 Micro to Nano, Wateringweg, Netherlands) using cyan acrylic glue and trimmed with a glass knife to a rectangle ~0.5 x ~0.75 mm with the tissue exposed

on all four sides. Silver paint (16062 – PELCO® Conductive Silver Pain, TedPella, Redding, CA, USA) was used to electrically ground the edges of the tissue block to the aluminium pin. The entire specimen was then sputter coated with a thin (25 nm) layer of gold (High Resolution Cressington Sputter Coater 208 HR sputter coater, TedPella Inc., Redding, CA, USA).

8.1 Data visualization and measurements

Serial block-face images are collected using a Gatan 3View system (Gatan, Pleasanton, CA) mounted in an FEI Quanta FEG 200 SEM operating at an accelerating voltage of 3 kV with a vacuum pressure of 10 Pa. Data will be collected at high magnification mode (10000x), used to visualize dendritic spines and PSD, with a pixel size of 6 nm in x-y plane and 50 nm along z-axis. The resulting datasets were assembled into volume files aligned using Digital Micrograph (Gatan), and then manually segmented into 3D models in Ilastik 0.5 and AMIRA 5.4.3 software package (FEI Visualization Science Group, Burlington, MA, USA). Three-dimensional structures in image stacks containing hundreds or thousands of 2D orthoslices were traced individually in each plane and are automatically surface rendered. The volumes of Amira 3D models were measured by the 'Material Statistics' modules of AMIRA. The data were expressed as mean ± SEM. Different groups were assessed by one- or two way analysis of variance (ANOVA) for multiple comparisons followed by post hoc Tukey's or by Kruskal-Wallis test and corrected with Dunn's multiple comparison procedure. All statistical analyses were done using software Prism, version 5 (GraphPad, CA, USA). The accepted level of significance was $P < 0.05$.

RESULTS

The protocol of intra-hippocampal DAB administration established in rats and described in Suzuki and colleagues (Suzuki et al., 2011) was adapted to mice. As in rat DAB was administered as 1μl of a solution 300 and 1000 μM (300 and 1000 pmol respectively), we injected bilaterally 0.5 μl of DAB (1000, 2000, 4000 and 8000 μM; 500, 1000, 2000 and 4000 pmol respectively) or vehicle (artificial cerebrospinal fluid) at a rate of 0.5 μl/side/60seconds. The lowest concentrations (500, 1000, 2000 pmol) were considered to be the relevant ones for our experimental set-up, in agreement with previous studies, while the highest dose (4000 pmol) was used to detect possible toxic effects of the drug on the treated mice.

1. Stereotactic coordinates for bilateral intra-hippocampal injection in mouse brain

To precisely identify the position of the site of injection and the correct diffusion of the drug into the hippocampus of mice, we performed bilaterally intra-hippocampal injection of Evans blue and histological analyses (Figure 1a-b).

The coordinates of the injection sites were defined according to the stereotactic plates of a mouse brain atlas (Paxinos and Franklin, 2001) with anterior–posterior coordinates (AP, -2 mm) referred to bregma, lateral coordinates (L, +/-1.9 mm) to the midsagittal suture line, and ventral coordinates (V, -1.9 mm) to the surface of the skull. The depth of the injection was carefully selected to reach the surface of the dorsal hippocampus, avoiding the direct contact of the cannula tips onto the basal dendrites region of CA1 to avoid micro-lesions.

To monitor the appropriateness of the settings and of the overall procedure, we injected 0.5 μl of Evans blue solution in a subset of animals (n=4). One hour after injection, the animals were sacrificed, the dissected brains were sectioned in 1 mm slices with a tissue chopper and the ex-vivo slices were directly viewed under a stereomicroscope. As shown in figure 1a, the Evans blue staining was visible only in the hippocampus of each injected hemisphere (Figure 1a).

The integrity of the dorsal hippocampus after micro-injection of 0.5 μl of vehicle was further verified by histological analyses. One hour after the injection, anesthetized mice were perfused and the brains dissected and processed for paraffin embedding (see Methods). Coronal brain sections stained with haematoxylin/eosin confirmed that the tip of the injection cannula reached the dorsal hippocampus, without directly touching it, and that no contact

lesions were evident in the area (Figure 1b). However, upon liquid injection, the neurons of the CA1, that were located immediately below the injection site, appeared to suffer from compression, a feature that is common for this type of experimental approach. The hippocampal areas affected by this compression artefact were never included in any further analysis.

Figure 1

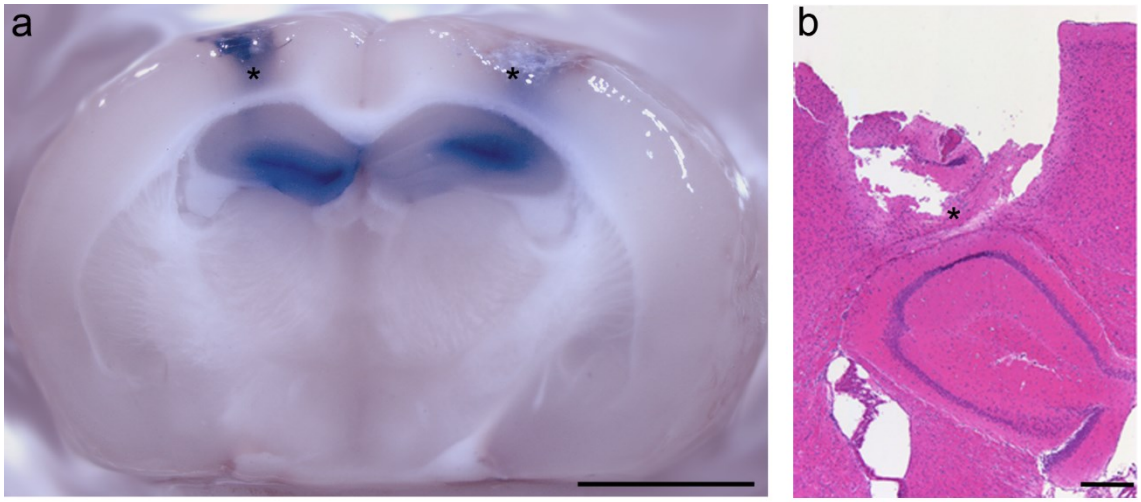

Figure 1. (a) *One hour after bilateral injection of 0.5 μl of Evans blue solution in the hippocampus of mice, the image confirmed the diffusion of the dye exclusively in the hippocampal region. The asterisks indicate the injection sites. (Scale bar = 4 mm).* ***(b)*** *Haematoxylin and eosin staining of a coronal section of the right hippocampus of a mouse injected with vehicle. The lesion caused by the cannula can be clearly seen in the cortex above the hippocampus (arrow). The layer of neuronal nuclei located below the injection site were typically slightly compressed by the pressure of the injected fluid (Scale bar = 300 μm).*

2. Intra-Hippocampal injection of vehicle or 1,4-Dideoxy-1,4-Imino-D-Arabinitol (DAB) did not affect mice spontaneous locomotor activity

To exclude unspecific effects of surgery or pharmacological treatments on mice behavior during the memory tasks, the mouse spontaneous locomotor activity was monitored. This was done by individually placing each animal in an activity cage with horizontal and vertical infrared sensors, where cumulative horizontal and vertical beam

breaks (corresponding to horizontal and vertical movements of the mouse) were automatically counted, every 5 minutes for a total of 30 minutes.

The spontaneous locomotor activity recordings showed that the number of the horizontal movements was unaffected by pharmacological treatment, while a slight but significant reduction of the vertical movements was observed only in treated animals with 1000 pmol DAB and not in mice treated either with vehicle or with 2000 and 4000 pmol DAB (Figure 2a-d and table 1).

Figure 2

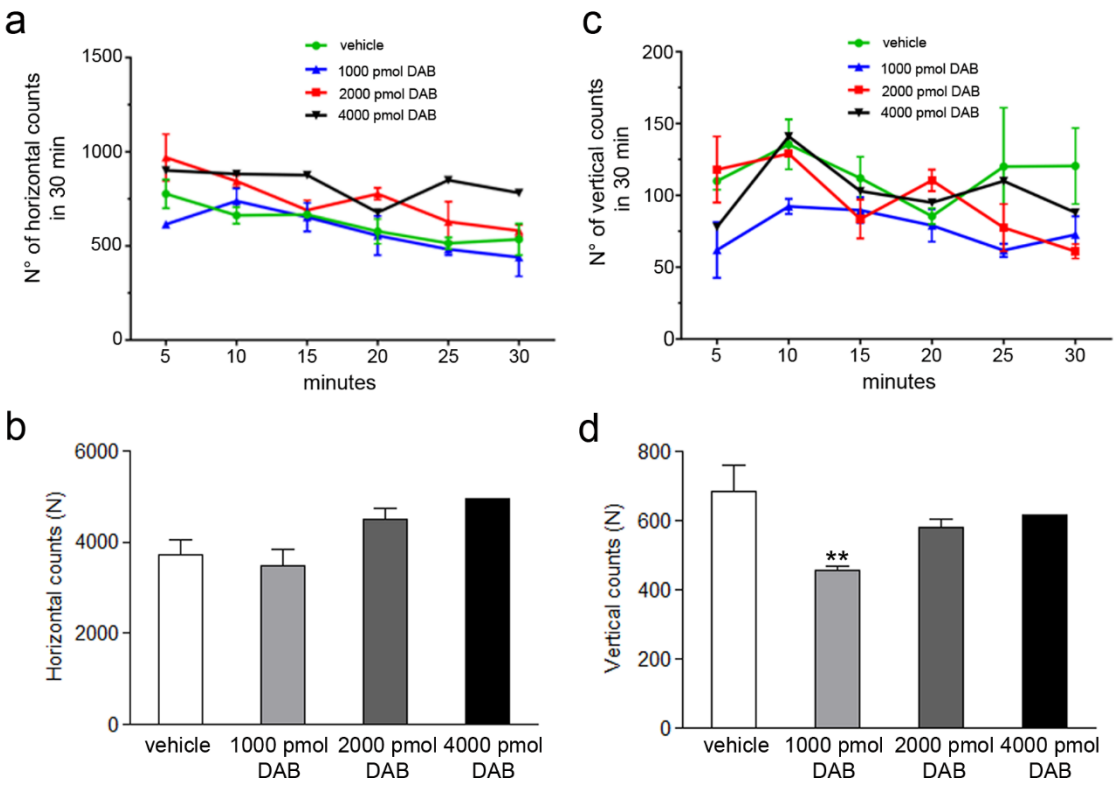

Figure 2. (a-d) *Spontaneous locomotor activity of mice treated with vehicle, 1000, 2000 and 4000 pmol DAB (Vehicle: n=2, 1000 pmol DAB: n=3, 2000 pmol DAB: n=2, 4000 pmol DAB: n=1) were tested for their horizontal* ***(a,b)*** *and vertical movements in 30' (c,d). **P < 0.01 vs vehicle group, unpaired Student t-test.*

Table 1

Spontaneous motor activity	Vehicle	1000 pmol DAB	2000 pmol DAB	4000 pmol DAB
Cumulative Horizontal movements (N)	3731 ± 314	3481 ± 369	4490 ± 269	4968 ± 0
Cumulative Vertical movements (N)	683 ± 76	457 ± 13	579 ± 26	615 ± 0

Table 1. *Spontaneous motor activity analyzed as number of horizontal/vertical counts (N). Data were expressed as mean ± SEM. We analyzed the movements of 2 mice injected with vehicle, 3 mice treated with 1000 pmol DAB, 2 mice treated with 2000 pmol DAB and one mouse injected with 4000 pmol DAB.*

3. Behavioural phenotyping of C57bl/6N mice bilaterally injected with DAB

To evaluate the effect of DAB administration on the formation of long-term memory, mice were submitted to two memory paradigms: Passive Avoidance (PA) and Novel Object Recognition (NOR) test.

3.1 Block of glycogen metabolism in mice hippocampus does not impair long-term memory formation after PA training

We first tested the effect of DAB administration on long-term memory using the Passive Avoidance Task, a fear-aggravated test used to evaluate learning and memory in rodents. In this test, mice learn to avoid an environment in which an aversive stimulus (foot-shock) was delivered during the acquisition phase/training (Figure 3b). DAB was injected 15 minutes before training and long-term memory was tested 24 hours after acquisition, as illustrated in figure 3a.

We knew from previous experience that visual impairment could deeply affect the result of this test, thus, before running the actual experiments, all animals were monitored

for visual acuity. Mice were tested by means of the Visual Cliff Test and only those with an acuity score higher than 70% were used for the experiments (data not shown).

The results obtained in the passive avoidance task of mice treated with 1000 and 2000 pmol DAB, are reported in figure 3c. Vehicle and DAB-treated mice had similar performances in the aversive long-term memory task ($F_{treatment}$ (2,26) = 1.95, P < 0.16), $F_{Pre\text{-}Post\ condition}$ (1,26) = 88.82 P < 0.0001, $F_{interaction}$ (2,26) = 3.437, P < 0.04, Two-way ANOVA, Bonferroni test).

Table 2

Latency time (seconds)	Acquisition phase	Test phase	P value
Vehicle	122.3 ± 24.8	294.0 ± 2.677	P < 0.0001
1000 pmol DAB	102.2 ± 14.5	278.8 ± 21.2	P < 0.0001
2000 pmol DAB	190.3 ± 34.7	298.0 ± 2.0	P < 0.0001

Table 2. *Latency time (seconds) evaluated during passive avoidance task in terms of acquisition (Acq) and memory retention (Test) after vehicle (n=4) or 1000 (n=7) and 2000 (n=5) pmol of DAB. Retention was assessed 24 h after training by measuring the latency to re-enter a context previously paired with a foot-shock. A single training event leads to a significant increase in latency in all groups (***P < 0.0001). Values are reported as mean ± SEM. P values obtained in the statistical analyses are reported.*

We observed only a slight but not significant decrease of the mean retention latency, expressed as difference (∆) between Acquisition phase and Test phase in seconds after treatment of 2000 pmol of DAB (Figure 3d and table 3).

Table 3

Passive Avoidance	Vehicle	1000 pmol DAB	2000 pmol DAB
Mean retention latency (Δ) (seconds)	177.7 ± 24.8	177.3 ± 19.9	109.7 ± 34.6

Table 3. *Difference between the mean latency time during acquisition and test (Δ) (reported as mean ± SEM) is comparable among the three groups.*

Figure 3

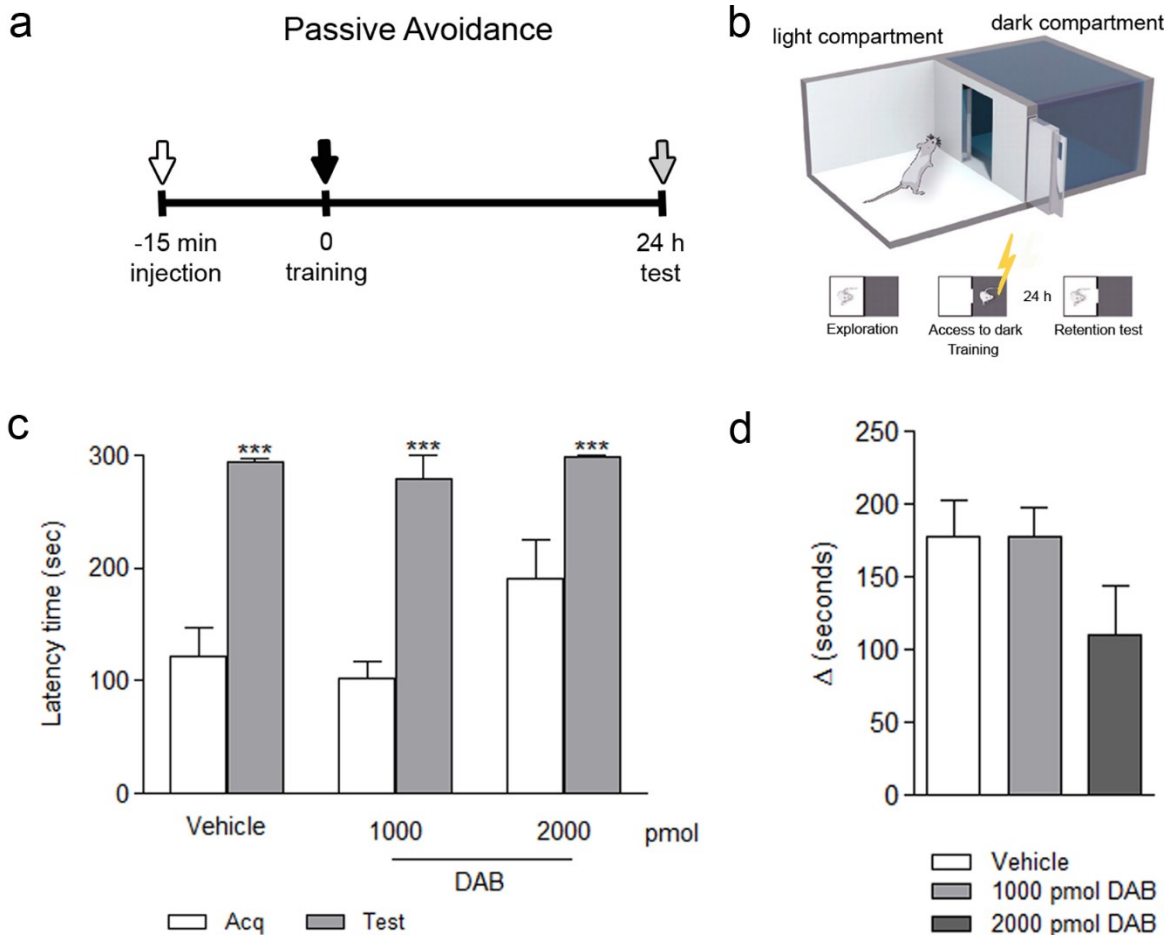

Figure 3. (a,b) *Passive avoidance test was used to study the long-term memory in mice 24 hours after DAB injection. We injected DAB 15 minutes before the training phase of the test (T0) where mice entered the dark compartment and received the foot shock. (The images in figure b was modified from Karlén et al., 2009)* ***(c)*** *Acquisition (Acq) and retention (Test) latency time are expressed as mean ± SEM, in mice treated with vehicle, 1000 and 2000 pmol/side DAB. Statistical*

analyses showed that DAB did not affect long-term memory in the passive avoidance test. ***(d)*** *Mean retention latency (difference Acquisition phase-Test phase (Δ)) is comparable among the three groups.*

3.2 Astrocytic glycogen metabolism is required in the hippocampus for intermediate- and long-term memory formation after NOR training

We then carried out the Novel Object Recognition test (NOR) to study intermediate and long-term episodic memory after DAB injection into the hippocampus following the protocol showed in figure 4a.

In rodents, the Novel Object Recognition (NOR) task is used to evaluate recognition memory. This test is based on the tendency of rodents to spend more time exploring a novel object (N) than a familiar (F) one. Exploring the novel object reflects the use of learning and recognition memory.

As shown in figure 4b, while 500 pmol DAB had no effect on memory formation, increasing doses of DAB (1000, 2000 and 4000 pmol/side) injected into the hippocampus induced memory alterations in terms of decreased mean discrimination index, defined as (N-F/N+F). There was a statistical difference among groups (treatment as between subject factor and time as within factor, treatment: $F(4,59) = 50.42$, $P < 0.0001$; time: $F(1,59) = 0.053$, $P=0.818$; treatment x time: $F(4,59) = 0.860$, $P=0.492$, 2-way ANOVA for repeated measures). Post-hoc comparisons revealed a significant decrease of mean discrimination index already at 120 minutes and up to 24 hours after treatment with 1000, 2000 and 4000 pmol DAB. (Figure 4b and table 4). The mean exploration time was different among groups (object as between subject factor and treatment + time as within factor, object: $F(1,196) = 3.788$, $P=0.05$; treatment + time: $F(14,196) = 2.909$, $P=0.0003$; object x treatment + time: $F(14,196) = 2.895$, $P=0.0005$, 2-way ANOVA for repeated measures). Post-hoc analysis revealed that there was no difference in the exploration time between the two objects in DAB treated animals at all the tested doses while there was a difference in vehicle group.

Table 4

Mean discrimination index (N-F/N+F)	Vehicle	500 pmol DAB	1000 pmol DAB	2000 pmol DAB	4000 pmol DAB
120 minutes	0.28 ± 0.03	0.27 ± 0.07	0.08 ± 0.05	-0.14 ± 0.02	-0.24 ± 0.03
24 hours	0.26 ± 0.03	0.26 ± 0.02	-0.01 ± 0.06	-0.12 ± 0.01	-0.18 ± 0.05
Mean exploration time	**Vehicle**	**500 pmol DAB**	**1000 pmol DAB**	**2000 pmol DAB**	**4000 pmol DAB**
Object 1 pre	14.09 ± 0.94	14.00 ± 1.05	12.17 ± 1.30	11.00 ± 1.19	12.00 ± 0.55
Object 2 pre	14.73 ± 0.97	16.00 ± 1.05	12.75 ± 1.00	12.29 ± 1.46	14.60 ± 2.04
Object 1 120'	8.50 ± 0.95	7.80 ± 1.98	6.62 ± 1.57	12.00 ± 1.87	14.40 ± 2.42
Object 2 120'	15.25 ± 1.73	12.40 ± 2.94	8.37 ± 1.99	9.14 ± 1.50	9.20 ± 1.85
Object 1 24h	9.73 ± 0.97	10.00 ± 1.30	11.00 ± 1.55	13.57 ± 1.66	11.60 ± 2.11
Object 2 24h	16.09 ± 1.32	16.20 ± 1.59	9.33 ± 1.12	10.71 ± 1.30	8.20 ± 1.39

Table 4. *Hippocampal injection of DAB (500 pmol (n=5), 1000 pmol (n=8), 2000 pmol (n=7) and 4000 pmol (n=5)), 15 minutes before the training phase, evaluated in the NOR, in terms of discrimination index and mean time exploration. The highest doses (1000, 2000 and 4000 pmol/side) impaired both intermediate (test 120 minutes after training) and long-term episodic memory (test 24 hours after training) in the object recognition test, compared to vehicle (n=8). DAB at 500 pmol/side (n=5) did not affect episodic memory.*

3.3 The effect of DAB administration in time

To evaluate whether a single hippocampal injection of DAB had persistent effects on memory formation in mice, we performed a new NOR experiment 7 days after drug treatment, following the protocol depicted in figure 4d.

Mice were injected with vehicle (n=3-11) or 1000 pmol DAB (n=4) 15 minutes before training and tested 24, 48 and 72 hours (Test 1) later. There was a statistical difference among groups (treatment as between subject factor and time as within factor, treatment: $F(1,36) = 16.61$, $P=0.0002$; time: $F(3,36) = 3.031$, $P=0.0417$; treatment x time: $F(3,36) = 6.486$, $P=0.0013$, 2-way ANOVA for repeated measures). Post-hoc comparisons revealed a significant decrease of mean discrimination index in DAB treated animals at 24, 48 and 72 hours while no difference was found in DAB treated animals when retrained 7 days after drug treatment (Figure 4e and table 5). The mean exploration time (Figure 4e-f) was different among groups (object as between subject factor and treatment + time as within factor, object: $F(1,124) = 12.01$, $P=0.0007$; treatment + time: $F(11,124) = 1.737$, $P=0.073$; object x treatment + time: $F(11,124) = 2.209$, $P=0.02$, 2-way ANOVA for repeated measures). Post-hoc analysis revealed that there was difference in the exploration time between the two objects in DAB and vehicle treated animals after retraining and only in vehicle treated groups at 24 and 48 hours of delay.

These findings indicated that DAB disrupts long-term memory formation during a limited time window.

Table 5

Mean discrimination index (N-F/N+F)	Vehicle	1000 pmol DAB
24 hours	0.26 ± 0.02	-0.070 ± 0.064
48 hours	0.31 ± 0.02	0 ± 0
72 hours	0.11 ± 0.08	-0.085 ± 0.03
24 hours after re-training	0.11 ± 0.02	0.250 ± 0.06

Mean exploration time	Vehicle	1000 pmol DAB
Object 1 pre	14.09 ± 0.94	12.17 ± 1.30
Object 2 pre	14.73 ± 0.97	12.75 ± 1.00
Object 1 24h	9.73 ± 0.97	11.00 ± 1.75
Object 2 24h	16.09 ± 1.32	9.33 ± 1.12
Object 1 48h	10.33 ± 0.33	15 ± 0.92
Object 2 48h	19.67 ± 0.33	15 ± 0.92
Object 1 72h	13.33 ± 1.20	13 ± 3.03
Object 2 72h	16.67± 1.20	11.25 ± 2.78
Object 1 2^{nd} pre	15.33 ± 1.45	13.75 ± 1.49
Object 2 2^{nd} pre	14.67 ± 1.45	16.25 ± 1.49
Object 1 2^{nd} 24h	13.33 ± 0.33	11.25 ± 0.95
Object 2 2^{nd} 24h	16.67 ± 0.33	18.95 ± 0.95

Table 5. *DAB (1000 pmol/side) microinjected into the hippocampus impairs long-term episodic memory evaluated in the NOR test, in terms of mean discrimination index and mean exploration time, for at least 72 hours after training. 24 hours after re-training no difference was found between DAB and vehicle injected mice Data are expressed as mean ± SEM. (n=3-11 per group).*

Figure 4

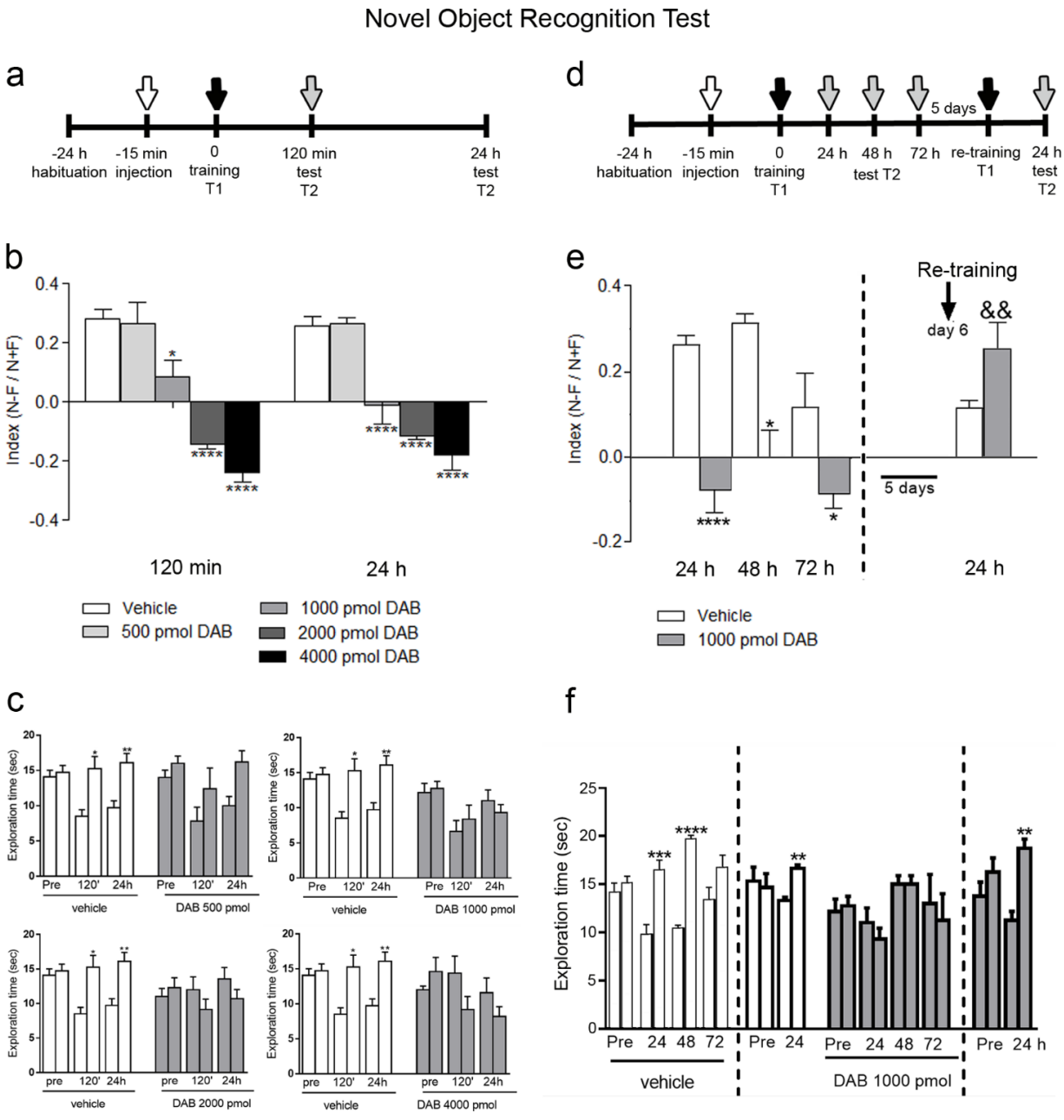

Figure 4. (a, b, c) *DAB (1000 – 2000 – 4000 pmol/side) microinjected into the hippocampus 15 minutes before the training phase impairs intermediate (120 minutes) and long-term episodic memory (24 hours) evaluated in the NOR test, in terms of mean discrimination index* ***(b)*** *and mean exploration time* ***(c)*** *and for at least 72 hours after training* ***(e)****. 24 hours after re-training* ***(d)*** *no difference was found between DAB and vehicle injected mice* ***(e, f)****. Data are expressed as mean ± SEM. (n=3-11 per group). (*P < 0.05, ****P < 0.0001 vs corresponding vehicle;* $^{\&\&}$*P < 0.01 vs DAB at 24 hours one-way ANOVA, Tukey's test).*

3.4 Rescue of behavioural alterations induced by DAB administration through hippocampal co-injections of L-lactate

As demonstrated in recent work, in rats brain the inactivation of glycogen metabolism, and the consequent decrease of lactate production in hippocampal astrocytes lead to an impairment of long-term memory (evaluated as a reduction in the mean latency during the inhibitory avoidance test), defects in long-term potentiation in hippocampal neurons, and a subsequent inhibition of immediately early genes (IEGs) expression, playing a pivotal role in synaptic plasticity and memory formation and their related synaptic structural changes. All these effects were rescued by L-lactate but not by D-lactate (Suzuki et al., 2011).

In agreement with these results, our behavioural data in mice suggested that: i) DAB (1000, 2000 and 4000 pmol) significantly affected intermediate- and long-term memory in a dose-dependent manner at both time points examined (2 and 24 hours after NOR training), ii) this effect was long lasting as, upon 1000 pmol DAB administration, memory impairment could be observed even 48 and 72 hours after NOR training and finally, iii) this effect was however not persistent as, 7 days after drug administration, if re-trained, treated animals completely recovered their ability to form new memories.

We then investigated if, as in the rat, in our mouse model L-lactate administration was able to revert this behavioural phenotype. L-lactate, at a dose of 100 nanomoles, was chosen to investigate its ability to revert the 1000 pmol DAB-induced memory impairment detected with the NOR task, 24 hours after training. This dose was selected based on previous work (Suzuki et al., 2011) and used as such in mice (see Methods). There was a statistical difference among groups (treatment as between subject factor and time as within factor, treatment: $F(3,55) = 11.55$, $P < 0.0001$; time: $F(1,55) = 0.81$, $P=0.3126$; treatment x time: $F(3,55) = 0.6820$, $P=0.5668$, 2-way ANOVA for repeated measures). Post-hoc tests demonstrated that , when co-injected with 1000 pmol DAB, 100 nmol L-lactate was able to rescue the DAB-induced memory impairment observed when T1 and T2 were 120 minutes or 24 hours apart (Figure 5a), while L-Lactate alone had no effect on mice behaviour. The mean exploration time (Figure 5c) was different among groups (object as between subject factor and treatment + time as within factor, object: $F(1,168) = 27.35$, $P < 0.0001$; treatment + time: $F(11,168) = 5.959$, $P < 0.0001$; object x treatment + time: $F(11,168) = 1.826$, $P < 0.05$, 2-way ANOVA for repeated measures). Post-hoc analysis revealed that there was a difference in the exploration time between the two objects in vehicle, L-lactate and the combination of both drugs treated animals.

Table 6

Mean discrimination index (N-F/N+F)	Vehicle	1000 pmol DAB	100 nmol L-lactate	1000 pmol DAB + 100 nmol L-lactate
120 minutes	0.28 ± 0.03	0.08 ± 0.06	0.17 ± 0.03	0.23 ± 0.05
24 hours	0.26 ± 0.03	-0.011 ± 0.06	0.15 ± 0.03	0.26 ± 0.05

Mean exploration time	Vehicle	1000 pmol DAB	100 nmol L-lactate	1000 pmol DAB + 100 nmol L-lactate
Object 1 pre	14.09 ± 0.94	10.25 ± 1.24	15.29 ± 0.99	12.14 ± 2.03
Object 2 pre	14.73 ± 0.97	12.13 ± 1.41	14.43 ± 0.87	14 ± 1.45
Object 1 120'	8.5 ± 0.95	6.62 ± 1.57	11.43 ± 0.65	7.14 ± 2.21
Object 2 120'	15.25 ± 1.73	8.37 ± 1.99	16.29 ± 0.92	9.57 ± 2.27
Object 1 24h	9.73 ± 0.97	9 ± 1.65	11 ± 0.87	9.14 ± 1.16
Object 2 24h	16.09 ± 1.32	8.75 ± 1.32	14.71 ± 1.06	15.86 ± 1.82

Table 6. *100 nmol of L-lactate co-injected with 1000 pmol DAB into the hippocampus rescued the intermediate and long-term episodic memory evaluated in the NOR test, in terms of mean discrimination index and mean exploration time. Data are expressed as mean ± SEM. (n=3-11 per group).*

Figure 5

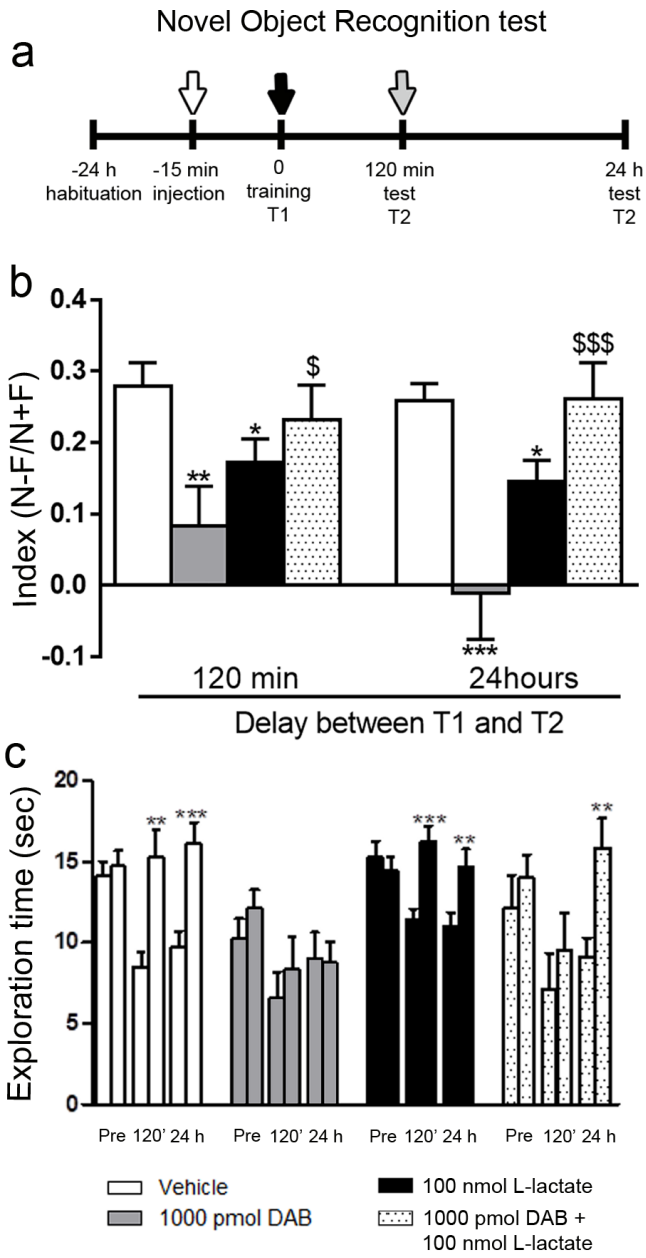

Figure 5. (a, b) *Hippocampal injection of 100 nmol L-lactate in combination with 1000 pmol DAB, infused 15 minutes before the training phase and tested at 120 minutes and 24 hours rescues the memory impairment in the NOR test (*P < 0.05, **P < 0.01, ***P < 0.001 vs corresponding vehicle group;* $^{\$}P < 0.05$, $^{\$\$\$}P < 0.001$ *vs DAB).* ***(c)*** *Mean exploration time for the familiar and the novel objects during training (T1) and test (T2). **P < 0.01, ***P < 0.001 vs corresponding familiar.*

4. DAB administration did not cause reactive astrogliosis 24 hours after hippocampal injection

To test whether the hippocampal injection of the inhibitor of glycogen phosphorylation with DAB led to reactive astrogliosis we performed confocal immunofluorescence experiments on cryostat sections with an antibody against GFAP (glial fibrillary acidic protein, a marker of astrocytes in the central nervous system) to evaluate possible increase of the number of these cells in the hippocampus. We evaluated the extent of GFAP signal in the CA1 of the hippocampus, in mice injected with vehicle or with 1000 pmol DAB, for a total analysed surface of 165 μm^2 for each brain derived from six different hippocampal sections (Figure 6a-b). The immunofluorescence experiments were run in parallel and the acquisition settings of the confocal microscope were kept constant throughout the imaging session (see Methods). For the quantitative analyses, we examined and compared the percentage of the area occupied by the GFAP signal (Figure 6e and Table 6) and the ratio between the mean fluorescence intensity measured in the CA1 region and the total surface area of the region itself (Figure 6f and Table 6). The results were statistically analysed with the software GraphPad Prism® 5 version, with unpaired Student t-test.

Table 6

GFAP positive area (%)	**Vehicle**	**1000 pmol DAB**	**P value**
CA1 hippocampus	86.83 ± 0.72	87.96 ± 0.39	P = 0.180

GFAP (a.u./μm^2)x10^{-3}	**Vehicle**	**1000 pmol DAB**	**P value**
CA1 hippocampus	0.288 ± 0.018	0.257 ± 0.009	P = 0.138

Table 6. *Percentage of the area occupied by GFAP fluorescence signal in CA1 region of hippocampus of mice injected with vehicle and with 1000 pmol DAB. Values are reported as mean ± SEM. Results were statistically analysed with the unpaired Student t-test.*
GFAP fluorescence intensity in arbitrary units (a.u.) per CA1 area in μm^2 measured in mice treated with vehicle or injected with 1000 pmol DAB. Values are reported as mean ± SEM. Results were statistically analysed with the unpaired Student t-test.

Figure 6

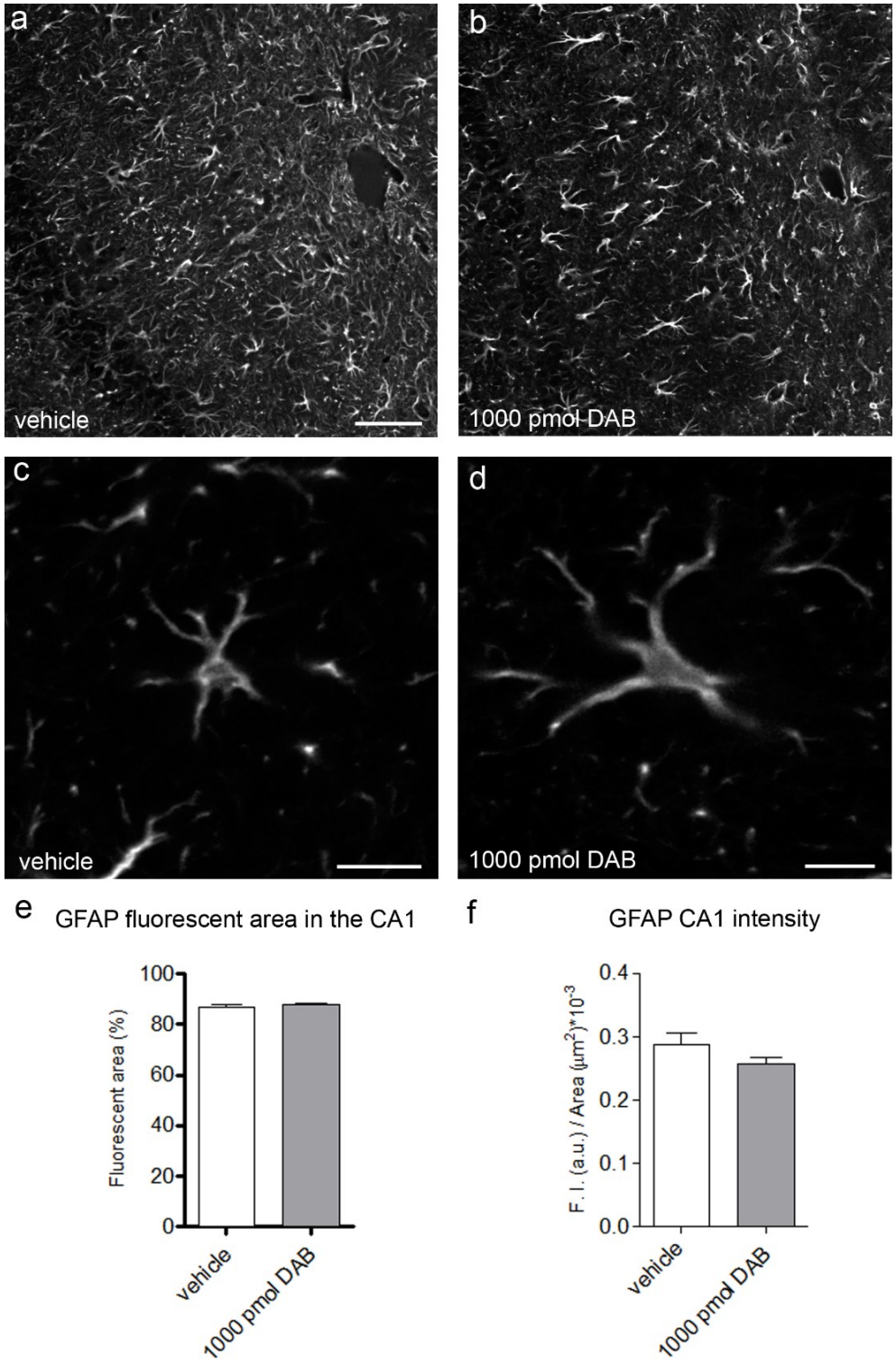

Figure 6. *Representative confocal images of GFAP immunofluorescence in the CA1 of the hippocampus acquired with low magnification* ***(a, b)*** *and a single astrocyte in the same area acquired at higher magnification* ***(c, d)****; in mice treated with vehicle* ***(a, c)*** *and 1000 pmol DAB* ***(b, d)*** *24 hours after injection (a: scale bar = 30 μm, c: scale bar = 10 μm, d: scale bar = 10 μm).* ***(e, f)*** *The graphs showed the quantification of GFAP fluorescent area (%) and the percentage of area covered by GFAP positive cells in the CA1 region of hippocampus. This analysis did not reveal differences*

between mice treated with vehicle and 1000 pmol DAB 24 hours after injection. Columns are reported as mean ± SEM. Results were statistically analysed with the unpaired Student t-test.

Our data demonstrated that, regardless of the method used to quantify the amount of GFAP-positive cells and/or puncta, there were no significant differences in the signal measured in the CA1 of the hippocampus among mice treated with vehicle or 1000 pmol DAB (Table 6).

5. Density of excitatory synapses in the CA1 region of the hippocampus

To determine whether behavioural defects were paralleled by defects in neuronal morphology and specifically in dendritic spine density, we performed preliminary low resolution analyses of spine density in apical dendrites from CA1 pyramidal neurons (*stratum radiatum*) by means of the Golgi-Cox staining technique (Figure 7a-b), 24 hours after training of mice treated with 1000 and 2000 pmol and challenged with both PA (Figure 7d) and NOR tasks (Figure 7e).

Table 8

Spine density (N° of spines/10 μm)	**Control**	**Vehicle**	**1000 pmol DAB**	**2000 pmol DAB**
PA (24 h)	10.32 ± 0.21	11.30 ± 0.21	9.73 ± 0.22	8.54 ± 0.21
NOR (24 h)	10.32 ± 0.21	11.04 ± 0.21	10.08 ± 0.17	8.56 ± 0.16

Table 8. *Spine density of the apical dendrites of the CA1 pyramidal neuron, measured as number of spine/10 μm of dendrites, values are presented as mean* ± SEM*. We measured the spine density 24 hours after passive avoidance and novel object recognition training in 3 mice injected with vehicle, 1000 pmol DAB and 2000 pmol DAB; as control we used 2 mice that underwent only surgery for cannula implantation. Data were statistically analysed by One-way Analysis of Variance (ANOVA) and corrected with Tuckey's post-test.*

24 hours after the training session of both PA and NOR task (Figure 7d, e), spine density was increased in mice treated with vehicle when compared to spine density measured in the same brain areas from pre-training mice that underwent only surgery for cannula implantation (One-way Analysis of Variance (ANOVA) and corrected with Tuckey's post-test). This increase in spine density induced by the memory training was not observed in dendrites from hippocampal pyramidal neurons of mice treated with both 1000 and 2000 pmol DAB. Indeed 24 hours after PA and NOR training, dendrites from 2000 pmol DAB treated mice were characterized by a reduced number of spines even when compared to samples from untrained and untreated mice. All numerical data derived from these experiments are reported in Table 8.

To strengthen the correlation between data from the NOR behavioral test and the analysis of dendritic spine density in CA1 pyramidal neurons, we analyzed spine density from hippocampal sections of those mice treated with vehicle or 1000 pmol DAB that were re-trained ad re-tested for memory formation 7 days after injection. As we have shown before, those animals recovered completely from the inhibitory effect of the drug, but not only DAB-treated mice were able to perform as well as vehicle-treated ones in the memory task (NOR), they also completely recovered in neuronal plasticity as their spine density after delayed re-training and re-testing was identical to vehicle treated mice (Table 9 and figure 7g, h). The results were statistically analysed with the software GraphPad Prism® 5 version, with unpaired Student t-test.

Table 9

Spine density (N° of spines/10 μm)	**Vehicle**	**1000 pmol DAB**	**P value**
NOR (7 days)	11.15 ± 0.18	11.05 ± 0.20	0.71

Table 9. *Spine density of the apical dendrites of the CA1 pyramidal neuron, measured as number of spines/10 μm of dendrites, values are presented as mean* ± SEM*. We measured the spine density 7 days after injection in 2 mice treated with vehicle and 2 treated with 1000 pmol DAB. Data were statistically analysed by unpaired student t-test and P value is showed in the table.*

Figure 7

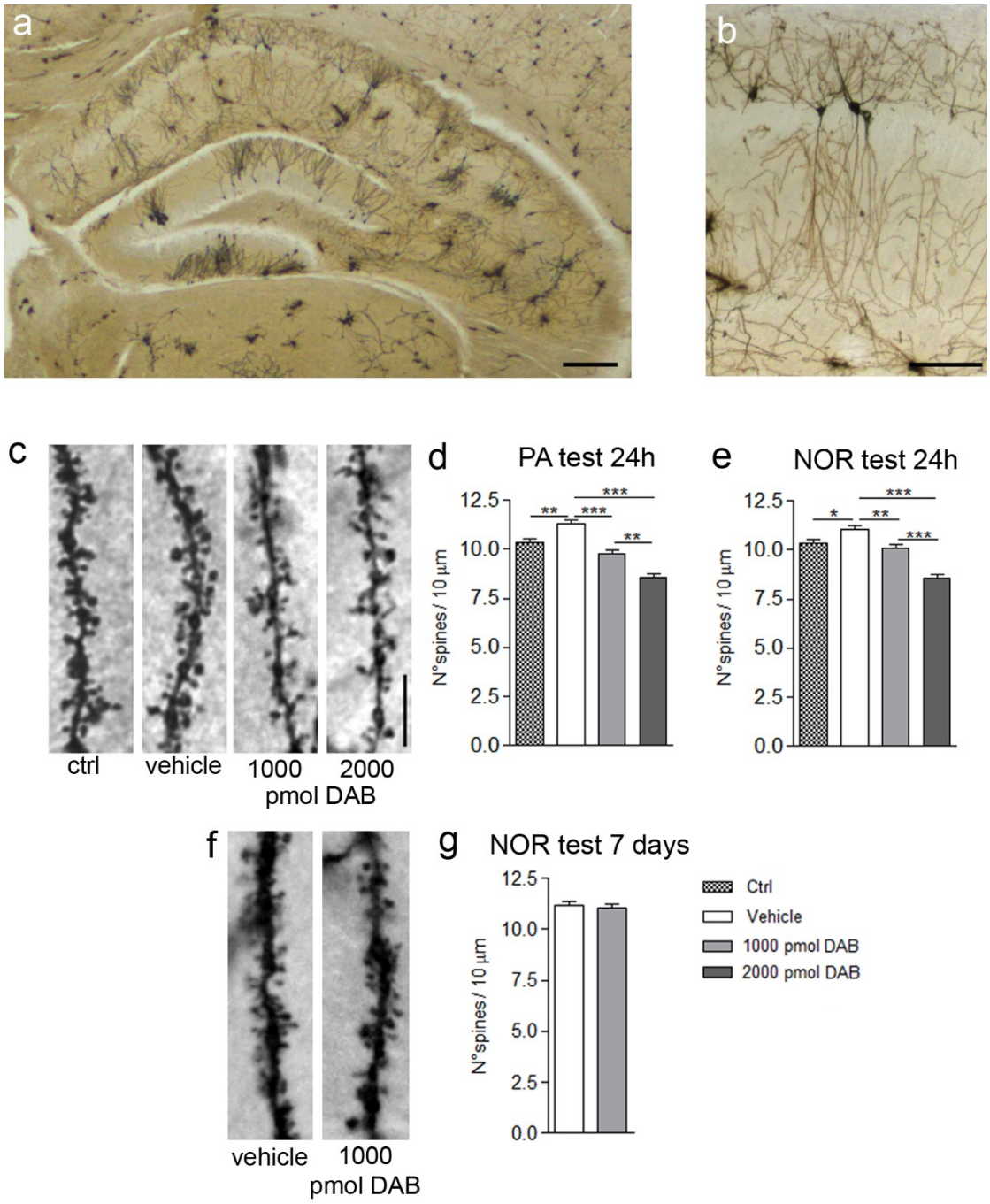

Figure 7. *Representative Images of 100 µm brain coronal section stained according to the Golgi-cox method.* ***(a)*** *Low magnification coronal section of hippocampus where the pyramidal neurons of the CA1 region are visible (black rectangle); scale bar: 300 µm.* ***(b)*** *Low magnification image of three CA1 pyramidal neurons fully impregnated with the Golgi staining solution. The basal (stratum oriens) and the apical dendrites (statum radiatum and moleculare) of the pyramidal neurons (stratum*

pyramidale) are visible (scale bar: 100 μm). ***(c)*** *Representative examples of Golgi-stained hippocampal neurons showing dendritic segments at high magnifications to highlight dendritic spines in the mice control (Ctrl) (n=2), injected with vehicle (n=3), 1000 pmol DAB (n=3) and 2000 pmol (n=3) (scale bar: 10 μm).* ***(d, e)*** *Quantitation of spine number per 10 μm dendritic segment by imageJ software. Note the fewer spines on the dendrites in the mice treated with both concentration of DAB both 24 hours after passive avoidance test and novel object recognition test (*P < 0.05, **P < 0.01, ***P < 0.001) (Scale bar: 10 μm).* ***(f)*** *Golgi-stained dendritic segment of mice injected with vehicle and 1000 pmol DAB, 7 days after injection.* ***(g)*** *Quantitative analyses of spine number per 10 μm of dendritic segment. We did not found any difference between the two groups of mice.*

6. Three-dimensional structure of dendritic spines and PSDs in the CA1 region of hippocampus 24 hours after PA and NOR training

As demonstrated in our behavioural results, blocking glycogenolysis in mice hippocampus impaired memory formation; this result was accompanied by a dramatic reduction of the spine density in the apical dendrites of the hippocampal CA1 region. Through Serial-Block Face Scanning Electron Microscopy (SBF-SEM), and consequent volume reconstruction, we studied the 3D architecture of dendritic spine and associate PSD as a consequence of DAB administration in mice after both the PA and NOR tasks.

Our analyses confirmed the preliminary data obtained on the Golgi-Cox stained section analysed at the optical microscopy level: the density of the dendritic spine was reduced in DAB treated animals and this reduction occurred in animals challenged with both the NOR and PA memory test.

First of all we evaluated the spine density as the ratio between the number of the spines and the volume of the dendrite associated, we reconstructed at least 20 dendrites for each animal group for a total volume of tissue analysed of 245 μm^3 (100 serial sections with a volume each of 7 μm x 7 μm x 0.05 μm). We analysed two animals for each group. We observed that DAB treatment significantly reduced the density of the dendritic spine in the hippocampal CA1 region respect to the mice injected with vehicle 24 hours after PA (*P < 0.05 both for 1000 and 2000 pmol DAB compared to vehicle) and NOR training (*P < 0.05 both for 1000 and 2000 pmol DAB compared to vehicle) (Figure 8a, figure 9b and table 10). In this analysis, no significant differences can be detected in the spine density examined between control and mice treated with vehicle.

To see whether the 3D architecture of the dendritic spines was affected by the block of the glycogenolysis we measured the spine head volume (Figure 8c) and the PSD volume (Figure 8d) in at least 70 spines in a total volume of tissue of 490 μm^3 (200 serial sections with a volume each of 7 μm x 7 μm x 0.05 μm) for each group of mice (2 animals for groups). DAB treatment did not affect the three-dimensional architecture of the dendritic spine if compared to control and mice injected with vehicle (24 hours after PA: figure 8b, c; 24 hours after NOR: figure 9c, d and table 10).

Table 10

Spine density (N° of spines/μm^3)	**Control**	**Vehicle**	**1000 pmol DAB**	**2000 pmol DAB**
PA (24 h)	2.668 ± 0.279	3.344 ± 0.175	2.497 ± 0.172	2.364 ± 0.185
NOR (24 h)	2.668 ± 0.279	3.044 ± 0.241	2.236 ± 0.166	2.030 ± 0.188

Spine head volume (μm^3)	**Control**	**Vehicle**	**1000 pmol DAB**	**2000 pmol DAB**
PA (24 h)	0.104 ± 0.008	0.113 ± 0.012	0.116 ± 0.009	0.118 ± 0.014
NOR (24 h)	0.104 ± 0.008	0.119 ± 0.009	0.113 ± 0.007	0.110 ± 0.009

PSD volume (μm^3)	**Control**	**Vehicle**	**1000 pmol DAB**	**2000 pmol DAB**
PA (24 h)	0.0066 ± 0.0004	0.0069 ± 0.0004	0.0065 ± 0.0005	0.0067 ± 0.0005
NOR (24 h)	0.0066 ± 0.0004	0.0071 ± 0.0003	0.0073 ± 0.0004	0.0068 ± 0.0005

Table 10. *3D analyses of dendritic spine of apical dendrites in the CA1 region of the hippocampus. We measured the spine density as the ratio between the number of the spine and the volume of the respective dendrite (μm^3), moreover we analysed the volume of the spine head and the PSD (μm^3). Data are reported as mean ± SEM. Data were statistically analysed by One-way Analysis of Variance (ANOVA) and corrected with Tuckey's post-test for the spine density and by Kruskal-Wallis test and corrected with Dunn's multiple comparison procedure for the analyses of spine head and PSD volume. Means were considered statistically different when $P < 0.05$.*

Figure 8

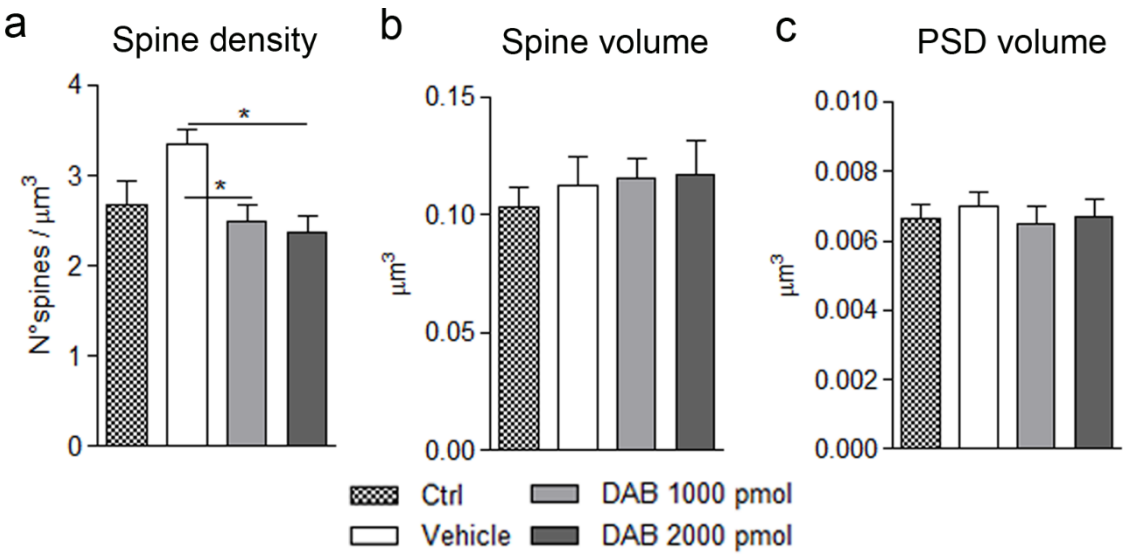

Figure 8. (a-c) *DAB treatment significantly reduced the spine density 24 hours after PA training* ***(a)*** *but did not affect the volume of the spine head* ***(b)*** *and the PSD* ***(c)*** *in mice treated with 1000 and 2000 pmol DAB compared to control mice and mice injected with vehicle. Columns of each graph represent mean ± SEM of the indicated parameter, calculated in 2 animals for each group. (*P < 0.05).*

Figure 9

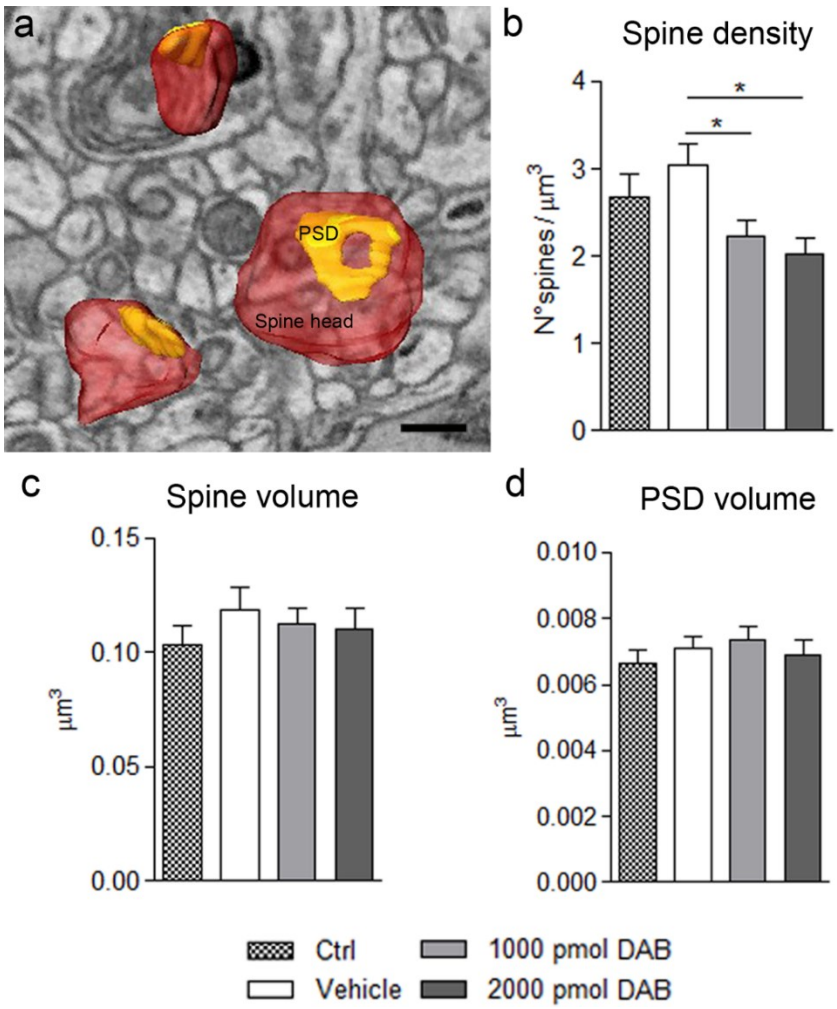

Figure 9. (a) *Example of three-dimensional reconstruction of dendritic spines heads (red) with their PSDs (yellow) that can be perforated (PSD) or not. (Scale bar = 300 nm). The 3D reconstruction of these three spines came from 15 serial sections for each structure, for a volume for each spine around 0.12* μm^3. ***(b, c, d)*** *DAB treatment significantly reduced the spine density 24 hours after NOR training* ***(b)*** *but did not affect the volume of the spine head* ***(c)*** *and the PSD* ***(d)*** *in mice treated with 1000 and 2000 pmol DAB compared to control mice and mice injected with vehicle. Columns of each graph represent mean ± SEM of the indicated parameter, calculated in 2 animals for each group. (*P < 0.05).*

7. Fine structure of hippocampal excitatory synapses in the CA1 of the hippocampus 24 hours after PA and NOR training

To evaluate if the decrease in dendritic spine number in mice treated with DAB, was associated to ultrastructural defects in the synaptic terminal we analysed the fine structure of hippocampal synapses of control mice, mice injected with vehicle, or 1000 and 2000 pmol DAB, 24 hours after PA and NOR training.

The pre-synaptic boutons of the synapses that contact the apical dendritic spines in the CA1 region of the hippocampus, contained many synaptic vesicles dispersed in the terminal and they often contained mitochondrial profiles. The pre-synaptic compartment was separated from the dendritic spine by a clearly visible synaptic cleft (Figure 9a-d). We measured pre-synaptic terminal mean surface (defined as the total surface of the terminal that was not occupied by mitochondrial profiles, if present) and the density of the synaptic vesicles, calculated as the ratio between the number of synaptic vesicle and the surface of the synapse (all the data are reported in table 11 and the histograms are shown in figure 9e-h). These morphometric analyses failed to reveal any change in the synaptic surface among excitatory synapses of the four groups of animals analysed. Instead, they revealed a significant difference in the density of the synaptic vesicle, that in mice treated with DAB (1000 and 2000 pmol) was strongly reduced compared to both control and vehicle-treated mice (Figure 9c, d, and Table 11). Statistical analyses revealed that 24 hours after PA training synaptic vesicle density was decreased in mice treated with 1000 and 2000 pmol DAB compared with untreated (***$P < 0.001$) and vehicle-treated animals (***$P < 0.001$). This observation was confirmed also in mice analysed 24 hours after NOR training where excitatory synapses in animals treated with 1000 pmol and 2000 pmol DAB were characterized by a reduction in synaptic vesicle density compared to control and vehicle-treated mice (*$P < 0.05$ and ***$P < 0.001$ respectively). Moreover, in this last experimental set-up, a significant difference in synaptic vesicle density can be detected also between the mice treated with 1000 and 2000 pmol DAB (**$P < 0.01$).

On the contrary, and despite the fact that we observed a significant decrease in spine density, the architecture of the post-synaptic density (PSD) remained unvaried in mice treated with DAB compared with animals injected with vehicle or control untreated mice. We measured PSD length and thickness, calculated as the ratio between PSD surface and PSD length, and we failed to detect changes in these parameters among the four groups analysed both 24 hours after PA and NOR training (Table 11). Accordingly, the 3D analyses confirmed

the observation made on 2D projections, namely that the spine head and PSD volume remained unvaried in mice untreated, treated with vehicle or DAB.

The results were statistically analysed with the software GraphPad Prism® 5 version, with Kruskal-Wallis test and corrected with Dunn's multiple comparison procedure. Means were considered statistically different when $P < 0.05$.

Table 11

Pre-synaptic surface (μm^2)	**Control**	**Vehicle**	**1000 pmol DAB**	**2000 pmol DAB**
PA (24 h)	0.202 ± 0.009	0.174 ± 0.011	0.177 ± 0.009	0.176 ± 0.008
NOR (24 h)	0.202 ± 0.009	0.191 ± 0.009	0.197 ± 0.012	0.186 ± 0.008

Vesicle density (N° vesicles / μm^2)	**Control**	**Vehicle**	**1000 pmol DAB**	**2000 pmol DAB**
PA (24 h)	196.1 ± 6.2	181.7 ± 5.9	132.2 ± 8.0	135.8 ± 6.6
NOR (24 h)	196.1 ± 6.2	200.4 ± 7.3	167.5 ± 6.1	136.5 ± 5.9

PSD length (nm)	**Control**	**Vehicle**	**1000 pmol DAB**	**2000 pmol DAB**
PA (24 h)	305.2 ± 10.4	286.8 ± 8.2	277.3 ± 11.5	280.6 ± 9.3
NOR (24 h)	310.3 ± 10.0	307.0 ± 11.09	275.8 ± 9.1	282.5 ± 8.3

PSD thickness (nm)	**Control**	**Vehicle**	**1000 pmol DAB**	**2000 pmol DAB**
PA (24 h)	61.4 ± 1.5	66.1 ± 3.8	65.9 ± 3.9	68.0 ± 2.3
NOR (24 h)	62.0 ± 1.6	63.3 ± 3.2	65.4 ± 2.3	59.8 ± 1.5

Table 11. *Morphometric analyses of excitatory synapses of apical dendrites in the CA1 region of the hippocampus. We measured the pre-synaptic surface and the synaptic vesicle density, in 75 synapses for each experimental group. For the analyses of PSD length and thickness, at least 80 PSD for each experimental group were analysed, both 24 hours after PA and NOR training (2 control*

mice, 3 mice treated with vehicle, 3 mice treated with 1000 pmol DAB and 3 mice injected with 2000 pmol DAB). Values are reported as mean ± SEM. Measures were statistically analysed with Kruskal-Wallis test and corrected with Dunn's multiple comparison procedure. Means were considered statistically different when P < 0.05.

Figure 9

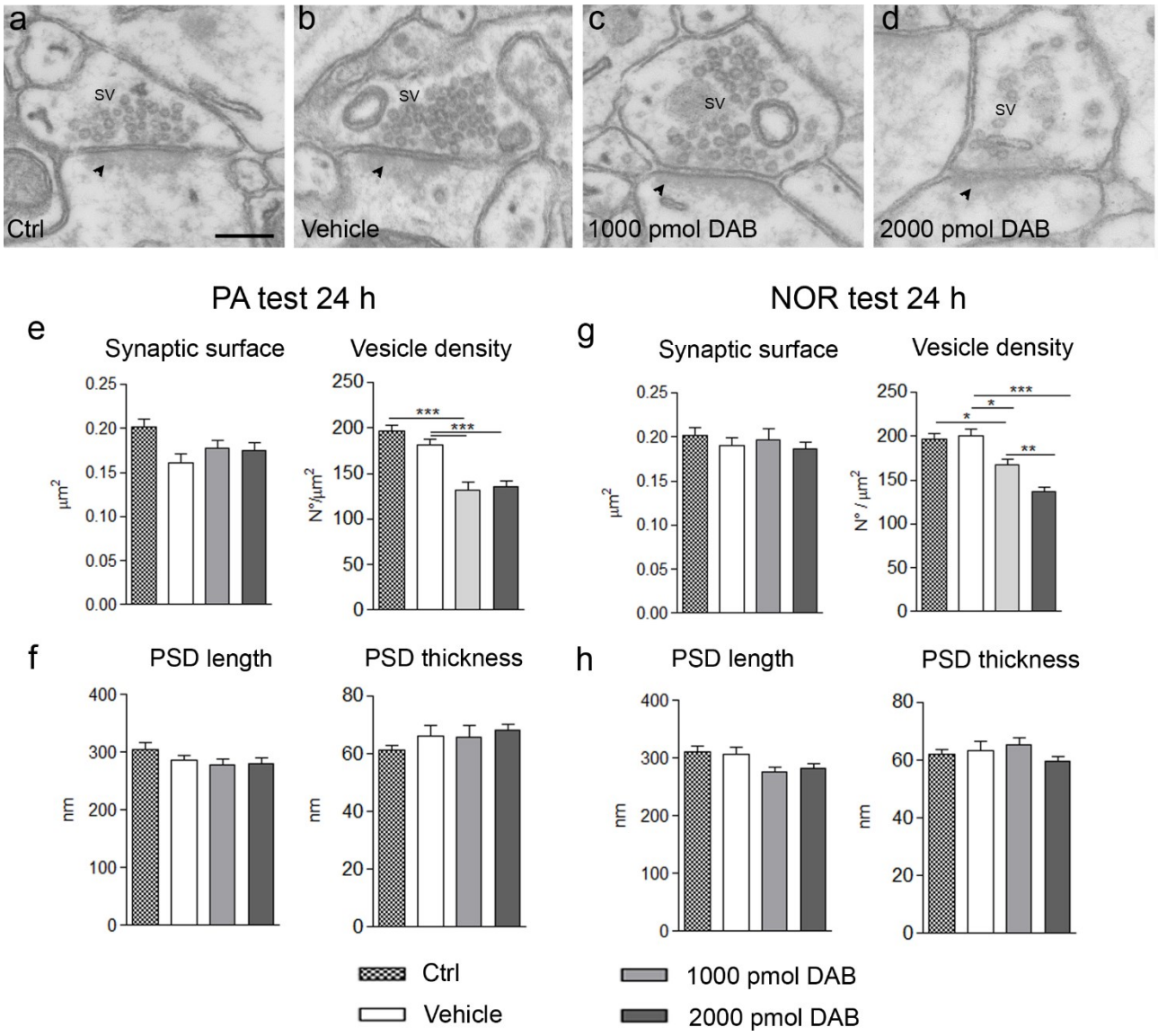

Figure 9. (a-d) *TEM images of excitatory synapses in the apical dendrites layer of the CA1 hippocampal region at 34000x showed a reduction in the vesicle density in the synapse of mice treated with 1000 pmol DAB and more evident in the synapses of mice injected with 2000 pmol DAB. The synaptic bouton with the synaptic vesicles (SV) and the dendritic spine associated with the classical PSD (arrowhead) are clearly visible in the four images. (Scale bar = 100 nm).* ***(e-h)*** *Quantitative analyses of synaptic features carried out both 24 hours after PA* ***(e, f)*** *and NOR training*

***(g, h)**. DAB treatment significantly reduced the synaptic vesicle density but did not affected the pre-synaptic surface and the features of the PSD. Columns of each graph represent mean ± SEM of the indicated parameter, calculated in 3 animals for each group. (*P < 0.05, **P < 0.01, ***P < 0.001).*

We have previously shown that animals injected with DAB, 7 days before the NOR test, were able to form new memories again as well as mice injected with vehicle according to the same experimental paradigm. Accordingly, spine density was recovered as well. To determine whether, besides recovery of the function and of the postsynaptic compartment also the structure of the pre-synaptic terminals was recovered we compared the pre-synaptic surface and the vesicle density of excitatory synapses of the CA1 synapses in mice treated with vehicle and 1000 pmol DAB, 7 days before the NOR test.

Table 12

NOR (7 days)	**Vehicle**	**1000 pmol DAB**	**P value**
Pre-synaptic surface (μm^2)	0.206 ± 0.013	0.191 ± .0.014	P = 0.445
Vesicle density (N° vesicles / μm^2)	194.5 ± 8.6	205.7 ± 11.3	P = 0.4

***Table 12.** Morphometric analyses of excitatory synapses of apical dendrites in the CA1 region of the hippocampus 24 hours after retraining (7 days after DAB injection). We measured the pre-synaptic surface and the synaptic vesicle density, in 40 synapses for each experimental group, in 2 mice treated with vehicle and 2 treated with 1000 pmol DAB. Values are reported as mean ± SEM. Measures were statistically analysed with unpaired Students t-test and P values are showed in the table.*

Figure 10

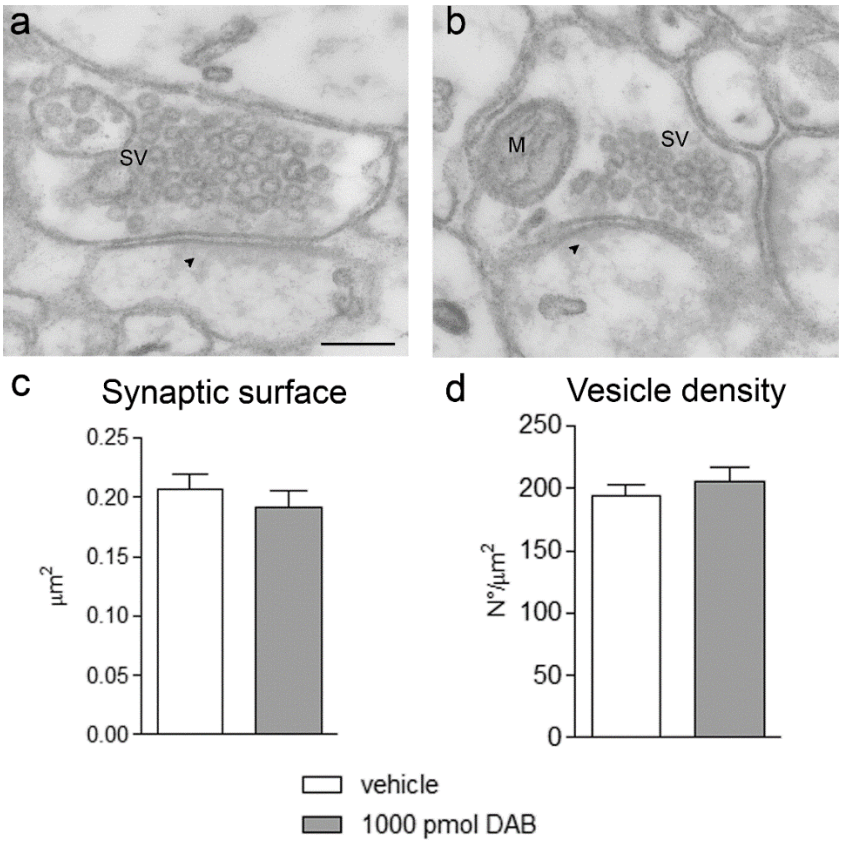

Figure 10. *TEM images of excitatory synapses in the apical dendrites layer of the CA1 hippocampal region at 46000x of mice injected with vehicle* ***(a)*** *and 1000 pmol DAB* ***(b)*** *7 days before NOR test. In the images are clearly visible the synaptic bouton with the synaptic vesicles (SV) and mitochondria (M) and the dendritic spine associated with the PSD (arrowhead). (Scale bar = 100 nm).* ***(c, d)*** *Quantitative analyses of synaptic surface and synaptic vesicle density 24 hours after retraining (7 days after DAB injection). Columns of each graph represent mean ± SEM of the indicated parameter, calculated in 2 animals for each group.*

8. Three-dimensional and fine structure of dendritic mitochondria in the CA1 region of hippocampus 24 hours after NOR training

Recent data demonstrated that altered brain metabolism is associated with changes in mitochondria dynamics (Zhang et al., 2016). Starting from these considerations, we decided to analyse mitochondrial structure, in order to verify whether block of glycogen metabolism affected the architecture of these specific organelles.

We observed significant changes in dendritic mitochondria number, shape, and volume in DAB-treated mice. We found that, compared to uniformly compact and well-separated mitochondria in the hippocampi of mice treated with vehicle, DAB (1000-2000 pmol) treated mice exhibited elongated mitochondria, in which two or more units were interconnected by thin, tubular membrane extensions containing mitochondrial matrix and cristae (Figure 12a-c). Dendritic mitochondria in DAB treated mice were longer, reduced in number (**P < 0.01 both for mice treated with 1000 and 2000 pmol DAB vs control and vehicle mice) and their total volume was broader compared to the dendritic mitochondria of mice treated with vehicle (*P < 0.05 both for mice treated with 1000 and 2000 pmol DAB vs control and vehicle mice) (Figure 11 and table 13). We calculated also the percentage of the dendritic volume occupied by the mitochondria, as the ratio between the mitochondria volume and the dendritic volume x 100, and we found a statistically increase of this parameter in mice treated with DAB respect to the control (*P < 0.05 ctrl vs 1000 pmol DAB) and vehicle mice (***P < 0.001 vehicle vs 1000 pmol DAB; **P < 0.01 vehicle vs 2000 pmol DAB) (Figure 11 and table 13).

Moreover, we frequently observed apposition of this elongated mitochondria and endoplasmic reticulum membranes at the junction between elongated mitochondrial profiles and their connecting double membranes (Figure 12d, e). Overall, these results suggested that the alteration of glycogen metabolism induced by DAB could be the basis of mitochondria dynamics changes.

Table 13

3D Dendritic mitochondria NOR (24 h)	Control	Vehicle	1000 pmol DAB	2000 pmol DAB
Mitochondrial density (N° / μm^3)	0.69 ± 0.07	0.60 ± 0.07	0.39 ± 0.04	0.37 ± 0.05
Dendrites volume (μm^3)	5.30 ± 0.64	5.94 ± 0.40	5.16 ± 0.36	4.55 ± 0.20
Mitochondrial volume (μm^3)	0.72 ± 0.06	0.66 ± 0.06	0.90 ± 0.05	0.91 ± 0.05
% mitochondrial volume / dendrites volume (μm^3)	13.68 ± 1.33	11.84 ± 1.15	18.03 ± 0.94	17.74 ± 1.15

Table 13. *Quantitative 3D analyses of dendritic mitochondria in the apical dendrites layer of the hippocampal CA1 region. We measured the mitochondrial density as the ratio between the number of the mitochondria and the volume of the dendrite associated; the dendrites and mitochondria volume (μm^3) and the percentage of the dendritic volume occupied by the mitochondria calculated as the ratio between the mitochondria volume (μm^3) and the dendritic volume (μm^3) x 100. These analyses were done on 2 animals for each group and at least 20 dendrites, in a total volume of tissue analysed of 980 μm^3 for animals (100 serial sections with a volume each of 14 μm x 14 μm x 0.05 μm). Values are reported as mean* ± SEM. *Measures were statistically analysed with Kruskal-Wallis test and corrected with Dunn's multiple comparison procedure. Means were considered statistically different when $P < 0.05$.*

Figure 11

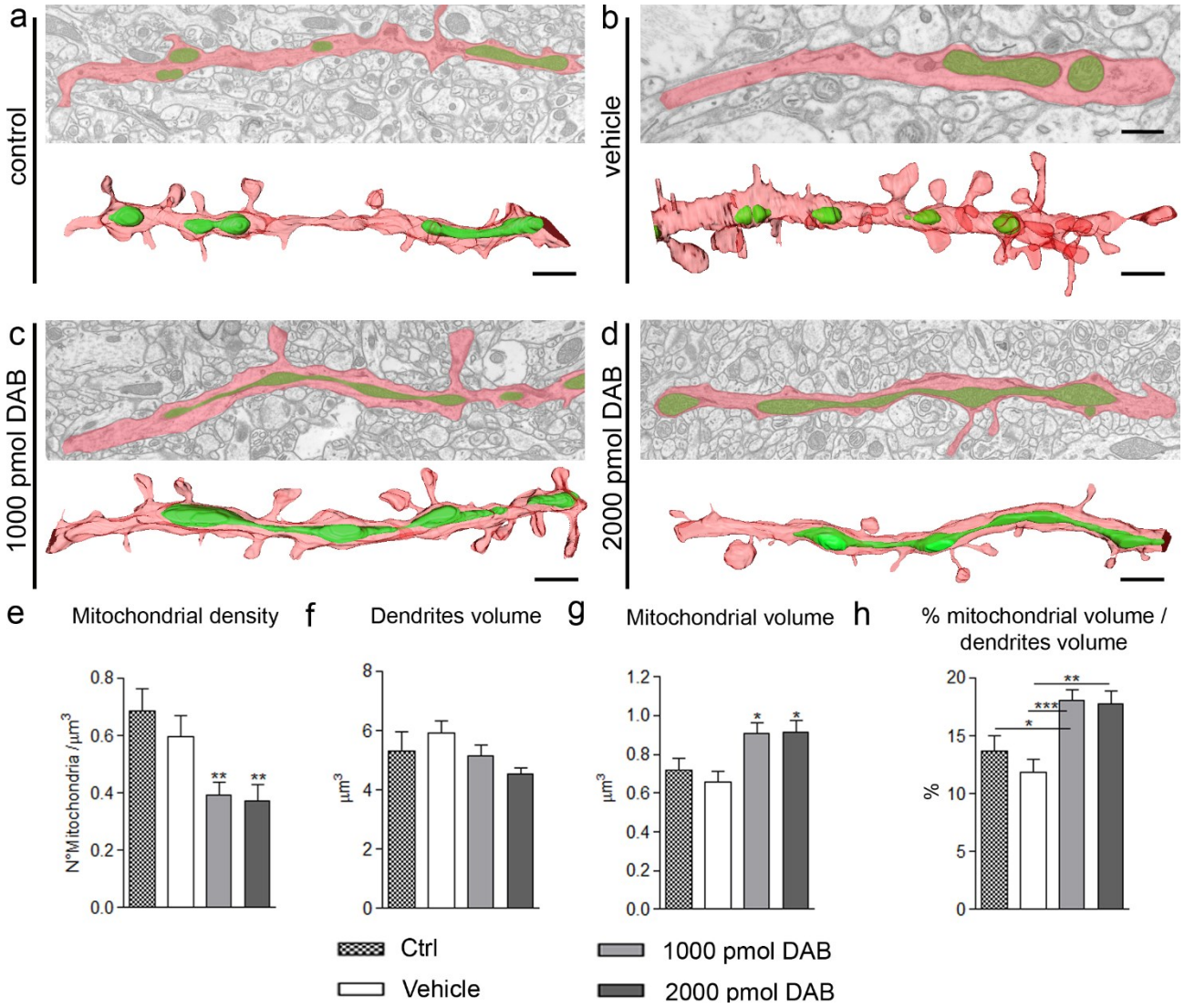

Figure 11. (a-d) *Examples of 2D TEM images and 3D reconstruction of dendrites with their spines (red) and mitochondria (green) in mice control (ctrl)* ***(a)****, injected with vehicle* ***(b)****, 1000* ***(c)*** *and 2000 pmol DAB* ***(d)****. (Scale bar = 1 µm and for the 2D image in the panel b the scale bar is 200 nm). In the images we could observe the reduction of spine density measured in mice treated with DAB* ***(c, d)*** *and the different mitochondrial morphology compared to control and vehicle treated mice* ***(a, b)****.* ***(e-h)*** *Graphs of 3D analyses of mitochondrial features, where we could note the decrease of mitochondrial density for µm³ of dendrite and the increase of mitochondrial volume (µm³) in DAB injected mice. Columns of each graph represent mean ± SEM of the indicated parameter, calculated in 2 animals for each group. (*P < 0.05, **P < 0.01, ***P < 0.001).*

Our 3D analyses revealed that DAB administration induced a significant effect on the dendritic mitochondrial architecture and number; in order to study more in details the fine structure of these organelles we performed 2D analyses on TEM images. Electron micrographs show the intact fine structure of dendritic mitochondria in control mice and mice injected with vehicle, 1000 and 2000 pmol DAB, they present intact and well-preserved outer and inner membrane, and the mitochondrial cristae were clearly visible (Figure 12a-e).

We performed the morphometric analysis of dendritic mitochondria measuring their surface (μm^2), length (μm), number of cristae and we calculated the mitochondrial cristae density as the ratio between the number of the cristae and the mitochondrial surface (μm^2). We detected a significant increase in the mean length (**P < 0.01 ctrl vs 1000 pmol DAB; ***P < 0.001 control vs 2000 pmol DAB and vehicle vs 1000 and 2000 pmol DAB) and surface (*P < 0.05 ctrl vs 1000 pmol DAB; ***P < 0.001 control vs 2000 pmol DAB and vehicle vs 1000 and 2000 pmol DAB) of dendritic mitochondria in DAB treated mice compared to control and vehicle animals (Figure 12f-l and table 14). Furthermore, we evidenced a decrease of cristae density in DAB treated mice respect to the ctrl and vehicle mice (*P < 0.05 ctrl and vehicle vs 1000 pmol DAB and ***P < 0.001 ctrl and vehicle vs 2000 pmol DAB) (Figure 12f-l and table 14). We analysed 70 mitochondria in the dendrites of 2 animals for each experimental group.

Table 14

2D Dendritic mitochondria NOR (24 h)	**Control**	**Vehicle**	**1000 pmol DAB**	**2000 pmol DAB**
Mitochondrial length (μm)	0.740 ±0.047	0.657 ± 0.036	1.080 ± 0.126	1.489 ± 0.149
Mitochondrial surface (μm^2)	0.165 ± 0.007	0.148 ± 0.009	0.225 ± 0.013	0.437± 0.041
Mitochondrial cristae density (N° cristae / μm^2)	72.56 ± 3.11	71.07 ± 2.88	57.08 ± 2.08	49.52 ± 1.92

Table 14. *Quantitative morphometrical analyses of dendritic mitochondria in the apical dendrites layer of the hippocampal CA1 region. We measured the mitochondrial surface, length and the mitochondrial cristae density. These analyses were done in 2 animals for each group and at least*

70 mitochondria for groups. Values are reported as mean ± SEM. *Measures were statistically analysed with Kruskal-Wallis test and corrected with Dunn's multiple comparison procedure. Means were considered statistically different when P < 0.05.*

Figure 12

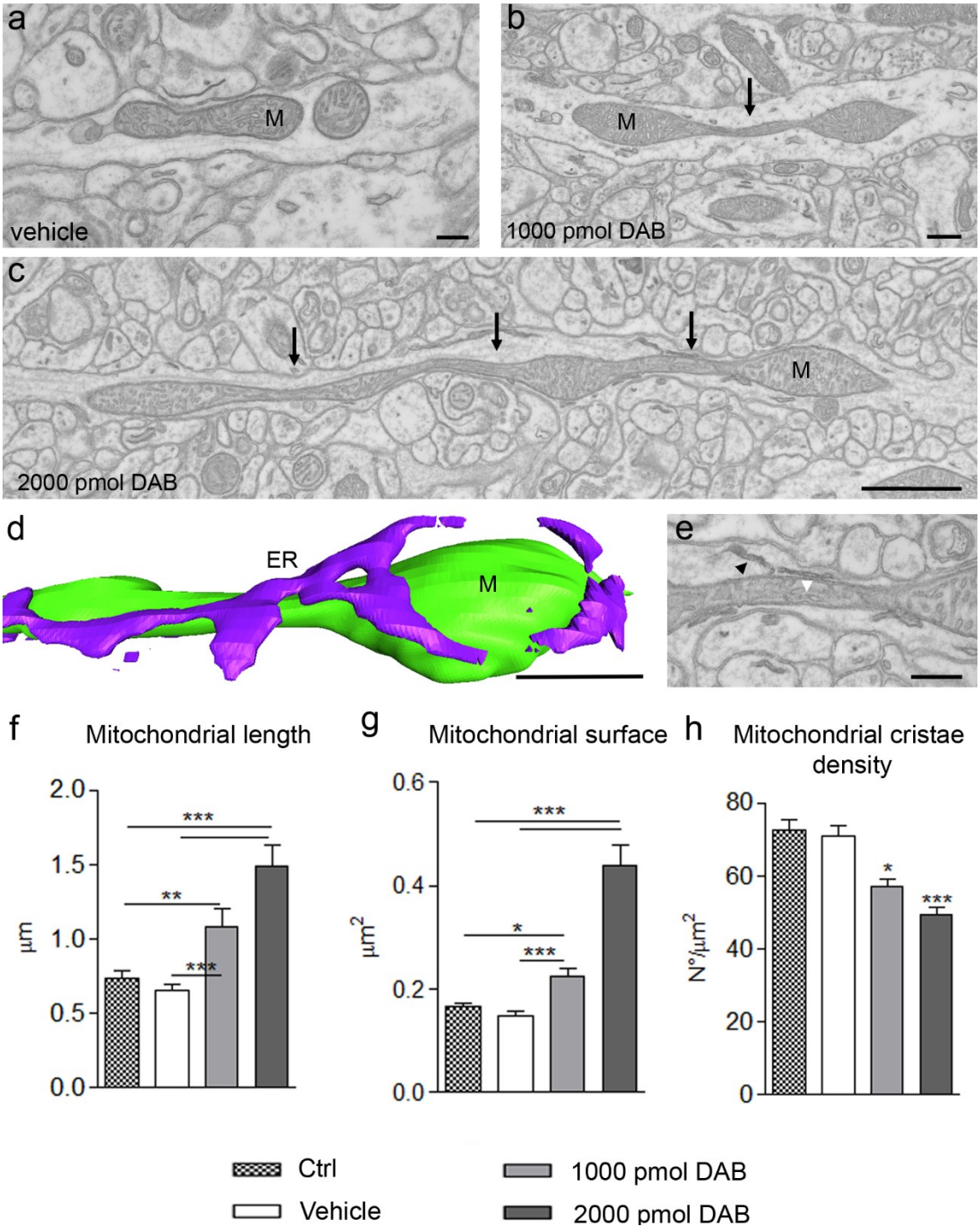

Figure 12. (a-c) *2D images of dendritic sections with at least one mitochondrial profile (M) in the hippocampal CA1 region of mice treated with vehicle* ***(a)****, 1000* ***(b)*** *and 2000 pmol DAB* ***(c)****. In these images is clearly visible the different mitochondrial morphology between the animals injected with DAB that presented elongated mitochondria, in which two or more units were interconnected by thin, tubular membrane extensions containing mitochondrial matrix and cristae* ***(arrows in image b and c; white arrowhead in the magnification in figure e)*** *and are often associated to the endoplasmic reticulum membrane (ER) in the restriction sites* ***(black arrowhead in e)*** *compared to the vehicle where are compact and well-separated. (Scale bar = 100 nm in a; 200 nm in b; 500 nm in c; 100 nm in e).* ***(d)*** *Example of three dimensional reconstruction of dendritic mitochondrion (green) with the endoplasmic reticulum (ER) (purple) that surround the elongated mitochondria in mice treated with 2000 pmol DAB. (Scale bar = 500 nm). The 3D reconstruction of this dendritic mitochondrion and ER membrane associated came from 20 serial sections.* ***(f-h)*** *DAB treatment significantly increase the mitochondria length* ***(f)****, surface* ***(g)****, and significantly reduced the mitochondrial cristae density* ***(h)****. Columns of each graph represent mean ± SEM of the indicated parameter, calculated in 2 animals for each group. (*P < 0.05, **P < 0.01, ***P < 0.001).*

9. Three-dimensional and fine structure of synaptic mitochondria in the CA1 region of hippocampus 24 hours after NOR training

To evaluate if the alterations in the dendritic mitochondria in the animals treated with DAB, were present also in the synaptic mitochondria we analysed the three-dimensional structure of these organelles in the pre-synaptic terminal of the hippocampal excitatory synapses (Figure 13a). In particular, with 3D reconstruction of 245 μm^3 (100 serial sections with a volume each of 7 μm x 7 μm x 0.05 μm) of tissue for a total number of pre-synaptic terminal analysed of 50 for each experimental group, we measured the pre-synaptic terminal volume (μm^3), the mitochondrial volume (μm^3) and the percentage of the pre-synaptic volume occupied by the mitochondrial volume (Table 15 and figure 13d-f). 3D analyses did not reveal any differences in mitochondrial characteristics among mice treated with DAB (1000 and 2000 pmol) and control or mice injected with vehicle. The same results were obtained with the quantitative analyses performed on 2D TEM images in which mitochondrial surface (μm^2) and mitochondrial cristae density of at least 70 mitochondrial profiles were evaluated (Table 16 and figure 13b, c).

Table 15

3D Synaptic mitochondria NOR (24 h)	Control	Vehicle	1000 pmol DAB	2000 pmol DAB
Pre-synaptic volume (μm^3)	0.248 ± 0.029	0.246 ± 0.022	0.266 ± 0.023	0.267 ± 0.046
Mitochondria volume (μm^3)	0.041 ± 0.005	0.049 ± 0.005	0.047 ± 0.005	0.045 ±0.011
Mitochondria cristae density (N° cristae / μm^2)	17.28 ± 1.50	18.71 ± 1.38	16.09 ± 1.38	14.57 ± 1.33

Table 15. *Quantitative 3D analyses of synaptic mitochondria in the apical dendrites layer of the hippocampal CA1 region. We measured the pre-synaptic and mitochondrial volume (μm^3) and the percentage of the synaptic volume occupied by the mitochondria calculated as the ratio between the mitochondrial volume (μm^3) and the pre-synaptic volume (μm^3) x 100. These analyses were done in 2 animals for each group and at least 40 synapse in a total volume of tissue analysed of 245 μm^3 (100 serial sections with a volume each of 7 μm x 7 μm x 0.05 μm) for animals. Values are reported as mean* ± SEM. *Measures were statistically analysed with Kruskal-Wallis test and corrected with Dunn's multiple comparison procedure. Means were considered statistically different when P < 0.05.*

Table 16

2D Synaptic mitochondria NOR (24 h)	Control	Vehicle	1000 pmol DAB	2000 pmol DAB
Mitochondria surface (μm^2)	0.165 ± 0.007	0.148 ± 0.009	0.147 ± 0.010	0.154 ± 0.009
Mitochondria cristae density (N° cristae / μm^2)	72.56 ± 3.11	66.51 ± 3.27	65.98 ± 2.39	65.31 ± 2.15

Table 16. *Quantitative analyses of synaptic mitochondria in the apical dendrites layer of the hippocampal CA1 region. We measured the mitochondrial surface (μm^2) and the mitochondrial cristae density. These analyses were done in 2 animals for each group and at least 70 mitochondria for groups. Values are reported as mean* ± SEM. *Measures were statistically analysed with Kruskal-*

Wallis test and corrected with Dunn's multiple comparison procedure. Means were considered statistically different when P < 0.05.

Figure 13

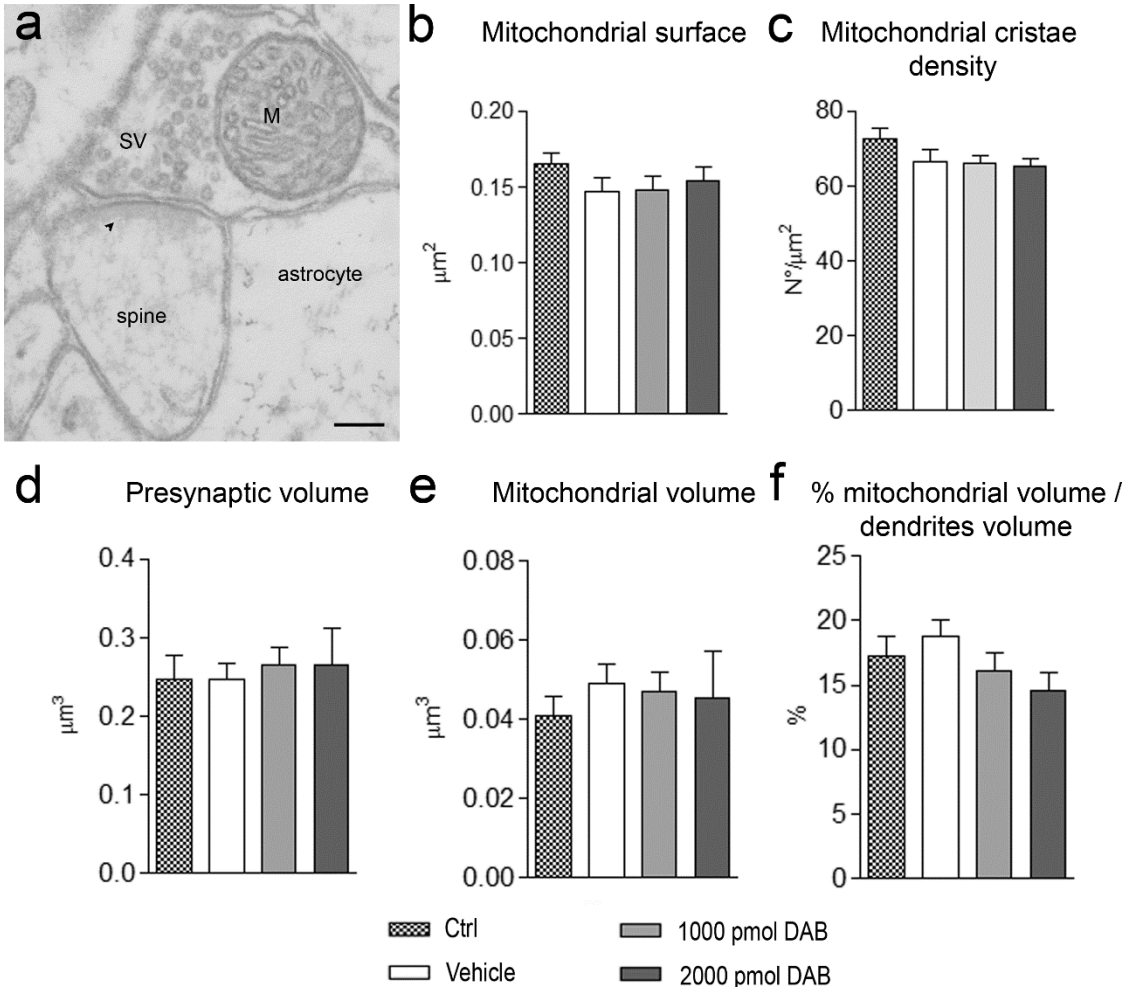

Figure 13. (a) *Example of 2D image of excitatory synapses with one mitochondrial profile (M) in the pre-synaptic terminal in the hippocampal CA1 region. In this image were indicated also the dendritic spine head with the PSD (arrowhead) and the astrocyte that surround the pre- and the post-synaptic terminal (Scale bar = 100 nm).* ***(b-c)*** *DAB treatment did not change the morphological features of synaptic mitochondria both the mitochondrial surface (μm^2)* ***(b)*** *and mitochondrial cristae density* ***(c)****. Moreover, the 3D analyses confirmed that the synaptic mitochondria preserved their architecture. We measured the pre-synaptic volume (μm^3), the mitochondrial volume (μm^3) and we calculated the percentage of pre-synaptic volume occupied by the mitochondria and DAB treated mice (1000 and 2000 pmol) presented the same values compared to mice injected with vehicle or control mice (ctrl). Columns of each graph represent mean ± SEM of the indicated parameter, calculated in 2 animals for each group.*

10. Rescue of morphological alterations induced by DAB administration through hippocampal co-injections of L-lactate

Our experiments revealed that intra-hippocampal injection of DAB in mice hippocampus was able to block long-term memory formation and caused important effects on spine number, synapse and dendritic mitochondrial morphology in hippocampal neurons from these animals. 24 hours after DAB treatment and following memory tests, the mice treated with DAB present a reduced spine density accompanied by an unaltered spines heads and PSDs volume, a reduction in the synaptic vesicle density and a significant change in the dendritic mitochondrial morphology. Our results indicated that block of glycogen metabolism led to an impairment in memory formation and altered number of hippocampal dendritic spines in the interested areas. Using behavioural and electrophysiological experiments, it was demonstrated that co-injection of L-lactate but not equicaloric concentration of glucose with DAB can rescue the phenotype (Suzuki et al., 2011). Given all these evidences, we decided to test whether, also in our experimental set-up, L-lactate co-injection was able to rescue the behavioural and morphological alterations. To answer this question, we studied the effect of 100 nmol L-lactate co-injected in mice hippocampus with 1000 pmol DAB. We observed that L-lactate treatment produced terrific effects on behavioural and at least some of the morphological defects induced by DAB alone. L-lactate injection significantly increased the spine density compared to mice injected with 1000 pmol DAB (*P < 0.05) (Table 17, figure 14a and 15g). In addition, L-lactate treatment significantly preserved the mitochondrial morphology that was now comparable to those of dendrites from neurons of mice injected with vehicle. With 3D analyses we measured the mitochondrial and dendrites volume in order to calculate the percentage of dendritic volume occupied by mitochondria and we demonstrated that mice treated with L-lactate all mitochondrial parameters measured were similar to those of mice injected with vehicle (*P < 0.05 between mice injected with 1000 pmol DAB and 1000 pmol DAB + 100 nmol L-lactate). On the contrary, L-lactate administration had no effect on synaptic vesicle density, that was still reduced with respect to that of mice injected with vehicle (*P < 0.05 vehicle vs 1000 pmol DAB + 100 nmol L-lactate) and similar to the value of recorded from 1000 pmol DAB treated samples (*P < 0.05 vehicle vs 1000 pmol DAB). As a control, we treated mice with only 100 nmol L-lactate, in order to monitor the effects of this compound alone and we confirmed that in all the parameters measured the results were comparable with the mice treated with vehicle (Tables 17-19 and Figures 14-16).

Table 17

2D analyses NOR (24 h)	Vehicle	1000 pmol DAB	100 nmol L-lactate	1000 pmol DAB + 100 nmol L-lactate
Spine density (N° spines / 10 μm)	11.04 ± 0.21	10.08 ± 0.17	10.80 ± 0.15	10.86 ± 0.18
Pre-synaptic surface (μm^2)	0.191 ± 0.009	0.197 ± 0.012	0.198 ± 0.011	0.184 ± 0.011
Synaptic vesicle density (N°vesicles / μm^2)	200.4 ± 7.3	167.5 ± 6.1	199.1 ± 7.1	176.0 ± 8.9

Figure 14

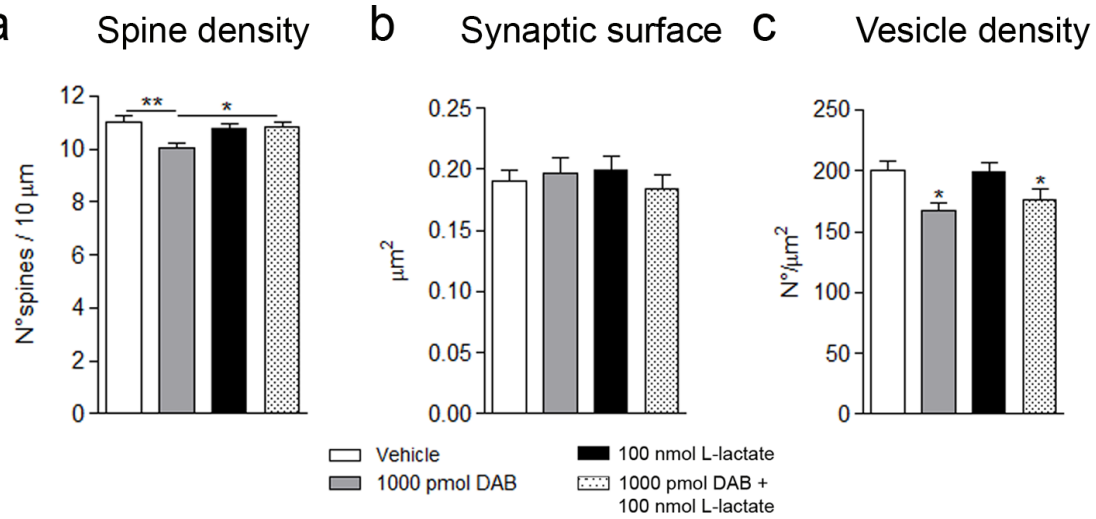

Table 17 and Figure 14. *Morphometric analyses of excitatory synapses of apical dendrites in the CA1 region of the hippocampus 24 hours after injection of vehicle, 1000 pmol DAB, 100 nmol L-lactate and 1000 pmol DAB + 100 nmol L-lactate. We measured the spine density after Golgi-cox staining in 10 stained neurons for each mouse; we analysed 3 mice for each experimental group* ***(a)****. 2D TEM images were used to evaluate the pre-synaptic surface* ***(b)*** *and the synaptic vesicle density* ***(c)****, in 75 synapses for each group, in 2 mice treated with vehicle and 2 treated with 1000 pmol DAB. Values are reported as mean ± SEM. Measures were statistically analysed with Kruskal-Wallis test and corrected with Dunn's multiple comparison procedure. Means were considered statistically different when P < 0.05. (*P < 0.05 and **P < 0.01).*

Table 18

3D Spine density and dendritic mitochondria NOR (24 h)	Vehicle	1000 pmol DAB	100 nmol L-lactate	1000 pmol DAB + 100 nmol L-lactate
Mitochondrial density (N° / μm^3)	0.598 ± 0.070	0.394 ± 0.042	0.640 ± 0.089	0.635 ± 0.089
Dendrites volume (μm^3)	5.942 ± 0.401	5.164 ± 0.366	5.975 ± 0.552	5.013 ± 0.358
Mitochondrial volume (μm^3)	0.656 ± 0.056	0.904 ± 0.058	0.641 ± 0.047	0.659 ± 0.049
% mitochondria volume / dendrites volume (μm^3)	11.84 ± 1.15	18.03 ± 0.94	11.99 ± 0.98	14.17 ± 0.94
Spine density (N° of spines/μm^3)	3.247 ± 0.222	2.407 ± 0.158	3.207 ± 0.191	3.234 ± 0.233

Table 18. *Quantitative 3D analyses of dendritic mitochondria in the apical dendrites layer of the hippocampal CA1 region. We measured the dendritic and mitochondrial volume (μm^3) and the percentage of the dendritic volume occupied by the mitochondria calculated as the ratio between the mitochondrial volume (μm^3) and the dendritic volume (μm^3) x 100. We calculated also the mitochondrial density as the ratio between the number of mitochondria and the dendritic volume associated. Moreover, we analysed the dendritic spine density as the ratio between the number of spines and the dendritic volume associated. These analyses were done in 2 animals for each group and at least 20 dendrites in a total volume of tissue analysed of 980 μm^3 for animals (100 serial sections with a volume each of 14 μm x 14 μm x 0.05 μm) for animals. Values are reported as mean* ± SEM. *Measures were statistically analysed with Kruskal-Wallis test and corrected with Dunn's multiple comparison procedure. Means were considered statistically different when P < 0.05.*

Figure 15

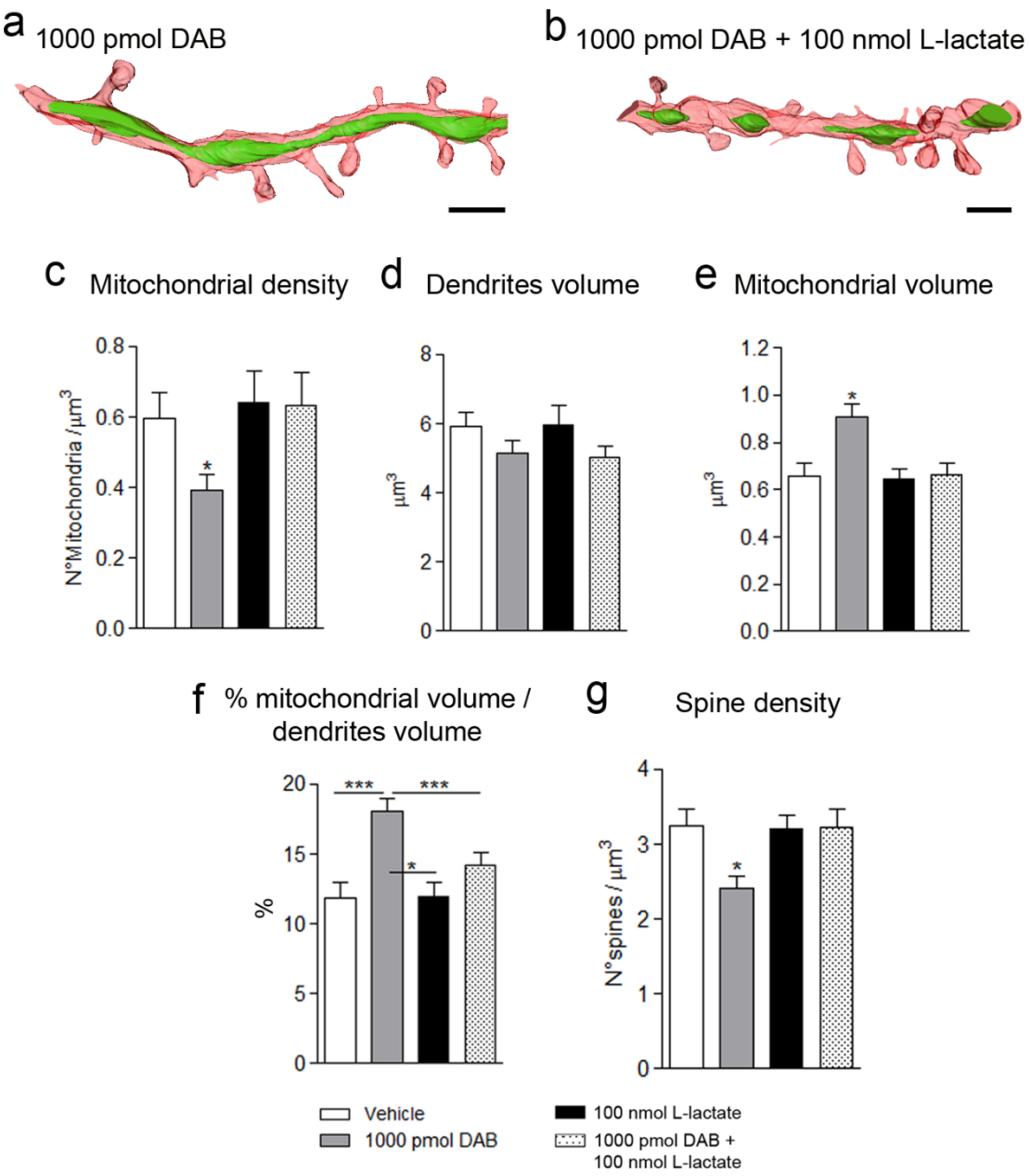

Figure 15. (a, b) *Examples 3D reconstruction of dendrites with their spines (red) and mitochondria (green) in mice injected with 1000 pmol DAB* ***(a)*** *and 1000 pmol DAB + 100 nmol L-lactate* ***(b)****. (Scale bar = 1 µm). In the images we could observe the rescue of mitochondrial morphology compared to 1000 pmol treated mice.****(c-f)*** *Graphs of 3D analyses of mitochondrial features, where we could note the increase of mitochondrial density for µm³ of dendrite, the rescue of mitochondrial volume (µm³) and the decrease of the percentage of dendritic volume occupied by the mitochondria in 1000 pmol DAB + 100 nmol L-lactate injected mice.* ***(g)*** *3D analyses of spine density rescue. Columns of each graph represent mean ± SEM of the indicated parameter, calculated in 2 animals for each group. (*P < 0.05, ***P < 0.001).*

To conclude the analysis of mitochondrial morphology we observed also the fine structure of these organelles, with a morphometrical analysis performed on 2D TEM images.
We measured the mitochondrial length (μm), surface (μm^2), the number of the cristae and we calculated the mitochondrial cristae density (N° cristae / μm^2). We found a significant rescue of mitochondrial length (*P < 0.05) and mitochondrial cristae density (Table 19 and figure 16e) in mice treated with 1000 pmol DAB + 100 nmol L-lactate compared to mice injected with 1000 pmol DAB (*P < 0.05). Mice injected only with 100 nmol L-lactate presented the same results compared with vehicle (Table 19 and figure 16c-e).

Table 19

2D Dendritic mitochondria NOR (24 h)	**Vehicle**	**1000 pmol DAB**	**100 nmol L-lactate**	**1000 pmol DAB + 100 nmol L-lactate**
Mitochondrial length (μm)	0.657 ± 0.036	1.080 ± 0.126	0.805 ± 0.053	0.742 ± 0.041
Mitochondrial surface (μm^2)	0.148 ± 0.009	0.225 ± 0.013	0.165 ± 0.009	0.171 ± 0.027
Mitochondrial cristae density (N° cristae / μm^2)	71.07 ± 2.87	57.08 ± 2.08	69.33 ± 2.09	67.93 ± 2.41

Table 19. *Quantitative morphometrical analyses of dendritic mitochondria in the apical dendrites layer of the hippocampal CA1 region. We measured the mitochondrial length, surface and the mitochondrial cristae density (N° cristae / μm^2). These analyses were done in 2 animals for each group and at least 70 mitochondria for groups. Values are reported as mean* ± SEM. *Measures were statistically analysed with Kruskal-Wallis test and corrected with Dunn's multiple comparison procedure. Means were considered statistically different when P < 0.05.*

Figure 16

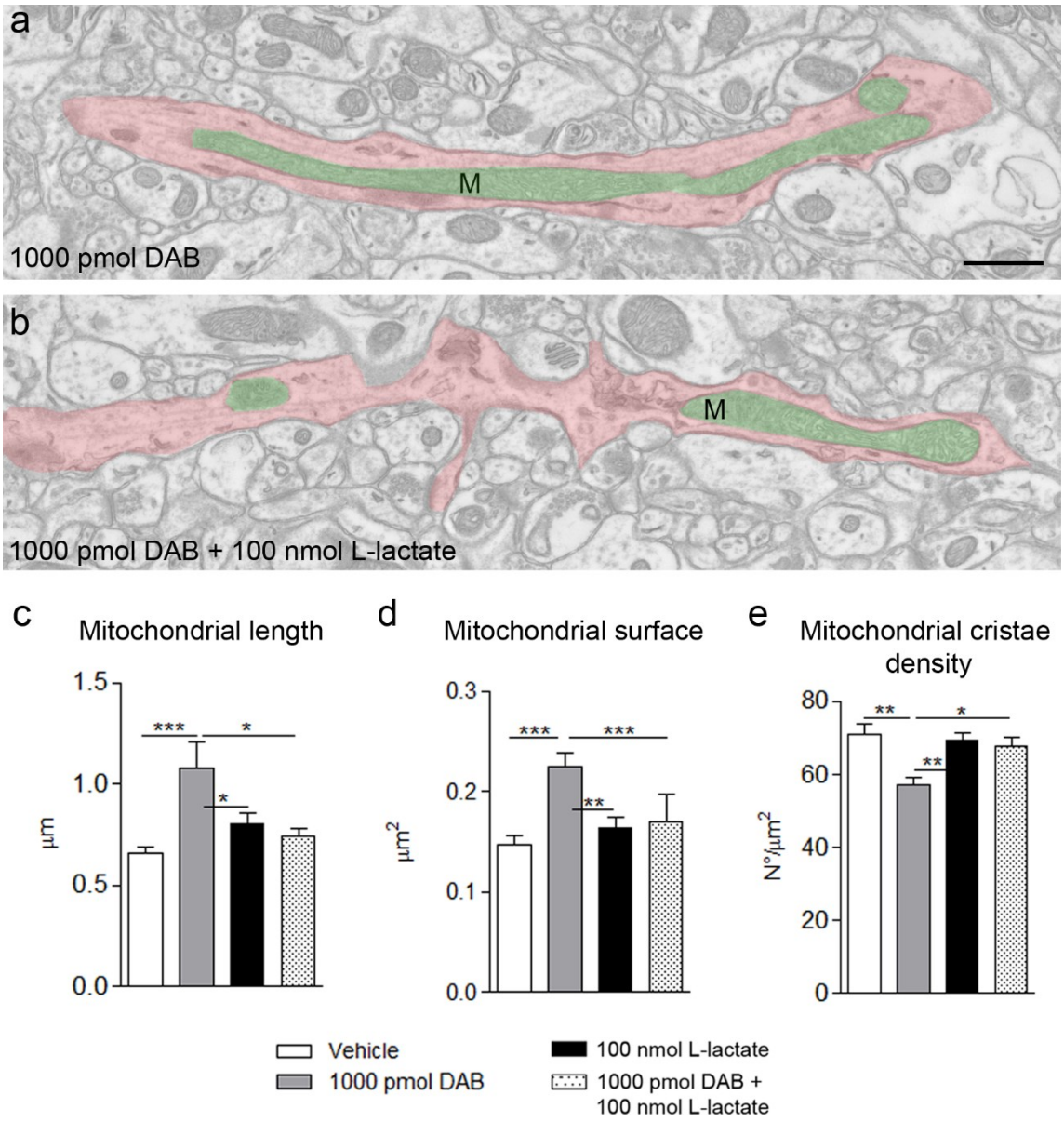

Figure 16. (a, b) *2D images of dendritic sections with at least one mitochondrial profile (M) in the hippocampal CA1 region of mice treated with 1000 pmol DAB* ***(a)*** *and 1000 pmol DAB + 100 nmol L-lactate* ***(b)****. In these images is clearly visible the different mitochondrial morphology between the animals injected with 1000 pmol DAB that presented elongated mitochondria (M) compared to the mice treated with 1000 pmol DAB + 100 nmol L-lactate where are compact and well-separated. (Scale bar = 500 nm).* ***(c-e)*** *Co-injection of L-lactate and DAB significantly rescue the mitochondria length* ***(c)****, surface* ***(d)****, and significantly increase the mitochondrial cristae density* ***(e)****. Columns of each graph represent mean ± SEM of the indicated parameter, calculated in 2 animals for each group. (*P < 0.05, **P < 0.01, ***P < 0.001).*

DISCUSSION

Here we show that blocking glycogenolysis in hippocampal astrocytes, with 1,4-dideoxy-1,4-imino-D-arabinitol, impairs intermediate- and long-term memory formation and affects the structure of excitatory synapses in mice CA1. While memory impairments are rescued by co-administration of L-lactate, the latter is only partially able to revert the anatomical defects at the synapse suggesting that, besides its well described effect on the decrease in lactate synthesis and shuttling from astrocytes to neurons, other, still undescribed, mechanisms of action of DAB might be at play during learning and memory in neurons from rodent brains.

It was previously shown that, in mice, brain glycogen synthesis is crucial for long-term memory formation and learning dependent synaptic plasticity (Duran et al., 2013). On the other hand, pharmacological interference with glycogenolysis using inhibitors of glycogen phosphorylase, leads to a decrease in lactate production in hippocampal astrocytes and its shuttling to neurons thus altering their metabolic coupling. The pharmacological properties of DAB as an inhibitor of glycogen phosphorylase and synthase have been extensively described and it was shown that, not only DAB treatment has profound effects on both glycogen synthesis and degradation (Gibbs et al., 2006; Walls et al., 2008 and references therein), but it also reduces lactate release from astrocytes in vivo (Suzuki et al., 2011). The specificity of DAB on glycogen metabolism in glial cells is mainly a consequence of the fact that glycogen has never been found in neurons of the hippocampus and neocortex of adult rodent brain (Magistretti, 2008 and references therein).

1. Lactate derived from glycogen metabolism has a critical role in intermediate- and long-term memory formation

Here we evaluated the effect of DAB administration on memory formation, with two memory paradigms, passive avoidance (PA) and novel object recognition (NOR) (Antunes and Biala, 2012).

We first tested the effects of DAB administration on long-term memory by means of the PA task, a fear-aggravated test, used to evaluate learning and memory in rodents and we observed that, unlike previous experimental data in rats (Suzuki et al., 2011), DAB did not affect long-term memory when evaluated with this behavioural test. We then carried out the NOR test to study intermediate- and long-term episodic memory after DAB injection and, here, we were able to show that the pharmacological treatment affected both intermediate-

and long-term episodic memory, in a dose dependent manner.

Our results from mice behavioural tests extend previous findings showing that, in different animal models and brain circuits, lactate reduction impairs intermediate- and long-term memory formation. Indeed the first report about an amnesic effect of DAB, dates back to 2006, when it was shown that the administration of this drug interfered with learning memory formation in young chicks (Gibbs et al., 2006). The relevance of the astrocyte-neuron lactate transport in this phenomenon was elegantly demonstrated in further experiments in rats, where, besides intra-hippocampal DAB administration, the effects of neuronal and astroglial lactate transporters downregulation were examined. Here the authors not only demonstrated that synaptic plasticity and long-term memory formation were dependent on the presence of lactate, but that these events were also critically dependent on the capability of the astrocytes to transfer lactate into the extracellular space and of the neurons to internalize it from this same compartment, through the expression of the specific lactate transporters (Suzuki et al., 2011). Recently, it was also shown that different kind of memory circuits are affected by the lack of maintenance of the the astrocyte–neuron lactate transfer, as its integrity is also crucial in the retrieval of addictive drug memories. In fact, also in this context, DAB injection into basolateral amigdala in rat brains was able to persistently reduce conditioned responses to cocaine (Boury-Jamot et al., 2015).

In agreement with all the previous published data, also in our experimental set-up in mice, the simultaneous administration of DAB and L-lactate completely removes the block to long-term memory formation when mice are challenged with the NOR task 24 hours after treatment and training. These pieces of evidences confirm that metabolic coupling between astrocytes and neurons via lactate is required for hippocampal long-term memory formation also in mice. Similarly our experiments also confirm that the effect of intra-hippocampal injection of DAB on memory formation, although long-lasting, was transient as if re-trained (six days after drug administration) and re-tested 24 hours after the new training, treated mice were able to properly form new memories.

2. The critical role of lactate in learning-induced post-synaptic changes

Lactate transfer from astrocytes into neurons is essential for memory formation and for the induction of all the molecular changes that are required for this process to occur. In fact, upon learning and memory training, a number of genes and proteins are either up-

regulated (Arc, c-Fos, and Zif268) (Yang et al., 2014) or post-translationally modified (i.e. CREB and cofilin are increasingly phosphorylated). pCREB is known to be critical for CREB-dependent gene expression regulation, while cofilin is the final effector of a signaling cascades that links extracellular stimuli to actin cytoskeletal dynamics and finally evokes those actin cytoskeletal rearrangements that are needed to dendritic spine remodeling during long-term memory and neural plasticity (Suzuki et al. 2011 and references therein).

It is known that long term-potentiation (LTP) and memory defects are often associated with alterations in dendritic spines morphology and density (Oertner and Matus, 2005; Segal, 2005; Bhatt et al., 2009; Caroni et al., 2012). We then firstly investigated - with a low resolution approach - if differences in the density of hippocampal dendritic spines were present and correlated with defects in long-term memory in mice treated with DAB, and if these defects were rescued by L-lactate administration. We thus performed analyses of spine density in apical dendrites from CA1 pyramidal neurons (*stratum radiatum*) by means of the Golgi-Cox staining technique focusing on the long-term memory effect (24 hours after training). Our data demonstrated that 24 hours after training a significant increase in dendritic spine density in the CA1 of the hippocampus is observed in tissues from trained vehicle-treated animals with respect to untrained ones. Interestingly, upon treatment with DAB before the memory tasks, hippocampal neurons showed a marked reduction in dendritic spine density compared to neurons from trained mice injected with vehicle. This reduction occurs independently from the memory paradigm used showing that, despite performing as well as vehicle-treated mice in the PA test, hippocampal neurons from DAB-treated mice experienced lactate deprivation and possibly underwent the same morphological alterations as hippocampal neurons from DAB-treated mice trained with the NOR. It is known that the neural circuits that mediate fear-aggravated learning in rodents comprise the amygdala and the medial prefrontal cortex and that these two brain areas play a fundamental role in the acquisition, consolidation and retrieval of fear memory (reviewed in Herry and Johansen, 2014). It is thus conceivable that hippocampal DAB injection alone would not elicit a measurable response in the memory test while still affecting the architecture of local memory circuits in the hippocampus.

Direct contact between astrocytic process and spines (through Ephrins and their receptors) is considered an important determinant of spine density and morphology in the hippocampus of adult mice. Based on the observations of Murai and colleagues (Murai et

al., 2003), a reduction in spine density could be expected if the volume of hippocampal astrocytes is increased (i.e. in case of reactive astrogliosis). To verify whether astrogliosis could, at least partially, account for the reduction in spine density we observed, we evaluated astrogliosis on hippocampal sections of vehicle and DAB-treated mice and found none, thus allowing us to exclude any influence of astrocytes swelling on the decrease in dendritic spine density in our experimental model.

To confirm, with higher resolution, the data derived from the Golgi-Cox method and to evaluate if the defect in spine density we observed with the low-resolution approach was associated with other ultrastructural defects in hippocampal excitatory synapses, we performed an in-depth high-resolution study based on morphometric analysis on 2D transmission electron microscopy images (Folci et al., 2016). Interestingly, despite the effect of DAB on spine density, individual spine was not affected as post-synaptic density (PSD) length and thickness were the same in animals treated with vehicle or DAB. Through Serial-Block Face Scanning Electron Microscopy (SBF-SEM) (Denk and Horstmann, 2004) and subsequent volume reconstruction and measurements, we confirmed the results obtained with both the Golgi-Cox and 2D EM analyses: the density of the dendritic spine was reduced while the PSD volume remained unchanged in mice treated with DAB. Enlargement of the head is a characteristic of dendritic spines that is related to increased synaptic strength during structural plasticity upon learning; however -and in agreement with the observation that PSD volume is unchanged upon DAB treatment- spine head size was unchanged. It has to be stressed however that transient changes in spine head size (associated with increased level of glutamate receptors and accumulation of F-actin) (Segal, 2005) might have occurred at shorter intervals from training and testing (minutes to few hours) and as we have performed ultrastructural analyses only at 24 hours after the learning session, we might have failed to detect them. Instead, at this time interval, we were able to highlight the effect of DAB in reducing the number of dendritic spines. Formation of new spines upon learning is indeed a phenomenon that, depending on the learning protocols and systems used, might occur with delays of several hours (up to 18 hours) from the learning session (Caroni et al., 2012 and references therein), thus our observation about changes in spine density, besides being temporally associated with the formation of long-term memory as it is described in the literature and as we recorded in our experimental set-up, fits well with the time course of spine formation and maintenance upon learning, according to the large body of literature.

3. Mitochondrial structure in apical dendrites is deeply affected by DAB treatment

Recent data have demonstrated that altered brain metabolism is associated with changes in mitochondria dynamics by interfering with their continuous cycles of fission and fusion (Youle and Van der Blieck, 2012). The major proteins that regulate the assembly and stability of the respiratory chain, the remodelling of mitochondrial cristae and mitochondrial morphology are sensitive to the energetic demand of the cell, which directly affects the development and maintenance of synapse. In the pre-synaptic terminals, mitochondria are needed to support neurotransmission by generating ATP and by buffering Ca^{2+} ions; while in dendrites they are needed for activity-dependent synaptic formation and to support synaptic density (Li et al., 2004). Given our pharmacological interference with neuronal energy metabolism in the hippocampus, we asked ourselves whether mitochondrial structure was affected in our experimental model. Indeed, in 3D reconstructed dendrites of DAB-treated mouse hippocampi, we observed a significant change in mitochondria number, shape, and volume. We found that, instead of uniformly compact and well-separated mitochondria as seen in dendrites from vehicle-treated samples, the apical dendrites of neurons from mice treated with DAB contained elongated mitochondria, in which two or more tubular units were interconnected by long and thin membrane extensions containing matrix and cristae. Dendritic mitochondria in DAB treated mice were longer, reduced in number and bigger compared to the dendritic mitochondria of mice treated with vehicle. Both 2D EM projections and 3D volume reconstructions strongly suggest that pharmacological inhibition of glycogen metabolism with DAB could affect dendritic mitochondria dynamics by specifically interfering with their fission and possibly with their transport. Besides being crucial for their proper functioning, mitochondria fusion and fission are also relevant to ensure mitochondria transport and localization in neurons. It has been recently demonstrated that altered mitochondrial transport could affect synaptic homeostasis and it is a shared common feature in many neurodegenerative diseases like Alzheimer's and Parkinson's diseases (Cai and Tammineni, 2016; Zhang et al., 2016 and references therein).

4. DAB administration induces pre-synaptic changes

Unexpectedly, our ultrastructural analyses showed a profound and significant reduction of synaptic vesicle density in terminals of mice treated with DAB, while the size of the pre-synaptic compartment was once again unaffected. Even if the size of the synaptic vesicle pool and the mitochondrial energy supply are indeed tightly connected, we failed to detect any difference in the architecture of mitochondria in these compartments thus allowing us to exclude an effect of the last upon the first one. Interestingly, as mentioned above, pre-synaptic terminal profiles are not enlarged or swelled. This allowed us to exclude a defect in the endocytic step required for local vesicle recycling and there, has been up to date, no evidence about massive exocytosis. Our preliminary observations did not allow us to explain the reasons for this specific effect of DAB on synaptic vesicle density, we could only hypothesize a couple of scenarios that will need further investigation: the first is that the drug, through some direct or indirect mechanism, interferes with the local vesicle recycling possibly at the level of the bulk endosome: the second is that it might interfere with the transport of synaptic vesicle precursors from neuronal soma.

5. Hippocampal co-injection of L-lactate rescues post- but not pre-synaptic defects

As mentioned before, co-injection of DAB and L-lactate is able to revert the memory impairment induced by the drug as already described in chicks and rats (Gibbs et al. 2006; Suzuki et al., 2011). Interestingly, besides behavioural rescue, Golgi-Cox staining showed that, in apical dendrites of CA1 pyramidal neurons 24 hours after DAB administration and NOR training, spine density was rescued as well, bringing back spine density to control level. These data were confirmed with ultrastructural analyses through volume reconstruction and once again strongly indicated that the mechanism of action of DAB in the inhibition of long-term memory formation and in dendritic spine plasticity is mediated by the inhibition of lactate release from astrocytes and impaired shuttling of this energetic substrate to neurons. In support of the direct involvement of lactate in mediating these post-synaptic events there are all the data pointing to an exclusive post-synaptic localization of the neuronal isoform of the lactate transporter (MCT-2). Indeed numerous reports demonstrated that this molecule

is present exclusively on the plasma membrane of the dendritic spine, associated with the post-synaptic density and in vesicular intracellular compartments where it co-localize with NMDA receptors (Pellerin et al., 2005; Chiry et al., 2008). Simultaneous administration of L-lactate with DAB was also able to completely abolish the described effects of the drug on dendritic mitochondria giving further support to the relevance of the metabolic coupling between astrocytes and neurons in promoting synaptic plasticity and brain homeostasis.

Anyway, when analysing the ultrastructure of excitatory synapses, we found that vesicle density in pre-synaptic terminals was not rescued by lactate co-administration as it was comparable to vesicle density of pre-synaptic terminals of DAB only treated mice. This observation, supported also by the lack of experimental evidence about the presence of lactate transporters at the pre-synaptic terminal in different brain areas in both rodents and humans, seems to suggest that, besides its well described effect on the decrease in lactate synthesis, other, still undescribed, mechanisms of action of DAB might be at play during learning and memory in neurons from rodent brains.

CONCLUSION

Our results indicate that, bilateral intra-hippocampal injection of DAB caused an impairment of long-term memory formation at 24 hours as evaluated with novel object recognition (NOR) test. This behavioural alteration was accompanied by important morphological alteration of excitatory hippocampal synapses and dendritic mitochondria.

L-lactate was able to rescue the behavioural and the spine density impairment induced by DAB, but not the pre-synaptic effect, namely the reduction in synaptic vesicle density on excitatory hippocampal synapses.

Finally, our data for the first time demonstrated that the interference with lactate supply from astrocytes to neurons, beside behavioural and electrophysiological effects, exerts also anatomical effects on neuronal connectivity.

REFERENCES

Adeva-Andany, M., López-Ojén, M., Funcasta-Calderón, R., Ameneiros-Rodríguez, E., Donapetry-García, C., Vila-Altesor, M., & Rodríguez-Seijas, J. (2014). Comprehensive review on lactate metabolism in human health. Mitochondrion, 17, 76-100.

Alberini, C. M. (2009). Transcription factors in long-term memory and synaptic plasticity. Physiological reviews, 89(1), 121-145.

Allaman, I., Bélanger, M., & Magistretti, P. J. (2015). Methylglyoxal, the dark side of glycolysis. Glycolysis at 75: Is it Time to Tweak the First Elucidated Metabolic Pathway in History?, 75.

Almeida, A., Moncada, S., & Bolaños, J. P. (2004). Nitric oxide switches on glycolysis through the AMP protein kinase and 6-phosphofructo-2-kinase pathway. Nature cell biology, 6(1), 45-51.

Andersen, B., Rassov, A., Westergaard, N., & lundgren, K. (1999). Inhibition of glycogenolysis in primary rat hepatocytes by 1, 4-dideoxy-1, 4-imino-D-arabinitol. Biochemical Journal, 342(3), 545-550.

Anderson, C. M., & Swanson, R. A. (2000). Astrocyte glutamate transport: review of properties, regulation, and physiological functions. Glia, 32(1), 1-14.

Antunes, M., & Biala, G. (2012). The novel object recognition memory: neurobiology, test procedure, and its modifications. Cognitive processing, 13(2), 93-110.

Attwell, D., & Laughlin, S. B. (2001). An energy budget for 106arburg106et in the grey matter of the brain. Journal of Cerebral Blood Flow & Metabolism, 21(10), 1133-1145.

Bailey, C. H., Kandel, E. R., & Harris, K. M. (2015). Structural components of synaptic plasticity and memory consolidation. Cold Spring Harbor perspectives in biology, 7(7), a021758.

Bak, L. K., Schousboe, A., & Waagepetersen, H. S. (2006). The glutamate/GABA - glutamine cycle: aspects of transport, neurotransmitter homeostasis and ammonia transfer. Journal of neurochemistry, 98(3), 641-653.

Balestrino, M., Aitken, P. G., & Somjen, G. G. (1986). The effects of moderate changes of extracellular K+ and Ca 2+ on synaptic and neural function in the CA1 region of the hippocampal slice. Brain research, 377(2), 229-239.

Barros, L. F., Bittner, C. X., Loaiza, A., & Porras, O. H. (2007). A quantitative overview of glucose dynamics in the gliovascular unit. Glia, 55(12), 1222-1237.

Barros, L. F. (2013). Metabolic 107arburg107et by lactate in the brain. Trends in neurosciences, 36(7), 396-404.

Baylor, D. A., & Nicholls, J. G. (1969). Changes in extracellular potassium concentration produced by neuronal activity in the central nervous system of the leech. The Journal of physiology, 203(3), 555.

Benveniste, H., Drejer, J., Schousboe, A., & Diemer, N. H. (1984). Elevation of the extracellular concentrations of glutamate and aspartate in rat hippocampus during transient cerebral ischemia monitored by intracerebral microdialysis. Journal of neurochemistry, 43(5), 1369-1374.

Berg, J. M., Tymoczko, J. L., & Stryer, L. (2002). Biochemistry. 5th.

Bergles, D. E., & Jahr, C. E. (1998). Glial contribution to glutamate uptake at Schaffer collateral–commissural synapses in the hippocampus. The Journal of neuroscience, 18(19), 7709-7716.

Berkich, D. A., Ola, M. S., Cole, J., Sweatt, A. J., Hutson, S. M., & LaNoue, K. F. (2007). Mitochondrial transport proteins of the brain. Journal of neuroscience research, 85(15), 3367-3377.

Bhatt, D. H., Zhang, S., & Gan, W. B. (2009). Dendritic spine dynamics. Annual review of physiology, 71, 261-282.

Bittar, P. G., Charnay, Y., Pellerin, L., Bouras, C., & Magistretti, P. J. (1996). Selective distribution of lactate dehydrogenase isoenzymes in neurons and astrocytes of human brain. Journal of Cerebral Blood Flow & Metabolism, 16(6), 1079-1089.

Bittner, C. X., Loaiza, A., Ruminot, I., Larenas, V., Sotelo-Hitschfe, T., Gutiérrez, R., ... & Barros, L. F. (2010). High resolution measurement of the glycolytic rate. Frontiers in neuroenergetics, 2, 26.

Boumezbeur, F., Petersen, K. F., Cline, G. W., Mason, G. F., Behar, K. L., Shulman, G. I., & Rothman, D. L. (2010). The contribution of blood lactate to brain energy metabolism in humans measured by dynamic 13C nuclear magnetic resonance spectroscopy. The Journal of Neuroscience, 30(42), 13983-13991.

Bourne, J. N., & Harris, K. M. (2008). Balancing structure and function at hippocampal dendritic spines. Annual review of neuroscience, 31, 47.

Boury-Jamot, B., Halfon, O., Magistretti, P. J., & Boutrel, B. (2016). Lactate release from astrocytes to neurons contributes to cocaine memory formation. BioEssays, 38(12), 1266-1273.

Boury-Jamot, B., Carrard, A., Martin, J. L., Halfon, O., Magistretti, P. J., & Boutrel, B. (2015). Disrupting astrocyte–neuron lactate transfer persistently reduces conditioned responses to cocaine. Molecular psychiatry.

Bouzier - Sore, A. K., Voisin, P., Bouchaud, V., Bezancon, E., Franconi, J. M., & Pellerin, L. (2006). Competition between glucose and lactate as oxidative energy substrates in both neurons and astrocytes: a comparative NMR study. European Journal of Neuroscience, 24(6), 1687-1694.

Braida, D., Sacerdote, P., Panerai, A. E., Bianchi, M., Aloisi, A. M., Iosuè, S., & Sala, M. (2004). Cognitive function in young and adult IL (interleukin)-6 deficient mice. Behavioural brain research, 153(2), 423-429.

Braida, D., Donzelli, A., Martucci, R., Ponzoni, L., Pauletti, A., Langus, A., & Sala, M. (2013). Mice discriminate between stationary and moving 2D shapes: application to the object recognition task to increase attention. Behavioural brain research, 242, 95-101.

Bramham, C. R. (2008). Local protein synthesis, actin dynamics, and LTP consolidation. Current opinion in neurobiology, 18(5), 524-531.

Bröer, S., Rahman, B., Pellegri, G., Pellerin, L., Martin, J. L., Verleysdonk, S., … & Magistretti, P. J. (1997). Comparison of Lactate Transport in Astroglial Cells and Monocarboxylate Transporter 1 (MCT 1) Expressing Xenopus laevis Oocytes expression of two different monocarboxylate transporters in astroglial cells and neurons. Journal of Biological Chemistry, 272(48), 30096-30102.

Brooks, V. B. (1986). The neural basis of motor control. Oxford University Press.

Brooks, G. A. (2009). Cell–cell and intracellular lactate shuttles. The Journal of physiology, 587(23), 5591-5600.

Brown, A. M. (2004). Brain glycogen re-awakened. Journal of neurochemistry, 89(3), 537-552.

Buttgereit, A., Lelios, I., Yu, X., Vrohlings, M., Krakoski, N. R., Gautier, E. L., ... & Greter, M. (2016). Sall1 is a transcriptional regulator defining microglia identity and function. Nature Immunology.

Cahn, R. D., Zwilling, E., Kaplan, N. O., & Levine, L. (1962). Nature and development of lactic dehydrogenases. Science, 136(3520), 962-969.

Cai, Q., & Tammineni, P. (2016). Alterations in Mitochondrial Quality Control in Alzheimer's Disease. Frontiers in cellular neuroscience, 10.

Cappello, V., Vezzoli, E., Righi, M., Fossati, M., Mariotti, R., Crespi, A., ... & Francolini, M. (2012). Analysis of neuromuscular junctions and effects of anabolic steroid administration in the SOD1G93A mouse model of ALS. Molecular and Cellular Neuroscience, 51(1), 12-21.

Caroni, P., Donato, F., & Muller, D. (2012). Structural plasticity upon learning: regulation and functions. Nature Reviews Neuroscience, 13(7), 478-490.

Cater, H. L., Benham, C. D., & Sundstrom, L. E. (2001). Neuroprotective role of monocarboxylate transport during glucose deprivation in slice cultures of rat hippocampus. The Journal of physiology, 531(2), 459-466.

Chaudhry, F. A., Lehre, K. P., van Lookeren Campagne, M., Ottersen, O. P., Danbolt, N. C., & Storm-Mathisen, J. (1995). Glutamate transporters in glial plasma membranes: highly differentiated localizations revealed by quantitative ultrastructural immunocytochemistry. Neuron, 15(3), 711-720.

Chen, L. Y., Rex, C. S., Casale, M. S., Gall, C. M., & Lynch, G. (2007). Changes in synaptic morphology accompany act110arburg110eting during LTP. The Journal of neuroscience, 27(20), 5363-5372.

Chiry, O., Fishbein, W. N., Merezhinskaya, N., Clarke, S., Galuske, R., Magistretti, P. J., & Pellerin, L. (2008). Distribution of the monocarboxylate transporter MCT2 in human cerebral cortex: an immunohistochemical study. Brain research, 1226, 61-69.

Chuquet, J., Quilichini, P., Nimchinsky, E. A., & Buzsáki, G. (2010). Predominant enhancement of glucose uptake in astrocytes versus neurons during activation of the somatosensory cortex. The Journal of Neuroscience, 30(45), 15298-15303.

De Pittà, M., Brunel, N., & Volterra, A. (2016). Astrocytes: orchestrating synaptic plasticity?. Neuroscience, 323, 43-61.

De Vivo, D. C., Trifiletti, R. R., Jacobson, R. I., Ronen, G. M., Behmand, R. A., & Harik, S. I. (1991). Defective glucose transport across the blood-brain barrier as a cause of persistent hypoglycorrhachia, seizures, and developmental delay. New England Journal of Medicine, 325(10), 703-709.

Debernardi, R., Pierre, K., Lengacher, S., Magistretti, P. J., & Pellerin, L. (2003). Cell-specific expression pattern of monocarboxylate transporters in astrocytes and neurons observed in different mouse brain cortical cell cultures. Journal of neuroscience research, 73(2), 141-155.

Denk, W., & Horstmann, H. (2004). Serial block-face scanning electron microscopy to reconstruct three-dimensional tissue nanostructure. PLoS Biol, 2(11), e329.

Duarte, J. M., Lei, H., Mlynárik, V., & Gruetter, R. (2012). The neurochemical profile quantified by in vivo 1 H NMR spectroscopy. Neuroimage, 61(2), 342-362.

Duran, J., Saez, I., Gruart, A., Guinovart, J. J., & Delgado-García, J. M. (2013). Impairment in long-term memory formation and learning-dependent synaptic plasticity in mice lacking glycogen synthase in the brain. Journal of Cerebral Blood Flow & Metabolism, 33(4), 550-556.

Durand, G. M., Kovalchuk, Y., & Konnerth, A. (1996). Long-term potentiation and functional synapse induction in developing hippocampus.

Fernie, A. R., Carrari, F., & Sweetlove, L. J. (2004). Respiratory metabolism: glycolysis, the TCA cycle and mitochondrial electron transport. Current opinion in plant biology, 7(3), 254-261.

Ferri, A. L., Cavallaro, M., Braida, D., Di Cristofano, A., Canta, A., Vezzani, A., ... & Nicolis, S. K. (2004). Sox2 deficiency causes neurodegeneration and impaired neurogenesis in the adult mouse brain. Development, 131(15), 3805-3819.

Fischer, A., Sananbenesi, F., Schrick, C., Spiess, J., & Radulovic, J. (2004). Distinct roles of hippocampal de novo protein synthesis and actin rearrangement in extinction of contextual fear. The Journal of Neuroscience, 24(8), 1962-1966.

Folci, A., Murru, L., Vezzoli, E., Ponzoni, L., Gerosa, L., Moretto, E., ... & Bähler, M. (2016). Myosin IXa Binds AMPAR and Regulates Synaptic Structure, LTP, and Cognitive Function. Frontiers in molecular neuroscience, 9.

Fonnum, F. (1984). Glutamate: a neurotransmitter in mammalian brain. Journal of neurochemistry, 42(1), 1-11.

Fosgerau, K., Westergaard, N., Quistorff, B., Grunnet, N., Kristiansen, M., & Lundgren, K. (2000). Kinetic and functional characterization of 1, 4-dideoxy-1, 4-imino-d-arabinitol: a potent inhibitor of glycogen phosphorylase with anti-hyperglyceamic effect in ob/ob mice. Archives of biochemistry and biophysics, 380(2), 274-284.

Gallagher, C. N., Carpenter, K. L., Grice, P., Howe, D. J., Mason, A., Timofeev, I., ... & Hutchinson, P. J. (2009). The human brain utilizes lactate via the tricarboxylic acid cycle: a 13C-labelled microdialysis and high-resolution nuclear magnetic resonance study. Brain, awp202.

Geinisman, Y. (2000). Structural synaptic modifications associated with hippocampal LTP a112arburg112etiral learning. Cerebral Cortex, 10(10), 952-962.

Gibbs, M. E., Anderson, D. G., & Hertz, L. (2006). Inhibition of glycogenolysis in astrocytes interrupts memory consolidation in young chickens. Glia, 54(3), 214-222.

Halassa, M. M., & Haydon, P. G. (2010). Integrated brain circuits: astrocytic networks modulate neuronal activity a112arburg112eior. Annual review of physiology, 72, 335.

Halestrap, A. P., & Price, N. T. (1999). The proton-linked monocarboxylate transporter (MCT) family: structure, function and regulation. Biochemical Journal, 343(2), 281-299.

Halestrap, A. P., & Meredith, D. (2004). The SLC16 gene family—from monocarboxylate transporters (MCTs) to aromatic amino acid transporters and beyond. Pflügers Archiv, 447(5), 619-628.

Halim, N. D., Mcfate, T., Mohyeldin, A., Okagaki, P., Korotchkina, L. G., Patel, M. S., ... & Verma, A. (2010). Phosphorylation status of pyruvate dehydrogenase distinguishes metabolic phenotypes of cultured rat brain astrocytes and neurons. Glia, 58(10), 1168-1176.

Haydon, P. G., & Nedergaard, M. (2015). How do astrocytes participate in neural plasticity?. Cold Spring Harbor perspectives in biology, 7(3), a020438.

Herrero-Mendez, A., Almeida, A., Fernández, E., Maestre, C., Moncada, S., & Bolaños, J. P. (2009). T113arburg113eticstic and antioxidant status of neurons is controlled by continuous degradation of a key glycolytic enzyme by APC/C–Cdh1. Nature cell biology, 11(6), 747-752.

Herry, C., & Johansen, J. P. (2014). Encoding of fear learning and memory in distributed neuronal circuits. Nature neuroscience, 17(12), 1644-1654.

Hertz, L., & Dienel, G. A. (2005). Lactate transport and transporters: general principles and functional roles in brain cells. Journal of neuroscience research, 79(1-2), 11-18.

Isaac, J. T., Nicoll, R. A., & Malenka, R. C. (1995). Evidence for silent synapses: implications for the expression of LTP. Neuron, 15(2), 427-434.

Itoh, Y., Esaki, T., Shimoji, K., Cook, M., Law, M. J., Kaufman, E., & Sokoloff, L. (2003). Dichloroacetate effects on glucose and lactate oxidation by neurons and astroglia in vitro and on glucose utilization by brain in vivo. Proceedings of the National Academy of Sciences, 100(8), 4879-4884.

Jakoby, P., Schmidt, E., Ruminot, I., Gutiérrez, R., Barros, L. F., & Deitmer, J. W. (2012). Higher transport and metabolism of glucose in astrocytes compared with neurons: a multiphoton study of hippocampal and cerebellar tissue slices. Cerebral cortex, bhs309.

Juel, C., & Halestrap, A. P. (1999). Lactate transport in skeletal muscle—role and regulation of the monocarboxylate transporter. The Journal of Physiology, 517(3), 633-642.

Karlén, A., Karlsson, T. E., Mattsson, A., Lundströmer, K., Codeluppi, S., Pham, T. M.,… & Sherling, M. A. (2009). Nogo receptor 1 regulates formation of lasting memories. Proceedings of the National Academy of Sciences, 106(48), 20476-20481.

KBJ, P. G. F., & Paxinos, G. (2001). The mouse brain in stereotaxic coordinates. San Diego: Academic Press, 200(1), 65-69.

Kerchner, G. A., & Nicoll, R. A. (2008). Silent synapses and the emergence of a postsynaptic mechanism for LTP. Nature Reviews Neuroscience, 9(11), 813-825.

Kontos, H. A. (1981). Regulation of the cerebral circulation. Annual Review of Physiology, 43(1), 397-407.

Latsis, T., Andersen, B., & Agius, L. (2002). Diverse effects of two allosteric inhibitors on the phosphorylation state of glycogen phosphorylase in hepatocytes. Biochemical Journal, 368(1), 309-316.

Laughton, J. D., Bittar, P., Charnay, Y., Pellerin, L., Kovari, E., Magistretti, P. J., & Bouras, C. (2007). Metabolic compartmentalization in the human cortex and hippocampus: evidence for a cell-and region-specific localization of lactate dehydrogenase 5 and pyruvate dehydrogenase. BMC neuroscience, 8(1), 35.

Li, Z., Okamoto, K. I., Hayashi, Y., & Sheng, M. (2004). The importance of dendritic mitochondria in the morphogenesis and plasticity of spines and synapses. Cell, 119(6), 873-887.

Liao D, Hessler NA, Malinow R (1995) Activation of postsynaptically silent synapses during pairing-induced LTP in CA1 region of hippocampal slice. Nature 375:400–404.

Liao, D., Zhang, X.' O'Brien, R., Ehlers, M. D., & Huganir, R. L. (1999). Regulation of morphological postsynaptic silent synapses in developing hippocampal neurons. Nature neuroscience, 2(1), 37-43.

Lovatt, D., Sonnewald, U., Waagepetersen, H. S., Schousboe, A., He, W., Lin, J. H. C., ... & Goldman, S. A. (2007). The transcriptome and metabolic gene signature of protoplasmic astrocytes in the adult murine cortex. The Journal of Neuroscience, 27(45), 12255-12266.

Magistretti, P. J., Pellerin, L., Rothman, D. L., & Shulman, R. G. (1999). Energy on demand. Science, 283(5401), 496-497.

Magistretti, P. J. (2000). Cellular bases of functional brain imaging: insights from neuron-glia metabolic coupling. Brain research, 886(1), 108-112.

Magistretti, P. J., & Ransom, B. R. (2002). Astrocytes (No. LNDC-CHAPTER-2010-003, pp. 133-145). Lippincott Villiam & Wilkins.

Magistretti, P. J., & Chatton, J. Y. (2005). Relationship between L-glutamate-regulated intracellular Na+ dynamics and ATP hydrolysis in astrocytes. Journal of neural transmission, 112(1), 77-85.

Magistretti, P. J. (2008). Brain energy metabolism (No. LNDC-CHAPTER-2010-001, pp. 271-293). Academic Press.

Magistretti, P. J. (2009). Role of glutamate in neuron-glia metabolic coupling. The American journal of clinical nutrition, 90(3), 875S-880S.

Magistretti, P. J., & Allaman, I. (2015). A cellular perspective on brain energy metabolism and functional imaging. Neuron, 86(4), 883-901.

Mantzur, L., Joels, G., & Lamprecht, R. (2009). Actin polymerization in lateral amygdala is essential for fear memory formation. Neurobiology of learning and memory, 91(1), 85-88.

Martin, K. C., Michael, D., Rose, J. C., Barad, M., Casadio, A., Zhu, H., & Kandel, E. R. (1997). MAP kinase translocates into the nucleus of the presynaptic cell and is required for long-term facilitation in Aplysia. Neuron, 18(6), 899-912.

Massaad, C. A., & Klann, E. (2011). Reactive oxygen species in the regulation of synaptic plasticity and memory. Antioxidants & red116arburg116eting, 14(10), 2013-2054.

Mergenthaler, P., Lindauer, U., Dienel, G. A., & Meisel, A. (2013). Sugar for the brain: the role of glucose in physiological and pathological brain function. Trends in neurosciences, 36(10), 587-597.

Moraga-Amaro, R., Jerez-Baraona, J. M., Simon, F., & Stehberg, J. (2014). Role of astrocytes in memory and psychiatric disorders. Journal of Physiology-Paris, 108(4), 240-251.

Murai, K. K., Nguyen, L. N., Koolpe, M., McLennan, R., Krull, C. E., & Pasquale, E. B. (2003). Targeting the EphA4 receptor in the nervous system with biologically active peptides. Molecular and Cellular Neuroscience, 24(4), 1000-1011.

Nedergaard, M., Ransom, B., & Goldman, S. A. (2003). New roles for astrocytes: redefining the functional architecture of the brain. Trends in neurosciences, 26(10), 523-530.

Nelson, D. L., Lehninger, A. L., & Cox, M. M. (2008). Lehninger principles of biochemistry. Macmillan.

Norenberg, M. D., & Martinez-Hernandez, A. (1979). Fine structural localization of glutamine synthetase in astrocytes of rat brain. Brain research, 161(2), 303-310.

Oertner, T. G., & Matus, A. (2005). Calcium regulation of actin dynamics in dendritic spines. Cell calcium, 37(5), 477-482.

Paxinos, G. F. K. B. J., & Franklin, K. B. (2001). The mouse brain in stereotaxic coordinates. 2. San Diego: Academic.

Pellerin, L., & Magistretti, P. J. (1994). Glutamate uptake into astrocytes stimulates aerobic glycolysis: a mechanism coupling neuronal activity to glucose utilization. Proceedings of the National Academy of Sciences, 91(22), 10625-10629.

Pellerin, L., & Magistretti, P. J. (2003). Food for thought: challenging the dogmas. Journal of Cerebral Blood Flow & Metabolism, 23(11), 1282-1286.

Pellerin, L., Halestrap, A. P., & Pierre, K. (2005). Cellular and subcellular distribution of monocarboxylate transporters in cultured brain cells and in the adult brain. Journal of neuroscience research, 79(1 - 2), 55-64.

Pellerin, L., Bouzier-Sore, A. K., Aubert, A., Serres, S., Merle, M., Costalat, R., & Magistretti, P. J. (2007). Activity-dependent regulation of energy metabolism by astrocytes: an update. Glia, 55(12), 1251-1262.

Petralia, R. S., Esteban, J. A., Wang, Y. X., Partridge, J. G., Zhao, H. M., Wenthold, R. J., & Malinow, R. (1999). Selective acquisition of AMPA receptors over postnatal development suggests a molecular basis for silent synapses. Nature neuroscience, 2(1), 31-36.

Proia, P., Di Liegro, C. M., Schiera, G., Fricano, A., & Di Liegro, I. (2016). Lactate as a Metabolite and a Regulator in the Central Nervous System. International Journal of Molecular Sciences, 17(9), 1450.

Raichle, M. E., & Gusnard, D. A. (2002). Appraising the br’in's energy budget. Proceedings of the National Academy of Sciences, 99(16), 10237-10239.

Ramos, M., del Arco, A., Pardo, B., Martínez-Serrano, A., Martínez-Morales, J. R., Kobayashi, K., ... & Satrústegui, J. (2003). Developmental changes in the Ca 2+-regulated mitochondrial aspartate–glutamate carrier aralar1 in brain and prominent expression in the spinal cord. Developmental Brain Research, 143(1), 33-46.

Ransom, B. R., Yamate, C. L., & Connors, B. W. (1985). Activity-dependent shrinkage of extracellular space in rat optic nerve: a developmental study. The Journal of neuroscience, 5(2), 532-535.

Ransom, C. B., Ransom, B. R., & Sontheimer, H. (2000). Activity - dependent extracellular K+ accumulation in rat optic nerve: the role of glial and axonal Na+ pumps. The Journal of physiology, 522(3), 427-442.

Roebroeck, A., Galuske, R., Formisano, E., Chiry, O., Bratzke, H., Ronen, I., ... & Goebel, R. (2008). High-resolution diffusion tensor imaging and tractography of the human optic chiasm at 9.4 T. Neuroimage, 39(1), 157-168.

Salem, R. D., Hammerschlag, R., Bracho, H., & Orkand, R. K. (1975). Influence of potassium ions on accumulation and metabolism of [14 C] glucose by glial cells. Brain research, 86(3), 499-503.

Schurr, A., Miller, J. J., Payne, R. S., & Rigor, B. M. (1999). An increase in lactate output by brain tissue serves to meet the energy needs of glutamate-activated neurons. The Journal of neuroscience, 19(1), 34-39.

Segal, M. (2005). Dendritic spines and long-term plasticity. Nature Reviews Neuroscience, 6(4), 277-284.

Shulman, R. G., & Rothman, D. L. (2001). The “glycogen shunt” in exercising muscle: a role for glycogen in muscle energetics and fatigue. Proceedings of the National Academy of Sciences, 98(2), 457-461.

Simpson, I. A., Carruthers, A., & Vannucci, S. J. (2007). Supply and demand in cerebral energy metabolism: the role of nutrient transporters. Journal of Cerebral Blood Flow & Metabolism, 27(11), 1766-1791.

Smith, D., Pernet, A., Hallett, W. A., Bingham, E., Marsden, P. K., & Amiel, S. A. (2003). Lactate: a preferred fuel for human brain metabolism in vivo. Journal of Cerebral Blood Flow & Metabolism, 23(6), 658-664.

Sokoloff, L., Mangold, R., Wechsler, R. L., Kennedy, C., & Kety, S. S. (1955). The effect of mental arithmetic on cerebral circulation and metabolism. Journal of Clinical Investigation, 34(7 Pt 1), 1101.

Sola-Penna, M. (2008). Metabolic regulation by lactate. IUBMB life, 60(9), 605-608.

Stehberg, J., Moraga-Amaro, R., Salazar, C., Becerra, A., Echeverría, C., Orellana, J. A., ... & Sáez, J. C. (2012). Release of gliotransmitters through astrogli119arburg119exin 43 hemichannels is necessary for fear memory consolidation in the basolateral amygdala. The FASEB Journal, 26(9), 3649-3657.

Suh, S. W., Bergher, J. P., Anderson, C. M., Treadway, J. L., Fosgerau, K., & Swanson, R. A. (2007). Astrocyte glycogen sustains neuronal activity duri119arburg119eticsmia: studies with the glycogen phosphorylase inhibitor CP-316,819 ([RR*, S*]-5-chloro-N-[2-hydroxy-3-(methoxymethylamino)-3-oxo-1-(phenylmethyl) propyl]-1H-indole-2-carboxamide). Journal of Pharmacology and Experimental Therapeutics, 321(1), 45-50.

Suzuki, A., Stern, S. A., Bozdagi, O., Huntley, G. W., Walker, R. H., Magistretti, P. J., & Alberini, C. M. (2011). Astrocyte-neuron lactate transport is required for long-term memory formation. Cell, 144(5), 810-823.

Taglialatela, G., Hogan, D., Zhang, W. R., & Dineley, K. T. (2009). Intermediate- and long-term recognition memory deficits in Tg2576 mice are reversed with acute calcineurin inhibition. Behavioural brain research, 200(1), 95-99.

Tekkök, S. B., Brown, A. M., Westenbroek, R., Pellerin, L., & Ransom, B. R. (2005). Transfer of glycogen-derived lactate from astrocytes to axons via specific monocarboxylate transporters supports mouse optic nerve activity. Journal of neuroscience research, 81(5), 644-652.

Toni, N., Buchs, P. A., Nikonenko, I., Bron, C. R., & Muller, D. (1999). LTP promotes formation of multiple spine synapses between a single axon terminal and a dendrite. Nature, 402(6760), 421-425.

Van't Veer, A., Bechtholt, A. J., Onvani, S., Potter, D., Wang, Y., Liu-Chen, L. Y., ... & Carlezon, W. A. (2013). Ablation of kappa-opioid receptors from brain dopamine neurons has anxiolytic-like effects and enhances cocaine-induced plasticity. Neuropsychopharmacology, 38(8), 1585-1597.

Vilchez, D., Ros, S., Cifuentes, D., Pujadas, L., Vallès, J., García-Fojeda, B., ... & García-Rocha, M. (2007). Mechanism suppressing glycogen synthesis in neurons and its demise in progressive myoclonus epilepsy. Nature neuroscience, 10(11), 1407-1413.

Walls, A. B., Sickmann, H. M., Brown, A., Bouman, S. D., Ransom, B., Schousboe, A., & Waagepetersen, H. S. (2008). Characterization of 1, 4-dideoxy-1, 4-imino-d-arabinitol (DAB) as an inhibitor of brain glycogen shunt activity. Journal of neurochemistry, 105(4), 1462-1470.

Wang, F., Yuan, T., Pereira Jr, A., Verkhratsky, A., & Huang, J. H. (2016). Glial Cells and Synaptic Plasticity. Neural Plasticity, 2016.

Ward, P. S., & Thompson, C. B. (2012). Metabolic reprogramming: a cancer hallmark ev120arburgurg did not anticipate. Cancer cell, 21(3), 297-308.

Westergaard, N., Sonnewald, U., & Schousboe, A. (1995). Metabolic trafficking between neurons and astrocytes: the glutamate/glutamine cycle revisited. Developmental neuroscience, 17(4), 203-211.

Yang, J., Ruchti, E., Petit, J. M., Jourdain, P., Grenningloh, G., Allaman, I., & Magistretti, P. J. (2014). Lactate promotes plasticity gene expression by potentiating NM121arburg121eting in neurons. Proceedings of the National Academy of Sciences, 111(33), 12228-12233.

Youle, R. J., & Van Der Bliek, A. M. (2012). Mitochondrial fission, fusion, and stress. Science, 337(6098), 1062-1065.

Zhang, L., Trushin, S., Christensen, T. A., Bachmeier, B. V., Gateno, B., Schroeder, A., ... & Gylys, K. H. (2016). Altered brain energetics induces mitochondrial fission arrest in Alzheimer's disease. Scientific reports, 6.

Zielke, R. H., Zielke, C. L., & Baab, P. J. (2009). Direct measurement of oxidative metabolism in the living brain by microdialysis: a review. Journal of neurochemistry, 109(s1), 24-29.

ACKNOWLEDGEMENTS

I would like to thank Prof. Panerai and Prof. Corsini, who, during these years, coordinated with great passion the Ph.D. School in Pharmacological Sciences.

I am grateful to Dr. Maura Francolini, who supervised me and gave me the opportunity to work and develop my technical skills as well as my great passion in microscopy since I started my studies at the University of Milan.

I sincerely acknowledge Prof. Andrea Falqui and Prof. Pierre Magistretti, who funded this project, gently hosted me in Saudi Arabia, and supported my work with their constructive scientific discussion.

Special thanks to Dr. Elisa Sogne and Dr. Corrado Calì, who helped me with serial block face scanning electron microscopy experiments as well as with 3D reconstructions, and who contributed to this project also with their scientific interest and passion.

I would like to thank Prof. Mariaelvina Sala, Dr. Luisa Ponzoni and Dr. Daniela Braida, who did the behavioural experiments of this project with great professionalism and accuracy.

I would also like to acknowledge Norma Lattuada, who worked with me and helped me in the lab daily life in the last year.

Last but not least, I would like to thank Simona Rodighiero and Lorena Benedetti, who taught me a lot and worked hard with me.